



**AUDENTES**

**FORTUNA IU VAT**

UNIVERSITA' DEGLI STUDI MILANO-BICOCCA

DOCTOR OF PHILOSOPHY IN MATERIALS SCIENCE

XXVI CYCLE

# **Organic Materials for Dye-Sensitized Solar Cells**

VALENTINA LEANDRI

Supervisor:  
Prof. Alessandro Abboto

Academic Year 2013-2014

## Special Acknowledgements



Pirelli & C. S.p.A. is an Italian company that operates in the tire sector. Through its subsidiary Pirelli Tyre, it designs, develops, manufactures and markets tires for motor vehicles, industrial vehicles and motorcycles. Its products are used by car maker partners such as Bentley, Aston Martin and Porsche, among others. Through its subsidiaries Pirelli & C. Eco Technology SpA, Pirelli & C. Ambiente S.p.A and PZero S.r.l, it is active in emissions control technologies, renewable energy sources and fashion.

### **CORIMAV**

Consortium for Research on Advanced Materials (CORIMAV) is a consortium between Pirelli and Milano-Bicocca University, whose objective is researching on advanced materials with a joint effort of the scientific and technological know-how of both University and Pirelli.

“We must not forget that when radium was discovered no one knew that it would prove useful in hospitals. The work was one of pure science. And this is a proof that scientific work must not be considered from the point of view of the direct usefulness of it. It must be done for itself, for the beauty of science, and then there is always the chance that a scientific discovery may become like the radium a benefit for mankind. ”

– Marie Curie

# List of Papers

This thesis is based on the following three papers, which are referred to in the text, by their Roman numerals I-III.

- I. A. Abbotto, V. Leandri, N. Manfredi, F. De Angelis, M. Pastore, J.-H. Yum, M. K. Nazeeruddin, M. Graetzel  
**Bis-Donor-Bis-Acceptor Tribranched Organic Sensitizers for Dye-Sensitized Solar Cells**  
*Eur. J. Org. Chem.*, **2011**, 31, 6195-6205.
- II. V. Leandri, V. Trifiletti, R. Ruffo, A. Abbotto  
**Asymmetric Tribranched Dyes: an Intramolecular Co-Sensitization Approach for Dye-Sensitized Solar Cells**  
*Eur. J. Org. Chem.*, **2013**, 30, 6793-6801.
- III. V. Leandri, H. Ellis, E. Gabrielsson, G. Boschloo, L. Sun, A. Hagfeldt  
**Organic Hydrophilic Dye for Water-Based Electrolyte Dye-Sensitized Solar Cells** (*in preparation for Energy Environ. Sci*)

# Abbreviations and Symbols

J	Joule
K	Kelvin
HOMO	Highest Occupied Molecular Orbital
LUMO	Lowest Unoccupied Molecular Orbital
CB	Conduction Band
WE, we	Working-Electrode
CE, ce	Counter-Electrode
$\eta_j$	Photocurrent efficiency
$\eta_{\text{abs}}$	Absorbed photons
$\eta_{\text{diss}}$	Hole-electron pairs dissociated
$\eta_c$	Charge collection efficiency
$\varepsilon$	Molar extinction coefficient
$J_{\text{sc}}$	Short-circuit photocurrent
$V_{\text{oc}}$	Open-circuit voltage
FF	Fill Factor
$P_{\text{in}}$	Power of incident light
IPCE	Incident Photon to Current Efficiency
$\lambda$	Wavelength
LHE	Light Harvesting Efficiency
APCE	Absorbed Photon to Current Efficiency
$\Phi_{\text{inj}}$	Electron injection efficiency
$L_n$	Electrode thickness
C	Concentration
NIR	Near-Infrared
ICT	Intramolecular Charge Transfer
MLCT	Metal to Ligand Charge Transfer
LMCT	Ligand to Metal Charge Transfer
<i>t</i> -BuOK	Potassium <i>tert</i> -butoxide
Pd(dppf)Cl <sub>2</sub>	1,1'-Bis(diphenylphosphino)ferrocene palladium(II) dichloride
Py	Pyridine
THF	Tetrahydrofuran

DMF	N-N-dimethylformamide
MeOH	Metanol
PhMe	Toluene
NBS	N-Bromosuccinimide
TBA(PF <sub>6</sub> )	Tetrabutylammonium hexafluorophosphate
PTSA	p-Toluenesulfonic acid
P(OEt) <sub>3</sub>	Triethylphosphite
CV	Cyclic Voltammetry
CDCA	Chenodeoxycholic acid
GuSCN	Guanidinium thiocyanate
<i>n</i> -BuLi	Normal-butyllithium
NaDS	Sodium dodecyl sulfate
EDOT	3,4-Ethylenedioxythiophene

# Table of Contents

1.	Introduction .....	1
1.1.	Energy from the Sun .....	1
1.2.	Photovoltaic .....	2
2.	Dye-Sensitized Solar Cells (DSSC) .....	3
2.1.	Working Principles and Components.....	4
2.2.	Characterization Parameters.....	5
3.	Dye Sensitizers .....	8
3.1.	Background .....	8
3.2.	Organic Dyes.....	9
3.3.	Aim of the Thesis .....	10
4.	The Challenge of Absorption Extension .....	11
5.	Design Modification: from Mono- to Tri-branched Dyes .....	12
5.1.	Introduction .....	12
5.2.	Aim of the Study .....	13
5.3.	Design and Synthesis .....	14
5.4.	Properties of the Sensitizers .....	18
5.5.	Photovoltaic Performance .....	22
5.6.	Conclusion .....	24
6.	Asymmetric Tribranched Dyes: Full Exploitation of Design Variability.....	25
6.1.	Introduction .....	25
6.2.	Aim of the Study .....	25
6.3.	Design and Synthesis .....	26
6.4.	Properties of the Sensitizers .....	32
6.5.	Photovoltaic Performance .....	35
6.6.	Conclusion .....	37

7.	Organic Hydrophilic Dye for Water-based DSSCs .....	40
7.1.	Introduction .....	40
7.2.	Aim of the study .....	40
7.3.	Design and Synthesis .....	41
7.4.	Properties of the Sensitizer .....	43
7.5.	Photovoltaic Performance .....	47
7.6.	Conclusion .....	53
8.	Concluding Remarks .....	54
	References .....	55
	Appendix 1 .....	62
	Acknowledgements .....	63



# 1. Introduction

From the 18<sup>th</sup> and 19<sup>th</sup> century, the whole world experienced the beginning of a great industrial change known as “industrial revolution”. Due to the rapid industrialization and mechanization of an always increasing number of tasks, vast territories benefited of a significant improved wellness. This eventually resulted in a dramatic increase in population that has not still reached its peak and will cause the global energy demand to double by the year 2040.<sup>1</sup> At the same time, pollution deriving from the emission of side-products from industrial processes such as CO, CO<sub>2</sub>, NO<sub>x</sub>, are having serious impacts on the climate, causing phenomena like the “greenhouse effect” and the “global warming”. In this scenario, the research for an alternative, efficient, and renewable energy is necessary.

## 1.1. Energy from the Sun

More energy from sunlight strikes the Earth in one hour ( $4.3 \times 10^{20}$  J) than all the energy consumed on the planet in a year ( $4.1 \times 10^{20}$  J),<sup>2</sup> therefore, solar energy is considered the most attractive clean option. The spectrum of the radiation emitted by the sun is very similar to that of a black body at around 5800 K (Figure 1).

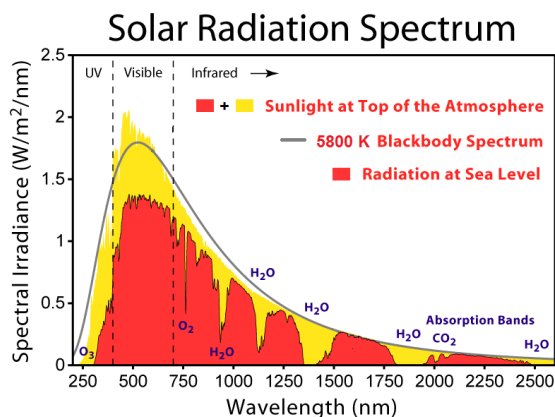


Figure 1. Emission spectrum of the Sun

Solar energy can be converted into electricity mainly using two different technologies currently available: solar thermal and photovoltaic.

## 1.2. Photovoltaic

Edmund Becquerel discovered the photovoltaic effect in 1839, while conducting experiments with an electrolytic cell in which two platinum electrodes were immersed. He observed that the intensity of the current produced increased when the cell was exposed to sunlight and was also the first one to realize that this effect depended on the wavelength of the incident light. Since its discovery, the ability to derive electricity from solar radiation, has aroused increasing interest in the world scenario and it is still one of the biggest scientific challenges. Photovoltaic research has diversified greatly over time, defining numerous types of devices and many applications. The entire technology is formally divided into three generations that reflect the chronological order in which different systems have made their appearance.

The first generation of photovoltaic devices exploits a p-n junction between differently doped semiconductors, such as silicon. The maximum experimental value currently achieved for a monocrystalline silicon cell, stood at 24.7%,<sup>3</sup> very close to the theoretical limit calculated, estimated to be around 30%. However, the high cost for the realization of these devices prevents them from being competitive on the market.

The efforts to contain material costs and reduce the energy payback time, led to the second generation, dominated by the thin-film technology. Thin films are films of semiconductor material whose thickness is around 100 nm. Solar cells manufactured with this technology, typically employ semiconductors like amorphous silicon, cadmium telluride (CdTe), or copper indium gallium diselenide (CIGS). Although high efficiencies, around 20% have been achieved,<sup>4</sup> the use of rare and toxic elements still limits the production costs.

The third generation sees as protagonists devices that try to overcome the 30% theoretical limit, based on a multi-junction approach like tandem solar cells. Great attention was addressed to the realization of cheaper and more environmental friendly devices based on organic materials, from which Organic Photovoltaics (OPVs) arose. Dye-Sensitized solar cells, at the center of the topic of this thesis, can be ascribed to this generation.

## 2. Dye-Sensitized Solar Cells (DSSC)

The DSSCs, more commonly known as DSCs, are last generation solar cells consisting of both organic and inorganic materials. In the field of organic and hybrid photovoltaic, DSCs are very promising systems in relation to production costs and conversion efficiencies. It is estimated that approximately 60% of the cost of a dye-sensitized solar cell is due to the conducting glasses.<sup>5</sup>

In 1991, Professors Michael Graetzel and Brian O'Regan, designed a new device inspired by a natural process for converting solar energy already exploited by plants and other organisms: the photosynthesis (Figure 2).<sup>6</sup>

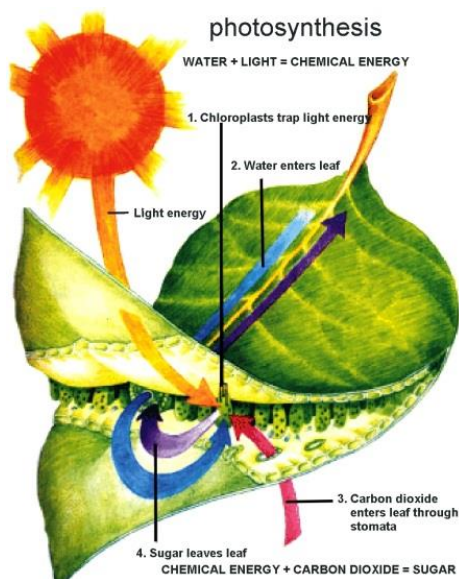


Figure 2. Pictorial representation of the photosynthesis.

In this process, organic pigments (chlorophyll, carotenoids, etc. ...) operate the absorption of light radiation and use the energy captured to promote an electron in the excited state. Subsequently, the charges are transferred to a specific reaction center and the neutrality of the chromophores is restored by electrons coming from the splitting of water molecules. The plant organism is thus able to acquire energy that will then be used in the processes of synthesis of organic substances, useful to its survival.

## 2.1. Working Principles and Components

The DSSCs, unlike conventional devices, provide a substantial distinction between optical absorption and charge separation. In the parallelism previously made with the photosynthesis, the function of the pigment is accomplished by the dye, while the redox couple has the role to transport the electrons necessary to restore the electroneutrality. The configuration and the working principle of a DSC is schematised in Figure 2.1.

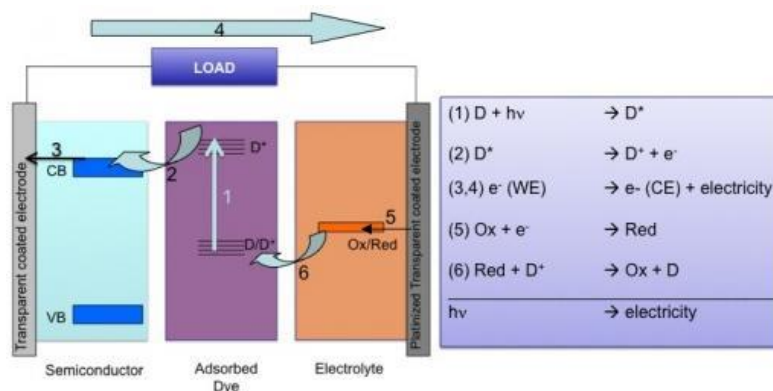


Figure 2.1. Operating principles and reactions occurring in a Dye-sensitized solar cell.

In the first step, the incident radiation is absorbed by the dye and its energy is used to promote an electron from the HOMO to the LUMO level (process 1 in Figure 2.1). From the LUMO level, the electron is injected into the conduction band (CB) of a semiconductor material, usually  $TiO_2$  (process 2 in Figure 2.1). In dark condition, the Fermi level of the  $TiO_2$  equals the redox potential of the redox couple, therefore no voltage is present and no current flows. Under illumination, the *quasi*-Fermi level is shifted up as the electron concentration in the conduction band increases, and a driving force for the electrons to perform electrical work is obtained (processes 3 and 4 in Figure 2.1).<sup>7</sup> The electrons accumulated at the counter-electrode perform the reduction of the oxidized part of the redox couple (process 5 in Figure 2.1), which concludes the photovoltaic cycle migrating at the working-electrode to restore the electroneutrality of the dye (process 6 in Figure 2.1). Common losses in the cells are due to the recombination of the injected electrons with the oxidized specie of the electrolyte, or with the oxidized dye. The latter aspect is strongly related to the electron lifetime of the dye employed, which is a crucial aspect for the correct operation of the device.

As can be deduced from the previous description, a DSSC is therefore composed of four main elements: a chromophore (dye), a redox couple, a working-electrode, and a counter electrode. Each individual part fulfills a great importance and has received thorough investigation during the last decades. The implementation of dye-sensitized solar cells requires joint efforts coming from different subject areas, and a clear interpretation and knowledge of the processes involved. For this reason, this kind of system currently offer a wide research margin.

## 2.2. Characterization Parameters

In order to achieve a better understanding of the operating principles of a dye-sensitized solar cell, it is necessary to perform a brief discussion including several guidelines used in the description of the photovoltaic performances. The parameters described later, represent a common reference point for all the photovoltaic devices and therefore allow to make an immediate comparison between different technologies.

### Energy Conversion Efficiency

The overall solar conversion efficiency ( $\eta$ ) is the most important parameter for a basic description of photovoltaic devices, as it allows direct comparison between different technologies. Its value represent the amount of incident radiation that the device is able to convert into electrical power. Equation (1) reports the most commonly known expression of the overall conversion efficiency for Dye-sensitized solar cells:

$$\eta = \frac{J_{sc} \cdot V_{oc} \cdot FF}{P_{in}} \quad (1)$$

where  $J_{sc}$  is the photocurrent produced per unit area ( $\text{mAcm}^{-1}$ ) under illumination, at shortcircuit conditions, while  $V_{oc}$  is the potential difference between the the *quasi*-Fermi level of the semiconductor and the redox couple at open-circuit conditions. FF, the *fill factor*, expresses the relative area between an imaginary rectangle representing the maximum power obtainable from the cell in ideal conditions, and the one drawn in order to get the maximum area inside the real  $J$ - $V$  curve (Figure 2.2). The FF value is an important indicator of the quality of a device, as it is directly affected by the series and shunt resistances in a solar cell.

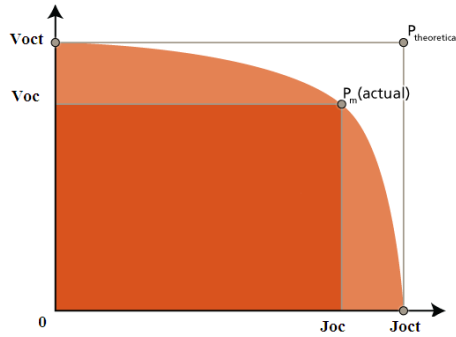


Figure 2.2. Evaluation of the *fill factor*. The smaller rectangle expresses the maximum area obtainable inside the *J-V* curve. The bigger rectangle is obtained from maximum  $J_{sc}$  and  $V_{oc}$ .

The electric current that a photovoltaic solar cell is able to produce is a very important element, as it is the aspect that offers more possibilities to improve the overall conversion efficiency. Its value depends on the fraction of photons absorbed ( $\eta_{abs}$ ), the number of electron-hole pairs that are dissociated ( $\eta_{diss}$ ) and the amount of the separated charges that reach the electrodes ( $\eta_{out}$ ).<sup>8</sup> All these factors affect the value of the photocurrent efficiency  $\eta_j$ , according to the following equation (2):

$$\eta_j = \eta_{abs} \cdot \eta_{diss} \cdot \eta_{out} \quad (2)$$

The fraction of photons absorbed is, in turn, affected by the absorption spectrum of the dye, its molar extinction coefficient  $\epsilon$ , the thickness of layers and multiple internal reflections. The key to efficient charge separation in DSSCs relies on the kinetically ultraslow interfacial recombination rate and the ability of electrolyte ions to surround each nanoparticle, thus neutralizing the electrostatic field between the photoinjected electron and the hole.<sup>9</sup> To reach the electrodes, the charge carriers need a net driving force, which generally results from the difference in the electrochemical potentials of the *quasi-Fermi* level of the semiconductor and the redox couple, under illumination.

### Incident Photon to Current Efficiency (IPCE)

Known with the acronym IPCE, the incident-photon-to-current-efficiency is one of the most essential photovoltaic parameters and provides information about the ability of the device to convert photons from monochromatic incident light, into

electrical current. Its principal physical expression is reported in the equation below (3):

$$IPCE(\lambda) = \frac{1240 \cdot J_{sc}(\lambda)}{P_{in}(\lambda)} \cdot 100 \quad (3)$$

Where  $\lambda$  is the wavelength of the monochromatic light that is harvested by the cell. The IPCE value is commonly expressed in percentage (%), that is the reason of the multiplication for a 100 factor.

### **Light Harvesting Efficiency (LHE) and Absorbed Photon to Current Efficiency (APCE)**

The value of IPCE can also be expressed as a function of two other important parameters, the Light Harvesting Efficiency (LHE) and Absorbed Photon to Current Efficiency (APCE).<sup>10</sup> Equation (4) shows their relationship:

$$IPCE(\lambda) = LHE(\lambda) \cdot \Phi_{inj} \cdot \eta_c = LHE(\lambda) \cdot APCE \quad (4)$$

$\Phi_{inj}$  and  $\eta_c$  are, respectively, the electron injection efficiency and the charge collection efficiency. LHE can be directly measured from the absorption spectrum of the dye absorbed on a sufficiently thin and transparent semiconductor layer, and converted into the desired variable by simply utilizing equation (5):

$$LHE(\lambda) = 1 - 10^{-\varepsilon(\lambda)L_n C} \quad (5)$$

Where  $L_n$  and  $C$  are, respectively, the electrode thickness and the concentration, determined by the effective photoanode roughness. As showed by equation (5), the ability of a dye-sensitized solar cell to efficiently harvest incident light is therefore related to the dye, as it is determined by the dye's absorption spectrum, molar extinction coefficient  $\varepsilon$ , and concentration on the surface. Through equation (4) it is possible to extract very useful information for the investigation of the single components into the device. Infact, by measuring IPCE and LHE, it is also possible to obtain information about the ability of the cell to convert the absorbed photons into current (APCE), simply applying equation (6), solved as a function of the desired parameter:

$$APCE = \frac{IPCE(\lambda)}{LHE(\lambda)} \quad (6)$$

In other words, through the simple measurements of IPCE and LHE, and the APCE calculation, it is possible to discriminate the component that is responsible for poor performances of the device.

### 3. Dye Sensitizers

In the DSC technology the photosensitizer plays a fundamental role, as it is strongly related to important parameters, as seen in the previous chapter.

An ideal dye must have a broad and strong absorption of the portion of solar radiation located in the visible and NIR wavelengths. In addition to functioning as photon absorber, the sensitizing dye performs a variety of other tasks, including rapid electron injection,<sup>11,12</sup> efficient hole regeneration,<sup>13,14</sup> and acting as an effective barrier to recombination.<sup>15-17</sup> In order to achieve high stable devices and efficient electron injection, the dye must be strongly bonded with the semiconductor, therefore it must necessarily have at least one anchoring group such as  $-\text{COOH}$ ,<sup>18-21</sup>  $-\text{SO}_3\text{H}$ ,<sup>22,23</sup>  $-\text{PO}_3\text{H}_2$ ,<sup>24,25</sup>  $-\text{Py}$ ,<sup>26,27</sup> or others.<sup>28-29,31</sup> Finally, energy levels of dye must fulfill some required parameters: the LUMO must necessarily be more negative than the CB edge of the semiconductor, and the HOMO level must be more positive than potential of the redox couple.

#### 3.1. Background

Ruthenium complex immediately revealed high potentiality, yielding performances around 7% from 1991.<sup>6</sup> The ability to absorb about 46% of the incident radiation combined with a remarkable stability, opened the possibility of further development in that direction.<sup>30</sup> Therefore, in the following years, many researches have focused on the realization of similar compounds, leading to photosensitizers that held the record efficiency for almost 20 years (Figure 3.).

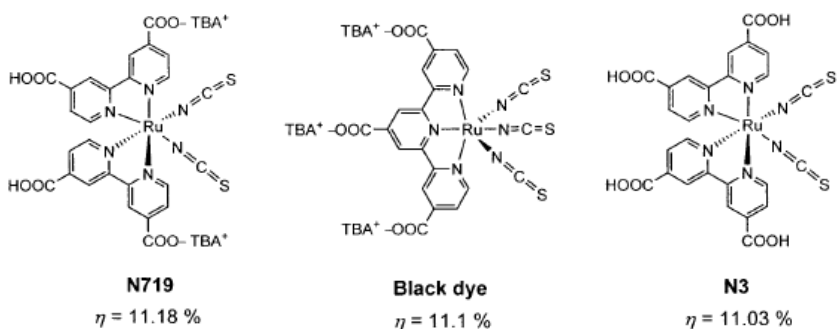


Figure 3. Ruthenium(II) complexes with polypyridyl and thiocyanate ligands.



The ruthenium complexes reported in Figure 3 resulted in very high performances in combination with  $I^-/I_3^-$  redox couple, but revealed to be inefficient when cobalt complexes were employed.<sup>32</sup> Recently, a new record was achieved exploiting a co-sensitization technique involving a porphyrin dye and a fully organic one (Figure 3.1).<sup>33</sup>

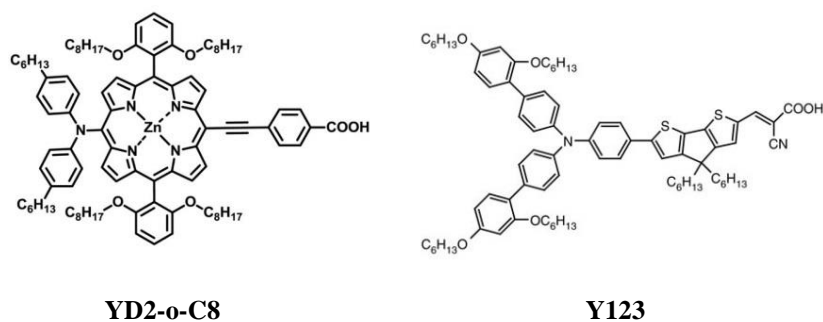


Figure 3.1. Record porphyrin (left) and organic (right) dye.

It is quite evident that metal-organic complexes detain great importance in DSSC. However, fully organic photosensitizers have been widely investigated because they offer several advantages with respect to the hybrid counterpart.

### 3.2. Organic Dyes

Fully organic sensitizers offer potentially endless possibilities to improve the desired properties through structural modification. Moreover, unlike the metal-organic compounds, can be purified in a more simple and economic way, have higher molar extinction coefficients, and do not involve expensive and rare metals such as Ruthenium, that would prevent their production on a big scale.<sup>34</sup>

A common way of designing organic dyes is to connect an electron donor (D), a conjugate bridge ( $\pi$ ) and an acceptor (A) building blocks, following a D- $\pi$ -A geometry (Figure 3.2). The dipole moment due to the D-A (push-pull) configuration is able to result, after excitation through light absorption, in an intramolecular charge separation responsible for the intramolecular charge transfer (ICT), necessary for electron injection.<sup>35</sup> In the last decades a vast number of organic structures have been synthesized by modifying all the components, with a great attention on the donor and the  $\pi$ -bridge. Coumarin,<sup>36,37</sup> indoline,<sup>38</sup> carbazole,<sup>39,40</sup> triphenylamine,<sup>41,42</sup> furan,<sup>43</sup> and thiophene, are just a few of the many of building blocks explored, whose various assembly resulted in hundreds of different compounds.

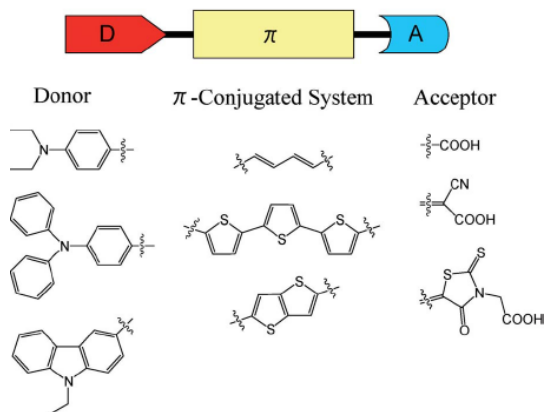


Figure 3.2. Schematic design of organic sensitizers (top), examples of building blocks (down).

### 3.3. Aim of the Thesis

The goals of this thesis were the design, synthesis and investigation of new organic dyes, with extended absorption properties, as photosensitizers for dye-sensitized solar cells. An important part of the work was focused on the synthetic paths to find new structures that could overcome the problems related to this class of materials.

A new design, rising from the evolution of the extension of the classical D- $\pi$ -A structure seen in the previous chapter, will be presented in Paper I. With the aim of further extending the optical properties we introduced another modification in Paper II, where we discovered surprising and interesting relationships between previous and new design. After the publication of Paper II, a new work was started in order to fully exploit the possibilities offered by the asymmetric structure introduced in Paper II. However, due to difficulties encountered in the synthetic route, the designed target could not be achieved within the available time. Paper III will deal with the use of water as solvent for DSSC and will present an organic hydrophilic dye that shows a remarkable stability in terms of desorption. In addition, the dye is able to give good performances with respect to the state-of-the-art for water systems.

## 4. The Challenge of Absorption Extension

From Chapter 3, Paragraph 3.1, resulted quite evident that the best performances have always been recorded employing organometallic compounds. Although significant results have been achieved employing fully organic sensitizers, a remarkable limit resides in the absorption spectrum of these compounds that typically show a single and narrow absorption band in the visible region (around 550 nm). These boundaries are imposed both by the type of building blocks used and, in general, more strongly by the design, constituted by a single D-A charge transfer. In order to achieve a significant breakthrough, it is fundamental to extend the absorption at longer wavelength, up to the NIR region. Infact, the presence of absorption bands in the near-infrared portion of the spectrum of metal complexes, is the main reason for their higher performances. Generally, Ru polypyridyl complexes show prominent absorption peaks at the UV region and the visible-NIR region, respectively. The absorption band appearing in the visible-NIR region is assigned as singlet to singlet metal-to-ligand charge transfer ( $^1\text{MLCT}$ ) from the metal core to the polypyridyl ligand.<sup>44</sup> The expansion of  $\pi$ -conjugation of polypyridyl ligand will lead to a decrease of the LUMO energy level and result in a bathochromic shift of the absorption band. Furthermore, small HOMO-LUMO gaps are known to be resulting not only from the metal-to-ligand or ligand-to-metal charge transfer (MLCT or LMCT), but also from the characteristic Q-bands, as in the case of porphyrins.<sup>45,46</sup> However, maintaining a large  $V_{oc}$ , while keeping the LUMO and HOMO levels at proper potentials, leaving enough driving force to have kinetically fast injection and regeneration, is a significant challenge for the realization of efficient NIR organic dyes.

## 5. Design Modification: from Mono- to Tri-branched Dyes

### 5.1. Introduction

Although promising, modified structures have rarely been considered in the field of organic sensitizers. In the case of Ruthenium-based sensitizers, the presence of more than one anchoring group has already been proved to have a positive effect on the stability and electron injection.<sup>47</sup> Taking inspiration from this fact, Abbotto *et al.* have applied the same concept to organic chromophores, developing new dibranched structures (Figure 5) characterized by the presence of two acceptor fragments,<sup>48</sup> each ending with a carboxylic, condensed to a donor group. The new design conferred enhanced stability, performances and optical properties to the dyes, increasing the photocurrent and broadening the absorption spectrum.

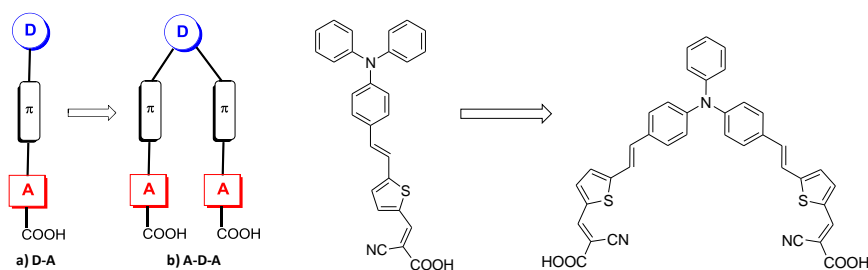
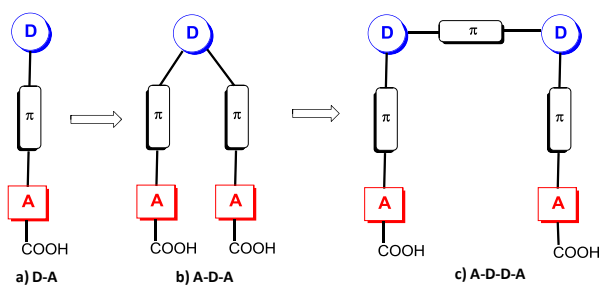


Figure 5. Schematic representation of mono-to-dibranched design (left), D5 monobranched dye (middle), DB1 dibranched dye (right).

In general, the multi-branch approach involves a number of advantages compared to the simple design D- $\pi$ -A, including a strengthening of the bond between dye molecules and semiconductor oxide particles, the extension of the  $\pi$  system for a more efficient absorption of sunlight, and a wider variety of structural possibility aimed to obtain a panchromatic response. Studies on donor functionality in organic photosensitizers suggest that dyes bearing donor fragments particularly electron-rich exhibit an increased photocurrent.<sup>49</sup> According to this observation and being aware that a limitation in the performances of the dibranched design could rise from the presence of only one donor moiety, the system was further modified.

## 5.2. Aim of the Study

The purpose of this study is therefore to investigate the optical and photovoltaic properties of a new dyes architecture which stems from a further extension of the dibranched one, deriving from the condensation of two units D- $\pi$ -A, to form one of the type A- $\pi$ -D- $\pi$ -D- $\pi$ -A (Figure 5.1).



*Figure 5.1* Schematic representation of the evolution from mono (a) to tribranched design (c).

Indeed, a significant broadening of the absorption spectrum moving from the monobranched to the dibranched design, was already observed.<sup>48,50,51</sup> Therefore, this study aimed to investigate the modulation of the absorption spectrum resulting from the addition of another donor unit. In addition, since the new geometry can also be regarded as two monobranched dyes connected through the donor moieties, it was also interesting to investigate its properties with respect to the analogous monobranched.

## 5.3. Design and Synthesis

### Design

To design the tribranched prototypes it was decided to employ simple building blocks widely used for organic sensitizers, with the aim of simplifying the synthetic path.

Triphenylamine derivatives have attained a great attention and have been extensively used as donor units.<sup>52-56</sup> We selected 4-methoxy-triphenylamine, instead of the more simple triphenylamine, because the methoxy group increases the donating character. Many different conjugated linkers are known, from simple vinylene to condensed aromatic units. The currently most common linkers are thiophene and their derivatives,<sup>57-59</sup> inspired by a work from Hara, who showed a good effect of their electron donating properties, resulting in bathochromic shift in the absorption spectra.<sup>60</sup> Therefore, we selected thiophene as a  $\pi$ -spacer to connect the single D-A moieties in the side-arms. 2-cyanoacrylic acid was used as acceptor, since it provides the best performances. Finally, in order to investigate the influence of the introduced  $\pi$ -bridge connecting the donor units, ethenyl and phenyldiethenyl building blocks were used.

Based on these premises, we decided to explore the new geometry by synthesizing two tribranched prototypes, called TB-1 and TB-2, starting from L1, a simple chromophore previously known in literature (Figure 5.2).<sup>61</sup>

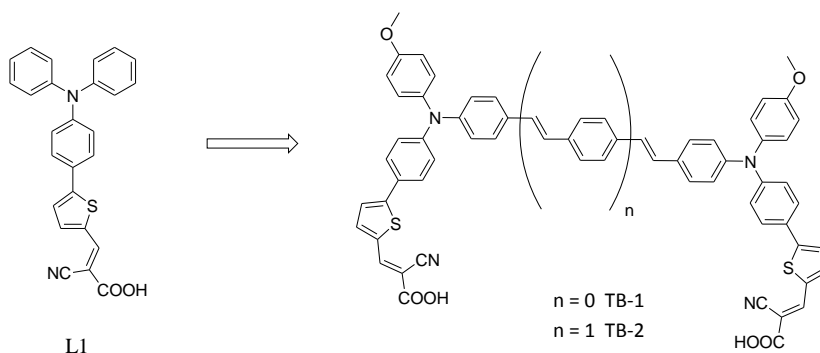
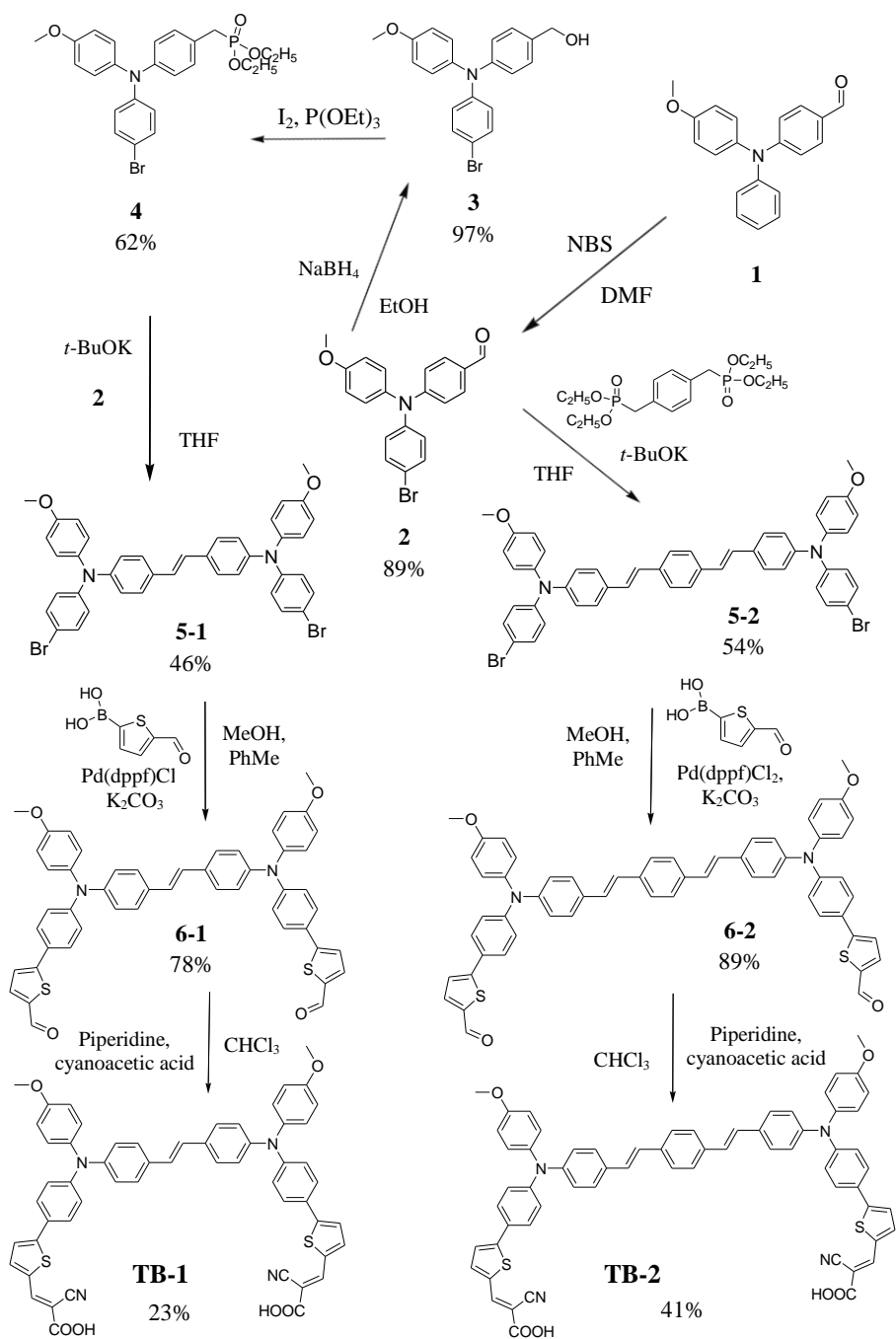


Figure 5.2 Chemical structures of monobranched L1 dye (left) and target tribranched molecules TB-1 and TB-2 (right).

## Synthesis

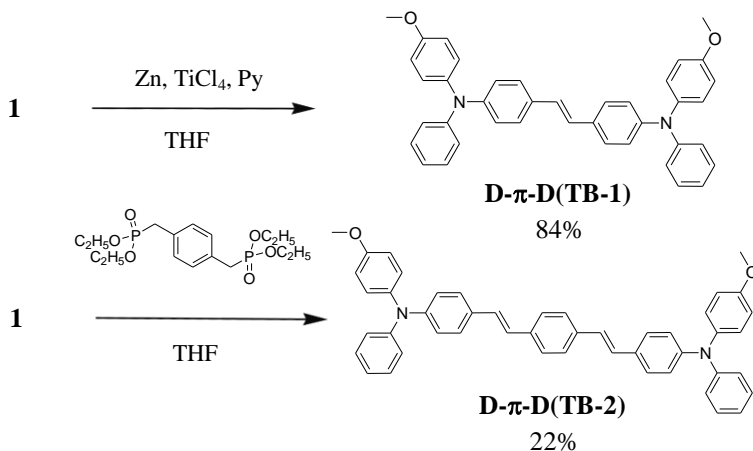
The first synthetic route that led to TB-1 and TB-2 dyes is based on a divergent approach starting from the triphenylamino donor moiety (Scheme 1). Therefore, commercially available 4-methoxytriphenylamine was formylated according to Vilsmeier-Haack procedure to afford intermediate **1**, previously known in literature. The brominated analogue **2**, key intermediate in this synthetic path, was obtained pure after bromination of **1** with recrystallized NBS. In this series, both the dibromo derivatives of the donor bridges D- $\pi$ -D, **5-1** and **5-2**, have been synthesized exploiting Horner-Wadsworth-Emmons condensation reaction between an aldehyde and a phosphonate. Tetraethyl 1,4-phenylenebis(methylene) diphosphonate,<sup>62</sup> was deprotonated using *t*-BuOK and aldehyde **2** was added to the solution, yielding desired intermediate **5-2**. For the synthesis of the analogue TB-1 donor bridge, phosphonate **4** was obtained from the one-pot halide and Michaelis-Arbuzov reaction of the reduced form of aldehyde **2**, alcohol **3**. Horner-Emmons reaction of phosphonate compound **4**, together with aldehyde **2**, was realized following the same procedure previously used, affording dibromo building block **5-1**. Suzuki-Miyaura cross-coupling reaction is a powerful technique to provide C-C bonds.<sup>63-65</sup> The discovery of this palladium-catalyzed reaction rewarded Akira Suzuki, its inventor, with a Nobel prize in 2010. The synthetic strategy we employed, involves a double Suzuki reaction on starting materials **5-1** and **5-2** with commercially available 5-formyl-2-thienylboronic acid, employing the widely used 1,1'-Bis(diphenylphosphino)ferrocene palladium(II) dichloride (Pd(dppf)Cl<sub>2</sub>) as catalyst. Both reactions were performed in a microwave reactor, affording bis-aldehydes **6-1** and **6-2**, that finally reacted with cyanoacetic acid *via* Knoevenagel condensation to give the desired final compounds **TB-1** and **TB-2**, respectively.



Scheme 1. Synthetic procedure of sensitizers TB-1 and TB-2.



With the purpose of investigating the nature of the optical contributions in the absorption spectrum (see Chapter 5.4) we further synthesized the donor D- $\pi$ -D cores of both TB-dyes (Scheme 2). In this occasion, we decided to explore a new and shorter route for the preparation of D- $\pi$ -D (TB-1), without the necessity to prepare the alcohol and phosphonate analogous of aldehyde **1**. Mc Murry reaction was therefore employed to synthesize the target molecule and provided **D- $\pi$ -D(TB-1)** in high yield. On the other hand, Horner-Emmons condensation performed on compound **1** and Tetraethyl 1,4-phenylenebis(methylene) diphosphonate, resulted in even lower yield than the one performed on reactant **2**.



*Scheme 2.* Synthetic procedure of D- $\pi$ -D(TB-1) and D- $\pi$ -D(TB-2).

## 5.4. Properties of the Sensitizers

### Optical Properties

Due to the extended conjugation, dyes TB-1 and TB-2 exhibit a remarkable broadening of the absorption spectra, that show two different transitions in the visible region (Figure 5.3).

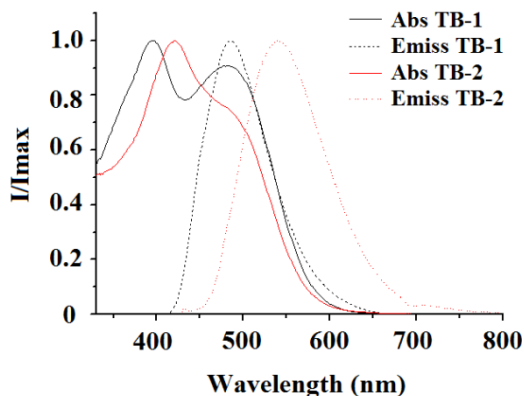


Figure 5.3. Normalized absorption and emission spectra of TB-dyes in DMSO.

After further investigations we were able to assign the two different absorption bands. Infact, the absorption spectra of the donor cores D- $\pi$ -D of both dyes in the same solvent, are perfectly matching the transitions at lower wavelengths (Figure 5.4).

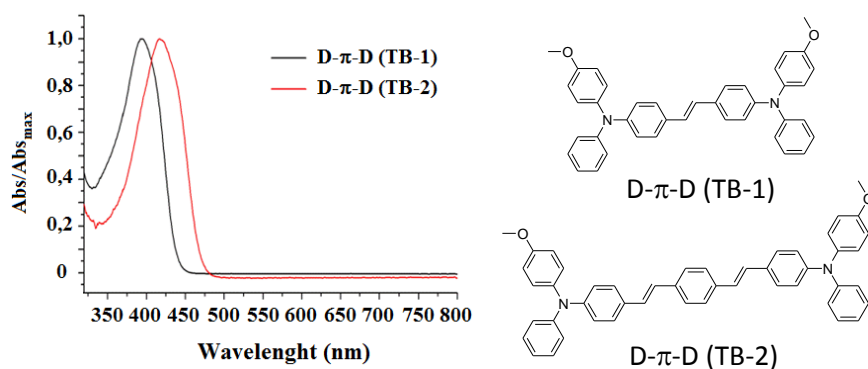


Figure 5.4 Normalized absorption spectra in DMSO (left), molecular structures of the donor cores (right).

This result, together with other measurements performed on TB-1 and TB-2 with chenodeoxycholic acid, commonly employed as disaggregating agent, in the UV-Vis solutions, allowed us to exclude the possibility that the bands at higher energies could be artefacts deriving from dye aggregation. Therefore, the 397 nm and 420 nm absorption bands were ascribable to the local transitions of the donor core, while the bands at higher wavelength were attributed to the  $\pi$ - $\pi^*$  transitions that correspond to the intramolecular charge transfer (ICT).

As expected, by increasing the conjugation exploiting the new design, the broadening of the absorption spectrum was combined with a significant improvement of the values of molar extinction coefficient. If compared to the monobranched dyes bearing the same buildings blocks, it is possible to notice that the molar extinction coefficients of TB-1 and TB-2 are almost doubled. Figure 5.5 contains the table that summarizes these properties.

Compound	$\lambda_{\text{abs}}/\text{nm}$ ( $\epsilon/\text{M}^{-1}\text{cm}^{-1}$ )	$\lambda_{\text{em}}/\text{nm}$ ( $\Phi$ ) <sup>[a]</sup>
<b>TB-1</b> <sup>[b]</sup>	397 (40900) 478 (35800)	485 (0.058) <sup>[b],[c]</sup>
<b>TB-2</b> <sup>[b]</sup>	421 (54000) 480 (40200)	540 (0.013) <sup>[d]</sup>
<b>L1</b> <sup>[e]</sup>	410 (25800)	549
<b>C213</b> <sup>[f]</sup>	514 (27500)	715

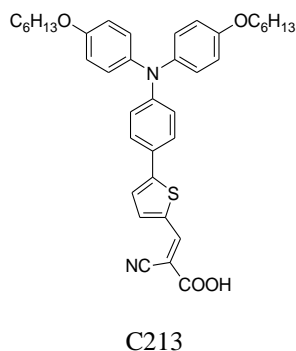


Figure 5.5. Table containing optical parameters (left) [a] Fluorescence quantum yield; standard: Coumarin 540A (0.58 in EtOH); [b] Spectra recorded in DMSO; [c]  $\lambda_{\text{exc}} = 397$  nm; [d]  $\lambda_{\text{exc}} = 421$  nm; [e] (*t*-butanol:CH<sub>3</sub>CN, 1:1);<sup>57</sup> [f] (THF).<sup>62</sup> C213 molecular structure (right).

Direct comparison between the values related to the maximum absorption wavelength is not possible due to the different solvents in which the measurements were performed. Solvatochromism plays a significant role in the detection of the maximum absorption wavelength and this effect results very clearly by making a comparison between L1 and C213 dyes that differ only in the length of the alkyl chains, not responsible for 100 nm bathochromic shift. However, the shape of the absorption spectrum and the molar extinction coefficient of the dyes are very poorly or not influenced by the solvent. Therefore, we can state that the goals of broadening the absorption spectrum and increase the molar extinction coefficient succeeded.

## Electrochemical Properties

The electrochemical properties of TB-dyes are summarized in Table 1.

Compound	$E_{(Ox)}$ [V] vs. NHE <sup>b</sup>	$E_{(Red)}$ [V] vs. NHE <sup>b</sup>	$E_{(0-0)}$ eV <sup>c</sup>
<b>TB-1<sup>a</sup></b>	+0.91	-0.87	1.8
<b>TB-2<sup>a</sup></b>	+0.98	-0.97	2.0

*Table 1.* Electrochemical parameters of TB-1 and TB-2. <sup>a</sup>Measurements performed in DMF solution: glassy carbon as we and Pt as ce, using 0.05 M TBA(PF<sub>6</sub>) as a supporting electrolyte, <sup>b</sup>Potentials measured vs. Fc+/Fc, converted into Normal Hydrogen Electrode (NHE) potentials by addition of +0.63 V, <sup>c</sup>Energy bandgap calculated from the reported values of  $E_{ox}$  and  $E_{red}$ .

It is interesting to notice that the reduction potentials (LUMO) reported, as well optical bandgaps, differ considerably from the values commonly known in literature for similar monobranchd dyes.<sup>50,57,66</sup> In particular, comparing the two dyes, it is possible to state that the more electron-rich character of the p-bridge in TB-2, causes a larger bandgap by moving the LUMO to more negative potentials and the HOMO toward more positive values.

## Computational Properties

Computational investigation performed on TB-1 detected two possible conformers: a more stable one with *transoid* arrangement of the two branches, and a less stable one corresponding to a *cisoid* arrangement of the two branches (Figure 5.6). The energy interconversion barrier between the two structures was computed to be around 5.3 kcal/mol. The *transoid* conformer is probably more stable due to the minimized interaction of the phenyl rings in the  $\pi$ -bridge. As can be noticed from Figure 5.6, the more stable conformer exhibits a non-optimal interaction with the TiO<sub>2</sub> surface, which might reduce the dye molecular packing, and, in turn, impact the photovoltaic performances.

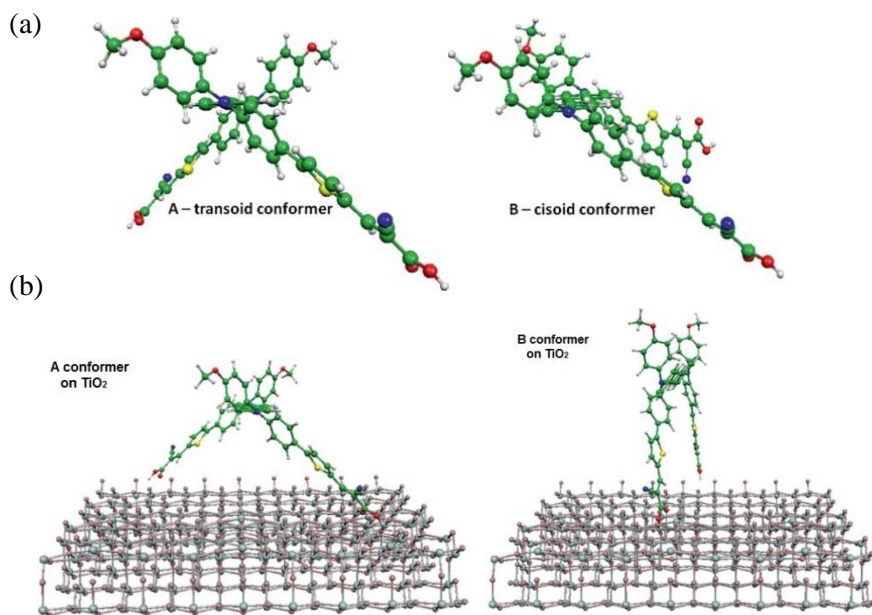


*Figure 5.6.* Optimized molecular structures of the TB-1 conformers (a); Possible interaction of TB-1 conformers with the TiO<sub>2</sub> substrate (b).

## 5.5. Photovoltaic Performance

The properties of the synthesized dyes were tested in DSSCs using  $I^-/I_3^-$  as redox couple. Figure 5.7 shows the IPCE spectrum of the different cells. Different data related to L1 are known in literature,<sup>57,67</sup> which makes hard to make a correct comparison. In Figure 5.7, it is possible to observe that TB-1 exhibits a high value at plateau (81%) and more than 70% from 400 to 560 nm. Although showing a photoelectrical response in the same region, dye TB-2 performs a slightly lower conversion of incident light into electrical work (75%). It may be interesting to speculate that the lower performances of dye TB-2 could be explained by analyzing its absorption spectrum. Although the maximum absorption wavelengths of both optical transitions result barely red-shifted in TB-2, it seems that the presence of an extended conjugation between the two donor units promotes the D- $\pi$ -D transition, rather than the ICT. This effect can be seen in the different intensities of the two transitions into play. Since the donor-donor transition does not contribute to electron-injection, it can actually be seen as a competitive phenomenon.

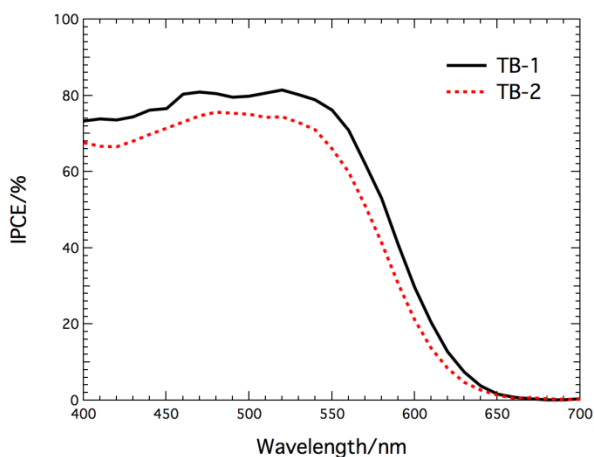


Figure 5.7. Incident-photon-to-current (IPCE) of TB-1 and TB-2 DSSCs.

The trend observed in the IPCE spectra reflects the photocurrent densities (Figure 5.8). All the main photovoltaic parameters are reported in Table 2.

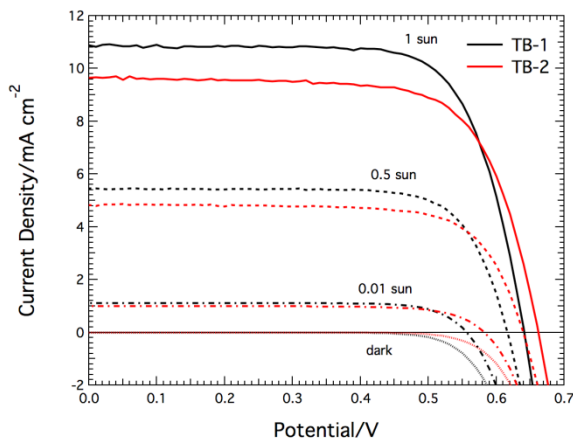


Figure 5.8. Light and dark current-voltage characteristics of DSCs based on TB-1 and TB-2.

Dye	$I_0/\text{sun}$	$J_{sc}/\text{mAcm}^{-1}$	$V_{oc}/\text{V}$	FF/%	$\eta/\%$
TB-1	1	10.9	641	72.5	5.05
	0.5	5.45	616	74.5	5.01
	0.1	1.10	558	76.6	4.75
TB-2	1	9.65	662	70.6	4.51
	0.5	4.84	640	72.6	4.50
	0.1	0.99	584	73.6	4.30
LI <sup>57,67</sup>	1	542	735	69	2.75
	1	12.8	620	66	5.20
C213 <sup>68</sup>	1	11.9	775	74.7	6.88

Table 2. Photovoltaic parameters of DSCs based on TB-1 and TB-2.

Measurements performed under AM 1.5 G irradiation. Electrolyte composition: 0.6 M N-methyl-N-butyl imidazolium iodide, 0.04 M iodine, 0.05 M LiI, 0.05 M GuSCN, and 0.28 M *tert*-butylpyridine in ACN/VN=85/15.

As previously said, it is not easy to make a comparison between our experimental data and the one in literature. However, Table 2. shows that the C213 best performance can be mainly ascribed to a 20% higher  $V_{oc}$  than TB-1. The long alkoxy chains in C213 could also be the main reason for its higher performances. Indeed, Hagberg et al. have recently shown a correlation between open-circuit voltage values and bulky butoxy chains.<sup>66</sup> Long alkoxy chains are in fact able to suppress dye aggregation, reducing recombination (increasing  $V_{oc}$ ) and current-loss ( $J_{sc}$ ) due to  $\pi$ - $\pi$  stacking.

## 5.6. Conclusion

Increasing the degree of conjugation in the sensitizers by introducing a new tribranched geometry resulted in a two-fold enhancement of the molar extinction coefficient. The absorption spectrum results widely broadened with respect to the commonly known monobranched counterpart. Stability test show good results due to the presence of two anchoring group in the molecular structure. Moreover, the tribranched molecular architecture provides more variety in the sensitizer chemical structure, allowing further structural optimization that can be tailored to achieve the desired properties. However, this work did not clearly detect the causes for lower photovoltaic performances with respect to the values found in literature for C213. Further investigation is therefore necessary.



## 6. Asymmetric Tribranched Dyes: Full Exploitation of Design Variability

### 6.1. Introduction

The previous chapter introduced a new design that possesses several optical advantages with the potentiality to result in improvement of photovoltaic performances. Moving from mono- and dibranched structures such as L1 and DB-1, to tribranched prototypes like TB-1, a remarkable broadening of the spectrum, due to the appearance of an additional transition, was found. In addition, the potentiality offered by the multi-branched architecture has not been fully exploited, yet. The tribranched design can be seen from two different point of view: as extension of the dibranched design, bearing an additional donor moiety, or as two monobranched dyes, connected through the donor units through a  $\pi$ -bridge (Figure 6.).

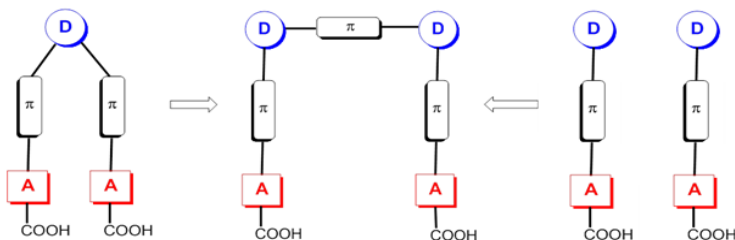


Figure 6. Different perspective approaches to the tribranched design.

### 6.2. Aim of the Study

By virtue of the monobranched-connected approach and encouraged from the modulation of the optical properties derived from the new structure, the design is here pushed to its limits. Therefore, the aim of this study is to explore the optical modulation and the photovoltaic performance of dyes with a new structure realized by introducing two different  $\pi$ -spacers in the side arms of the branches of the previous design. The result is an asymmetric tribranched dye with a A- $\pi_1$ -D- $\pi_2$ -A backbone (Figure 6.1). Interestingly, following the previous analysis, the architecture can also be considered as deriving from an intramolecular co-

sensitization approach, where two different dyes ( $D-\pi_1-D$  and  $D-\pi_2-D$ ), possessing diverse absorption features, are linked together through a conjugated bridge.

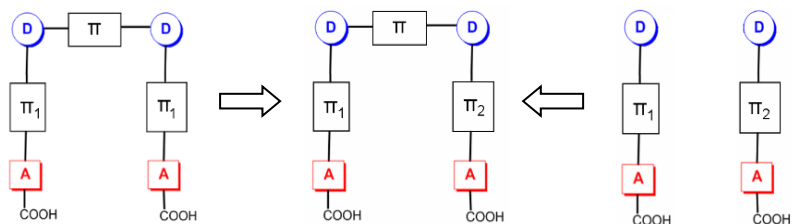


Figure 6.1. Symmetric tribranched (left), new design of asymmetric tribranched (middle), two different monobranched dyes (right).

## 6.3. Design and Synthesis

### Design

To design a prototype of the asymmetric tribranched geometry, similar general guidelines, as previously used for the symmetric analogous (Chapter 5, Paragraph 5.3), were followed. Aware of the synthetic complexity that generally characterizes asymmetric structures, the goal was to identify a simple prototype that could provide sufficient fundamentals to develop this study. Since thiophene, previously discussed, and phenyl rings, are the most common and simple building blocks,<sup>69-71</sup> they have been selected for this purpose. To verify that the two monobranched dyes carrying those spacers as building blocks have a difference in the absorption spectrum, a quick literature research was made. From this research, two chromophores with the desired characteristics were found: the already mentioned L1, and TC105 (Figure 6.2).<sup>61,72</sup> The difference reported in the maximum absorption wavelength is around 50 nm only, but still sufficient for the investigation of the optical modulation. Triphenylamine was still employed as a donor unit. For this series of dyes, however, it was decided to employ a longer alkoxy chain (hexyloxy), in order to provide higher solubility and study possible performance changes with respect to TB-1. Following the view of making a comparison with the dyes from the previous series and considering the better performances achieved by TB-1 with respect to TB-2, vinylene group was employed to connect the donor units and 2-cyanoacrylic acid was used as acceptor. Based on these premises, the properties deriving from the new geometry

were explored by the synthesis of an asymmetric tribranched prototype (TB-PT), and its two symmetric analogues (TB-T, TB-P) (Figure 6.2).

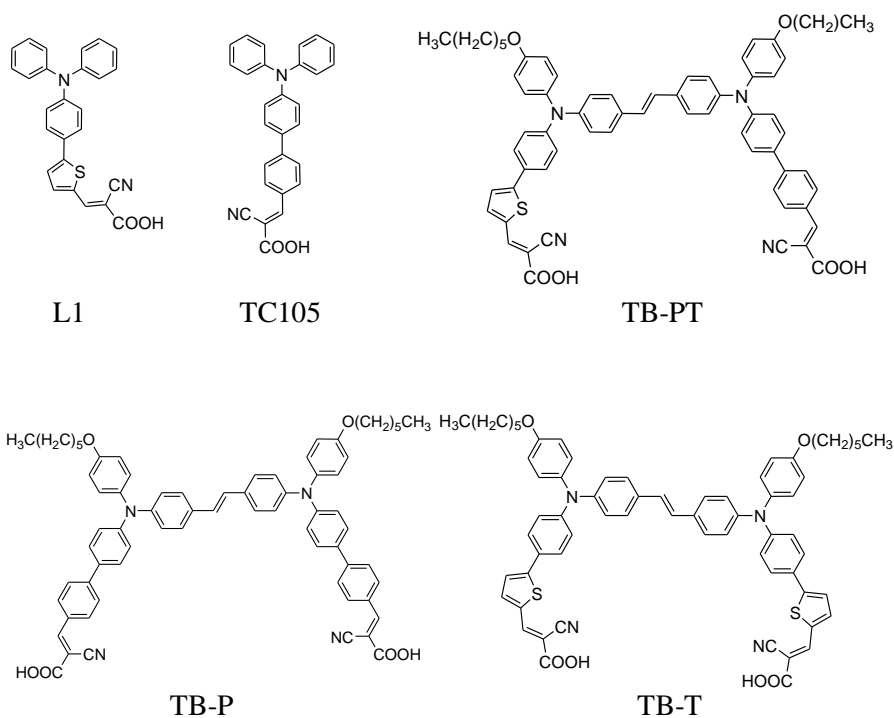
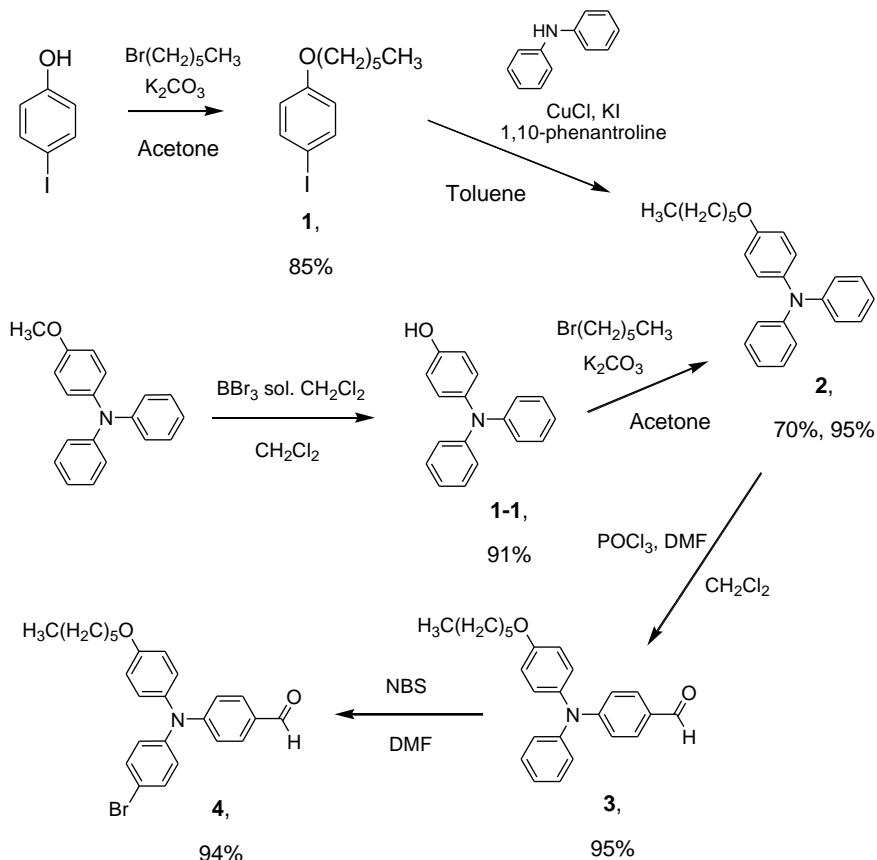


Figure 6.2. Molecular structures of: monobranched models L1 and TC105 (up, left); target asymmetric tribranched TB-PT (up, right); symmetric analogues TB-P and TB-T (down).

## Synthesis

The first target compound in the synthesis process is 4-hexyloxy-triphenylamine **2**, whose synthetic pathways are included in Scheme 3. The first synthetic approach, not reported, consisted in the Buckwald-Hartwig reaction between the bromo-analogue of the alkylated derivative **1**, and commercial N,N-diphenylamine. However, even after several attempts carried out in different conditions, the desired product was not obtained. Therefore, the strategy changed to the one here reported. Commercially available 4-iodophenol was alkylated according to a procedure known in literature,<sup>73</sup> with some modifications,<sup>74</sup> affording hexyloxy derivative **1**. The synthesis of triphenylamine donor **2**, is

performed by N-arylation of N,N-diphenylamine exploiting the versatile Ullmann coupling reaction with copper(I)chloride as catalyst.<sup>75-77</sup>



*Scheme 3.* Synthetic procedure of important intermediates **2** and **4**.

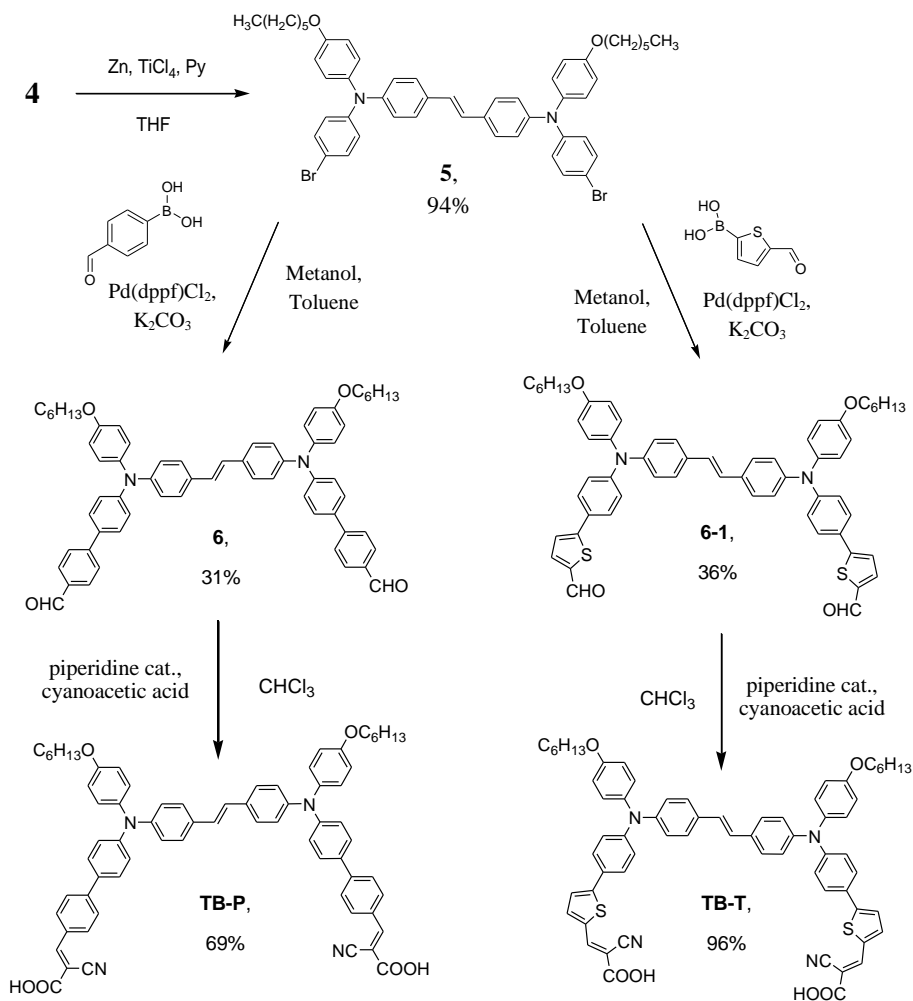
Although Ullmann reaction provided the desired compound in good yield (70%), the purification step results time consuming and requires, in order to perform the reaction on a big scale, the employment of big separation columns and a remarkable amount of solvents and materials. Therefore, with the aim of achieving the same intermediate in an easier way, another path was explored. Starting from commercially available 4-methoxytriphenylamine, the correspondent phenol **1-1** was obtained in remarkable yields from demethylation reaction by Boron tribromide. The following Williamson alkylation reaction, afforded intermediate **2** in high yield (95%). This synthetic path results much easier to handle and scalable with respect to the first one because the purification step of compounds **1-1** and **2**,

consist of a mere silica-gel filtration. Vilsmeier formylation reaction of starting material **2** gave excellent results when dichloromethane (CH<sub>2</sub>Cl<sub>2</sub>) was employed as solvent, affording aldehyde **3** in high yield. Bromination reaction with NBS resulted in the key intermediate **4** in quantitative yields.

From key intermediate **4**, different synthetic routes branch off for the realization of symmetric and asymmetric compounds. The identification of a synthetic path for symmetric compounds **TB-P** and **TB-T** traces the knowledge acquired for the achievement of **TB-1** and **TB-2**, shown in the previous chapter.

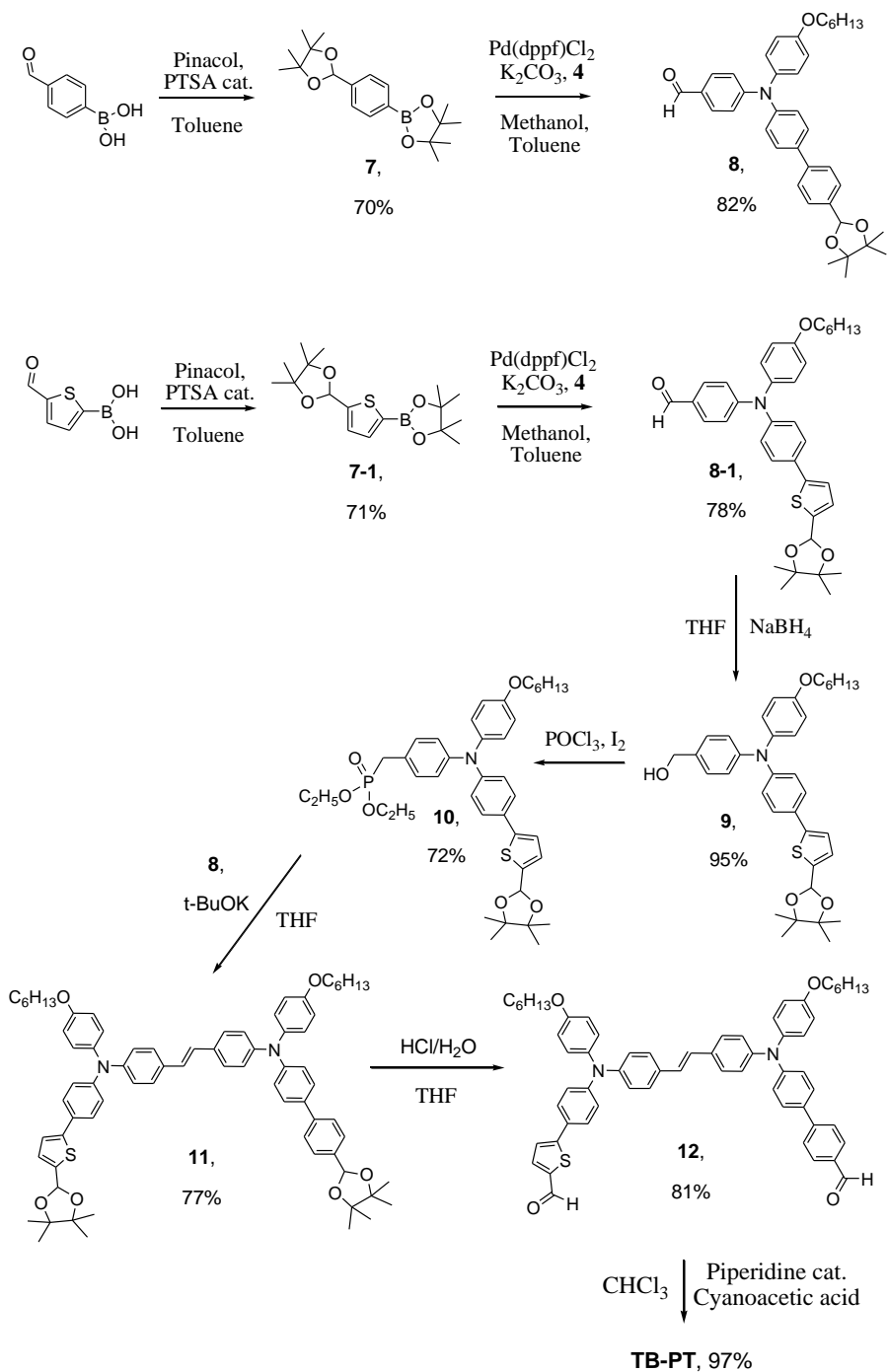
Divergent synthetic route (Scheme 4), as previously employed, started with Mc Murry reaction on the bromo-aldehyde **4**, affording dibromo derivative of the donor core **5**, in quantitative yield. Pd-catalyzed Suzuki-Miyaura reaction was carried out in the same conditions that led to the analogous compounds presented in Scheme 1, and bis-aldehyde derivatives **6** and **6-1** were obtained. Further Knoevenagel condensation with cyanoacetic acid resulted in the final desired compounds **TB-P** and **TB-T** in high yield.

The synthesis of asymmetric compound **TB-PT**, however, required a different approach. After several attempts, a convergent synthetic strategy based on the exploitation of protective group as key points, led to the target molecule. Scheme 5 presents this approach, based on the synthesis of the two separate side-arms of the structure **8** and **10**, condensed according to the classical Horner-Emmons reaction in one of the last steps.



*Scheme 4.* Divergent approach for the synthesis of **TB-P** and **TB-T** dyes.

The construction of the side-arms started from the pinacolic protection of commercially available 4-formylphenylboronic acid and 5-formyl-2-thienylboronic acid, using PTSA in catalytic amount, yielding acetals-boronic esters **7** and **7-1**, respectively. Both substrates underwent Suzuki cross-coupling reaction with the key intermediate **4**, in the same conditions, leading to aldehyde derivatives of side arms, **8** and **8-1**, respectively. In order to be able to perform Horner-Emmons condensation one aldehydic side-arm must be converted into its phosphonate analogous.



Scheme 5. Convergent approach for the synthesis of asymmetric TB-PT dye.

Therefore, aldehydic group of compound **8-1** was reduced with  $\text{NaBH}_4$  to give the correspondent benzyl alcohol derivative **9**. Subsequent one-pot nucleophilic substitution performed by  $\text{I}_2$ , followed by Arbuzov reaction with triethylphosphite, afforded the phosphonate derivative **10** in good yield. Horner-Emmons condensation between the properly functionalized side-arms **8** and **10**, resulted in the bis-protected derivative **11**. The aldehydic groups were deprotected in mild acidic conditions, leading to bis-aldehyde derivative **11** that, after double Knoevenagel condensation with 2-cyanoacetic acid, afforded the desired compound **TB-PT** in quantitative yield.

## 6.4. Properties of the Sensitizers

### Optical Properties

The synthesized dyes were characterized by UV-Vis absorption spectroscopy, revealing interesting insights on the optical modulation of the asymmetric compound TB-PT (Figure 6.3). TB-dyes exhibit two UV/Vis absorption bands, typical of the tribranched design,<sup>78</sup> as previously presented in Chapter 5, paragraph 5.4. The optical transitions at lower energies (430–490 nm) are related to intramolecular D– $\pi$ –A charge transfer of the side arms, while the bands at higher energies (385–395 nm) are due to a local transition of the donor core, D– $\pi$ –D. Table 3 summarizes the main optical parameters.

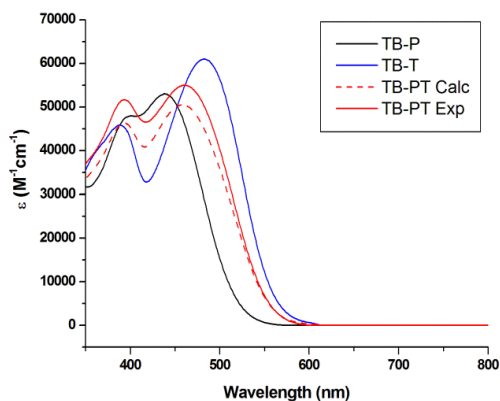


*Figure 6.3.* Absorption spectra of symmetric (i.e., TB-T, TB-P) and asymmetric (i.e., TB-PT) tribranched dyes in THF (solid line); calculated spectrum of TB-PT according to Equation (7) (dashed line).



In agreement with the geometry modification it is possible to notice that both the position of the donor core transition, and the maximum absorption wavelength correspondent to the ICT of TB-PT, are situated exactly at the average values with respect to TB-P and TB-T. Comparison of the molar extinction coefficients follows a similar trend. However, in this case, the absorption coefficient of TB-PT is closer to the lower value of TB-P, rather than standing exactly at the average. Nevertheless, TB-PT possesses the higher oscillator strength, indicating an enhancement effect of the different contributions.

Dye	$\lambda_{\max}$ <sup>[a]</sup>	$\epsilon/ \text{M}^{-1}\text{cm}^{-1}$ <sup>[a]</sup>	$f$ <sup>[a],[b]</sup>
<b>TB-T</b>	388	46000	1.96
	482	61000	
<b>TB-P</b>	401	48000	1.58
	439	53000	
<b>TB-PT</b>	394	52000	1.98
	460	55000	

*Table 3.* Main optical parameters of TB-P, TB-T, and TB-PT. [a] In THF; [b] Oscillator strength measured in the 350–800 nm range.

More interestingly, we discovered that the experimental spectrum of TB-PT could be nicely predicted (dashed line in Figure 6.3) by simply applying a 1:1 linear combination of the spectra of the symmetric dyes, as shown in Equation (7), where  $\epsilon$  is the molar absorptivity at each wavelength:

$$\epsilon_{\text{TB-PT}}(\lambda) = 0.50 \epsilon_{\text{TB-P}}(\lambda) + 0.50 \epsilon_{\text{TB-T}}(\lambda) \quad (7)$$

This aspect is very important in the view of a control of optical modulation because it states that, in principle, it is possible to predict the absorption spectrum of an asymmetric tribranched from its symmetric analogues, much easier to synthesize.

## Electrochemical Properties

The electrochemical properties of this series of TB-dyes were measured by cyclic voltammetry (CV) and are shown in Figure 6.4. All the oxidative waves observed exhibit a reversible behavior and, similarly to the absorption spectra, two oxidation peaks are present. We did not further investigate the peaks at higher potentials but it is reasonable to believe that, following the trend of the optical properties, they can be related to the oxidation of the donor core. HOMO and LUMO energies were converted into NHE values from cyclic voltammetry, using

0.69 V as conversion factor for  $\text{Fc}/\text{Fc}^+$  vs NHE. Curiously, they reveal that HOMO level of TB-PT has slightly more TB-P character, while the LUMO level is much more influenced by TB-T.

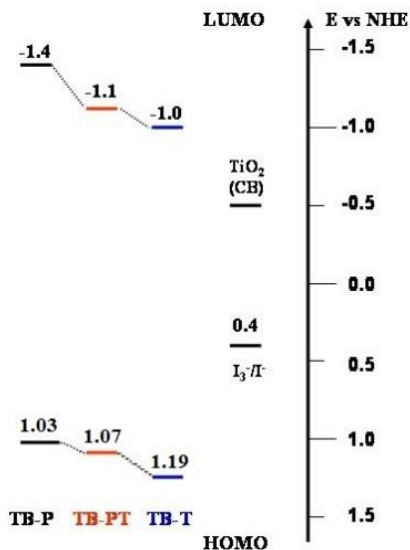
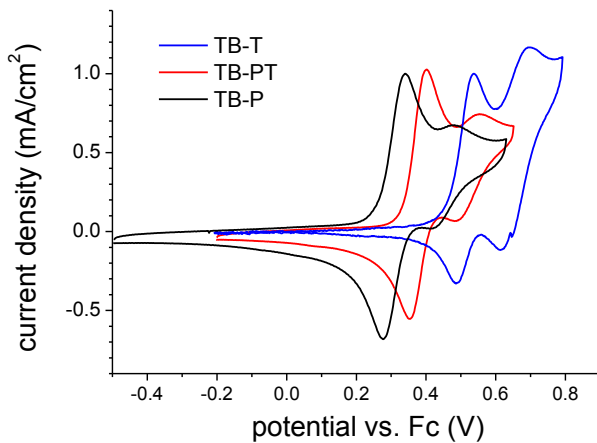


Figure 6.4. Cyclic voltammety of TB-P, TB-T and TB-PT, vs  $\text{Fc}/\text{Fc}^+$  (top); HOMO and LUMO energies vs. NHE (bottom).

## 6.5. Photovoltaic Performance

The performance of the synthesized dyes was tested in DSSCs employing  $I/I_3^-$  as redox couple. A preliminary study was performed on TB-PT, in order to find the best conditions for further investigation. Figure 6.5 shows the I/V curves of TB-PT dye employing two different standard electrolytes and diverse amount of chenodeoxycholic acid (CDCA), generally used as disaggregating agent.<sup>79-81</sup>

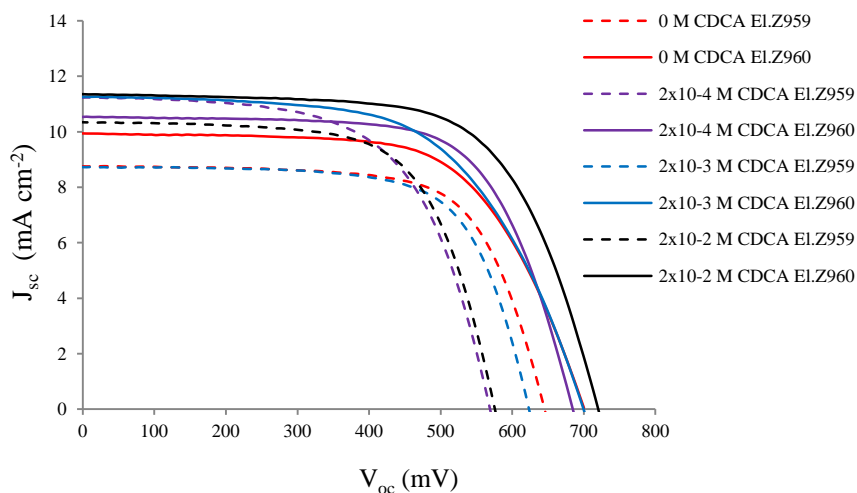


Figure 6.5. J-V curves of DSSCs sensitized with TB-PT dye and diverse amount of CDCA; Electrolytes: Z959 (1.0 M DMII, 0.03 M  $I_2$ , 0.1 M GuSCN, 0.5M TBP in ACN/VN=85/15), Z960 (1.0 M DMII, 0.03 M  $I_2$ , 0.05 M LiI, 0.1 M GuSCN, 0.5 M TBP in ACN/VN=85/15).

Table 4 reports in detail the photovoltaic parameters related to Figure 6.6.

CDCA:Dye	Electrolyte	$J_{sc}/mA\ cm^{-2}$	$V_{oc}/mV$	FF/%	$\eta/\%$
<b>0 : 1</b>	Z959	8.7	645	0.69	3.9
	Z960	9.9	701	0.64	4.5
<b>1 : 1</b>	Z959	11.2	568	0.61	3.9
	Z960	10.5	685	0.68	4.9
<b>10 : 1</b>	Z959	8.7	623	0.69	3.7
	Z960	11.3	699	0.60	4.7
<b>100 : 1</b>	Z959	10.3	575	0.66	3.9
	Z960	11.3	720	0.66	5.4

Table 4. Detailed photovoltaic parameters of the J-V curves in Figure 6.6.

This study shows the benefits deriving from the employment of CDCA and the addition of 0.05 M of LiI to the electrolyte composition. Although it seems to be not linearly dependent, the increase in the amount of CDCA produces better performances in combination with Z960 electrolyte. When Z960, with 0.05 M of LiI in addition, is employed, the photocurrent values show remarkable improvements, remaining constant in the cases 10:1 and 100:1 CDCA-dye. This may suggest that injection results to be more efficient because of the reduced amount of aggregates on the surface. Usually, in these cases, both  $V_{oc}$  and  $J_{sc}$  increase to a certain extent,<sup>79-82</sup> to decrease again when the amount of CDCA employed is too high to cancel its benefits. However, this behavior is not respected in this series, rendering hard the identification of the role that CDCA plays. Finally, the higher voltages observed by adding additional LiI are quite curious, since the addition of Lithium salts in the electrolyte is known to cause a downshift in the CB of  $TiO_2$ , lowering the voltage of the device.<sup>83</sup> However, none of the previously seen positive effects have been recorded in combination with Z959. Even worse power conversion efficiency were actually recorded when Z959 was employed in combination with 10:1/CDCA:dye.

TB-asymmetric dyes from this series were therefore tested employing Z960 as standard electrolyte and compared to the benchmark dye N719 [bis(2,2'-bipyridyl-4,4'-dicarboxylate)ruthenium(II) bis(tetrabutylammonium) salt].<sup>84</sup> Table 5. Reports the main photovoltaic data recorded.

Dye	CDCA:Dye	$J_{sc}/mA\ cm^{-2}$	$V_{oc}/mV$	FF/%	$\eta/\%$
<b>TB-P</b>	100:1	10.0	722	66	4.8
<b>TB-T</b>	100:1	10.9	687	65	4.9
<b>TB-PT</b>	100:1	11.7	708	66	5.4
<b>N719</b>	1:1	14.4	707	69	7.1

*Table 5.* Main photovoltaic parameters of DSSCs based on the TB-dyes from this series with Z960 electrolyte.

Table 5 proves that our new approach based on asymmetric tribranched is able to yield better performances with respect to the symmetric ones. Photocurrent value of TB-PT outperforms those of the symmetric analogous TB-P and TB-T, while the open-circuit voltage remains located at intermediate values.

In order to acquire a better understanding about the photovoltaic behavior, a further investigation was carried on. IPCE and LHE measurements (Figure 6.6) show that the performances could be enhanced from these point of view. Infact, despite the high values of molar extinction coefficient, the light-harvesting and, consequently, the incident photon-to-current efficiency result still limited.

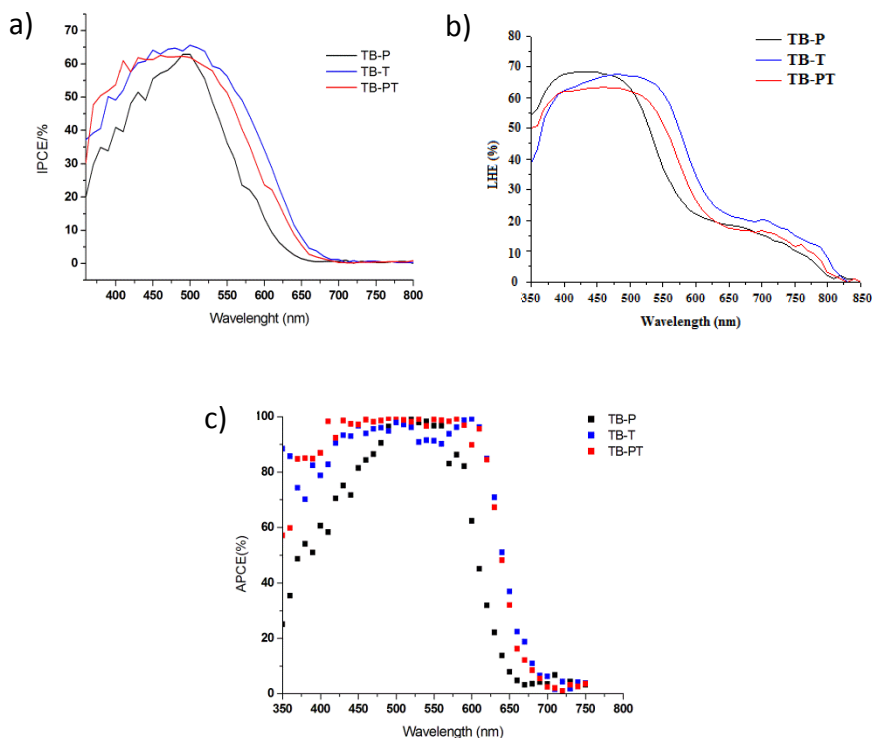


Figure 6.6. IPCE (a), LHE (b) and APCE (c) as a function of wavelength of DSSCs based on TB-P, TB-T and TB-PT.

However, the APCE clearly shows that TB-PT, like TB-T is able to convert all photons absorbed in the range 425-625 nm, into current.

## 6.6. Conclusion

Accurate analysis of absorption spectra demonstrates that the strategy employed for the modulation of the absorption properties, can actually be ascribed as deriving from a combination of two different molecules, possessing diverse optical features. Compared to its symmetric analogous, TB-PT exhibits enhanced photocurrent value that result in a higher power conversion efficiency. Furthermore, it is possible to predict and tune optical and photovoltaic performances analyzing the analogous monobranch and symmetric tribranch. Infact, Equation (7), which shows that the panchromatic behavior of a new sensitizer can be built by appropriately selected starting molecules with

complementary optical and photovoltaic properties, will facilitate the search for new efficient sensitizers. TB-PT dye was designed as prototype to study and understand the modulation of optical, electrochemical and photovoltaic performances deriving from the asymmetric design. In order to reach higher efficiency it is therefore necessary to realize an optimized structure by using the most efficient moieties.

# External Internship

Uppsala Universitet – Ångströmlaboratoriet,  
Sweden

Supervisors:

Prof. Anders Hagfeldt  
Prof. Gerrit Boschloo

# 7. Organic Hydrophilic Dye for Water-based DSSCs

## 7.1. Introduction

The idea of developing a photovoltaic device that could absorb light through molecules absorbed on the surface of a TiO<sub>2</sub> semiconductor layer, was formed gradually in the 1980s. At that time, several studies were investigating the use of chromophores absorbed on TiO<sub>2</sub> electrodes as photocatalyst for methane production and photodecomposition of water by absorption of visible light.<sup>85-87</sup> For this reason, the pioneering studies conducted on dyes absorbed on TiO<sub>2</sub> for photovoltaic application, were naturally performed in aqueous media.<sup>88-90</sup> However, water is known to decrease significantly photovoltaic performances inducing photocurrent losses due to dye detachment,<sup>91</sup> formation of iodate,<sup>92</sup> and reduced electron lifetime.<sup>93</sup> Therefore, water was quickly replaced by organic solvents and additives, able to provide much higher performances, that made DSSCs a promising candidate for future commercialization.<sup>6,32,33</sup> However, these components are often inflammable and toxic for human health and the environment. Therefore, the idea of developing simple, efficient and completely environmental friendly devices is still attractive.

Recently, several studies employing water-based electrolytes have been published.<sup>94-96</sup> In particular, remarkable results have been achieved by O'Regan *et al.*, and Spiccia *et al.*<sup>97-99</sup> In all these studies, the approach consists in employing hydrophobic dyes to avoid their desorption from the surface. However, without employing additional surfactant compounds, this approach would prevent interaction of the electrolyte with the dye, avoiding dye regeneration and blocking the completion of the photovoltaic cycle.

## 7.2. Aim of the study

To provide sufficient surface interaction and pores wettability, different surfactants are generally added to the electrolyte composition. However, it is still critical to enhance pore wettability, and such additives complicate the system, vanishing the efforts to develop a non-toxic, simple and environmental friendly system. Therefore, we proposed an innovative approach that consisted in tailoring the molecular structure of the dye to make it hydrophilic, in order to have great surface interaction without surfactants, but not water-soluble, in order to limit desorption problems. Dye D35 is a robust and efficient dye,<sup>66</sup> whose hydrophobic



character was turned into hydrophilic by substitution of alkyl chains with glycolic ones. The resulting V35 (Figure 7) dye was tested in 100% water electrolytes, yielding remarkable results.

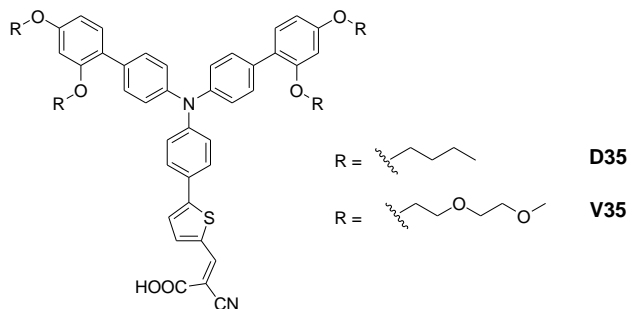


Figure 7. Molecular structures of dyes D35 and V35.

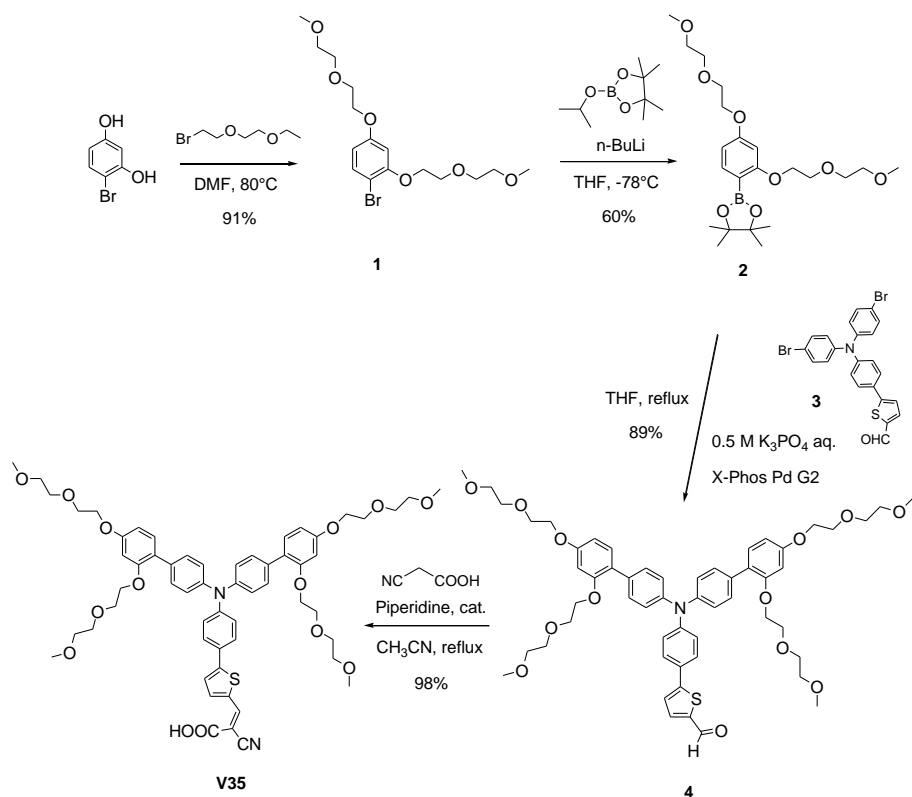
### 7.3. Design and Synthesis

#### Design

Glycolic functionality has well-known hydrophilic properties and dyes with glycolic chains have already been reported in literature with different purposes.<sup>100-102</sup> Particularly interesting is the study published by Kang *et al.*, who investigate dyes with glycolic chains of different lengths, for hydrogen production.<sup>103</sup> Furthermore, surfactants based on high molecular weight PEG (Polyethylene Glycol), have already been employed in water-based DSSCs systems.<sup>99</sup> For these reasons, and for their easy insertion in the dyes structure, glycolic chains were selected to provide good interaction with water. The length of the employed chains was established with the aim of provide great surface interaction, without hindering the core of the dye and provide an easy synthetic route. Therefore, it was decided to use the (methoxyethoxy)ethane length, whose bromo-derivative was commercially available, and that already gave good results.<sup>103</sup> Dye D35 was selected as a reference point because it represents an excellent compromise between efficiency and ease of synthesis. Another more performing dyes, such as LEG4,<sup>104</sup> was initially taken into account for this study but, finally, we opted for a more simple chromophore as prototype to test the new approach.

## Synthesis

The synthetic procedure for the realization of V35, is reported in Scheme 6. Starting from commercially available 4-Bromoresorcinol and 1-bromo-2-(2-methoxyethoxy)ethane, Williamson alkylation reaction afforded the glycolic building block **1** in high yield. Reaction of the bromo-derivative **1** with *n*-BuLi resulted in the formation of the correspondent lithium salt that, reacting with Isopropoxy-dioxaborolane yielded the boronic ester **2**. Intermediate **3** was already known in literature and synthesized according to the reported procedure.<sup>66</sup> Suzuki-Miyaura cross-coupling reaction of boronic pinacol ester **2** and di-bromo intermediate **3**, afforded the desired compound **4** in high yield. Final Knoevenagel condensation step of aldehyde **4** with cyanoacetic acid and a catalytic amount of piperidine, resulted in the desired dye, V35.



Scheme 6. Synthetic route of dye V35.

## 7.4. Properties of the Sensitizer

In order to investigate its properties and possible modifications induced by the presence of glycolic chains, V35 was optically and electrochemically characterized. Furthermore, the interaction of V35 and D35 with water, was tested by measuring the contact angles. Desorption studies in neutral and acidic conditions, up to five months, were made.

### Optical Properties

Dye V35 was optically characterized by UV-Vis absorption spectroscopy, emission spectroscopy, and molar extinction coefficient. Figure 7.1 reports absorption and emission spectra of V35 and D35, showing no significant difference.

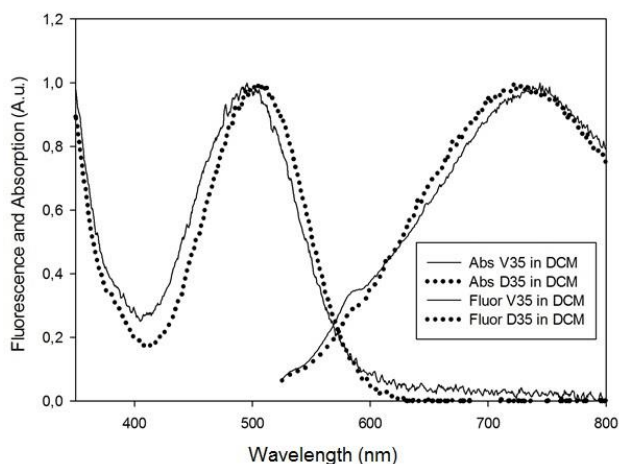


*Figure 7.1* Normalized absorption (left) and emission (right) spectra of V35 (solid lines) and D35 (dotted line).

The maximum absorption wavelength of V35 results only slightly hypsochromically shifted with respect to D35, and the maximum emission wavelength results slightly bathochromically shifted.

## Electrochemical Properties

The oxidation potential of V35 have been measured by cyclic voltammetry (CV) and its oxidation profile is reported in Figure 7.2.

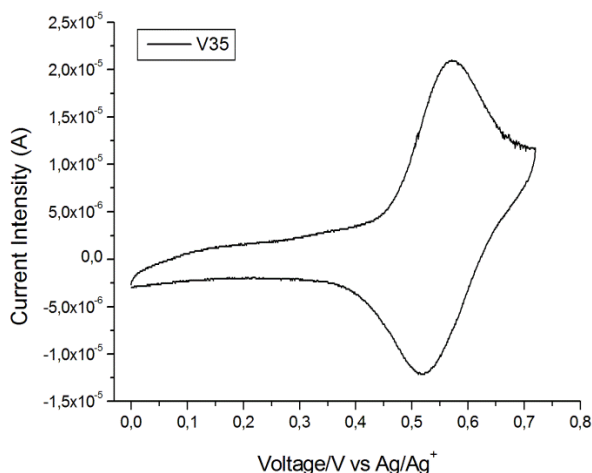


Figure 7.2 Cyclic voltammetry of V35 in CH<sub>3</sub>CN vs Ag/Ag<sup>+</sup>.

Table 6 reports the main optical and electrochemical parameters for V35 and D35.

Dye	$\lambda_{\text{abs}}$ (nm) <sup>a</sup>	$\lambda_{\text{emiss}}$ (nm) <sup>a</sup>	$\epsilon$ (M <sup>-1</sup> cm <sup>-1</sup> ) <sup>a</sup>	$E_{\text{HOMO}}$ (NHE) <sup>b</sup>	$E_{\text{LUMO}}$ (NHE) <sup>d</sup>	$E_{0-0}$ (eV) <sup>c</sup>
V35	495	722	27500	1.07	-1.11	2.18
D35	503	740	31000 <sup>e</sup>	1.04	-1.12	2.16

Table 6 Main optical and electrochemical parameters of V35 and D35. <sup>a</sup>Recorded in CH<sub>2</sub>Cl<sub>2</sub>, <sup>b</sup>Measured by CV (V35 0.2 mM, LiClO<sub>4</sub> 0.1M in CH<sub>3</sub>CN) vs Ag/Ag<sup>+</sup>. Reference electrode calibrated against an internal Fc/Fc<sup>+</sup> reference (using  $E^\circ(\text{Fc}/\text{Fc}^+) = 0.63$  V vs NHE), <sup>c</sup>Estimated from the interception of the normalized absorption and emission spectra, <sup>d</sup>Estimated by subtracting  $E_{0-0}$  from the oxidation potential, <sup>e</sup>Value reported in literature.<sup>104</sup>

From direct comparison of optical and electrochemical data, it is possible to state that no remarkable differences emerged from the replacement by glycolic chains. V35 and D35 dyes differ modestly exclusively in terms of light harvesting ability, reflected in the values of molar extinction coefficient. Therefore, it is possible to

conclude that the introduction of glycolic chains causes, in terms of the optical and electrochemical measurements performed, only slightly reduced ability of the dye to harvest light.

## Hydrophilic/Hydrophobic Properties

The hydrophilicity/hydrophobicity of a surface can be easily and quickly evaluated by measuring its contact angle. As previously reported, the surface interaction of the dye with water is fundamental to provide good performances and this approach is grounded on it. It has been shown that the optical properties and the redox potentials of the dyes examined, do not differ significantly. Indeed, the aim was only to turn the hydrophobic character of D35, into hydrophilic. Figure 7.3 shows the recorded images used for the evaluation of the contact angles ( $\theta_c$ ) of D35 and V35. The measurement was performed by taking working electrodes screen-printed with 2 layers of active paste (total thickness around 4.5  $\mu\text{m}$ ), sensitized with the different dyes. The deposition of a water drop on the sensitized  $\text{TiO}_2$ , reveals the dramatic difference in its interaction with D35 and V35.

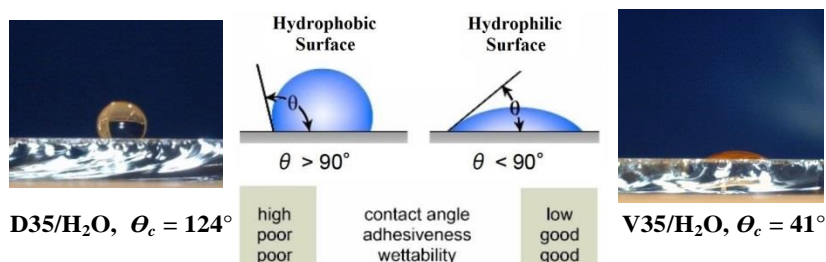


Figure 7.3 Cross-sections of distilled water positioned on the top of working electrodes sensitized with D35 (left) and V35 (right).

As depicted in Figure 7.3, contact angles greater than  $90^\circ$  indicate hydrophobic character of the surface while, lower than  $90^\circ$  reveal hydrophilic interactions. This trend is perfectly respected by hydrophobic D35, and hydrophilic dye V35, exhibiting a  $124^\circ$  and  $41^\circ$  contact angles, respectively.

## Desorption Properties

To test the tendency of V35 to desorb from the surface, transparent working electrodes were sensitized with V35 and placed into 5 mL of water. The

absorption spectra recorded show the desorption of the dye from the surface (Figure 7.4).

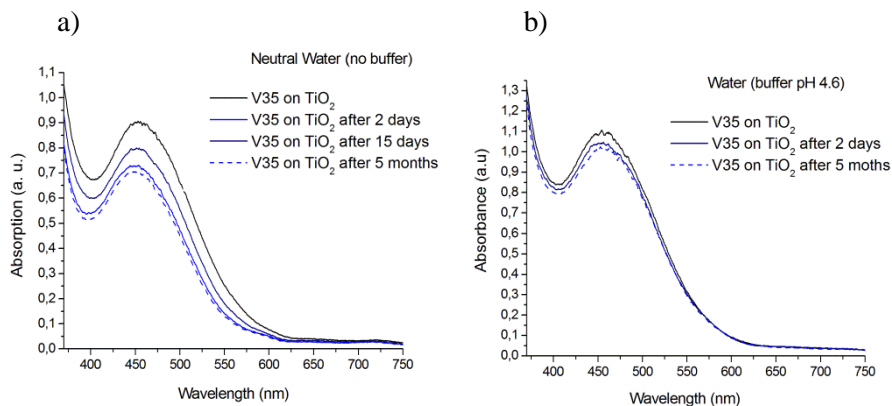


Figure 7.4 Desorption spectra of V35 in distilled water (a) and a distilled water buffer solution at pH 4.6 (b).

The mechanism that causes dye desorption has not been fully understood yet. However, it is commonly known that in acidic solutions, dyes exhibit much lower or no desorption problem. For this reason, water-soluble ruthenium complexes have always been tested at pH values around 3.<sup>90,97</sup> It should be also pointed out that the volume of water is enormously bigger compared to the one injected in the devices, therefore the equilibrium is completely shifted in favor of desorption. No desorption in neutral water occurred inside the assembled devices. In addition, test performed on the complete devices at different pHs buffer show very good and stable data for cells until pH 9.0. The data here reported show that the most significant desorption of dye occur in the initial 48 hours and then, suddenly slows down until stabilization.

## 7.5. Photovoltaic Performance

Dye V35 was tested in DSSCs employing  $I/I_3^-$  as redox couple. Previous attempts to use the Co(II)/Co(III) redox couple introduced by Spiccia *et al.* failed,<sup>99</sup> due to the very poor solubility of the  $[Co(bpy)_3](NO_3)_2$  complex in water. Therefore, the tests performed on V35 were inspired by the study recently reported by O'Regan *et al.*<sup>97</sup> According to this paper, CDCA and guanidinium salts acts as surfactant. Therefore, it was decided to avoid these components in the initial tests, starting from an electrolyte composed by NaI and  $I_2$  in 100% distilled water, and some variations. Figure 7.5 reports preliminary data obtained with these electrolytes.

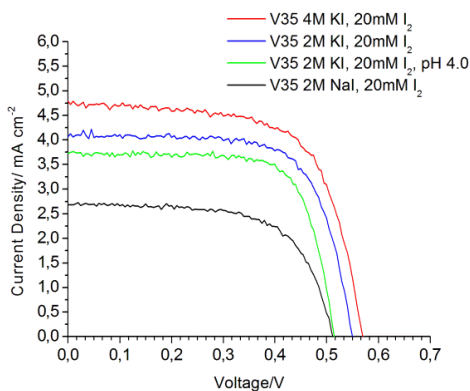


Figure 7.5 J-V curves of DSSCs based on V35 dye, in 100% distilled water electrolytes, platinum counter electrodes.

Table 7 reports in detail the photovoltaic parameters related to Figure 7.5.

Dye	Electrolyte	Jsc (mAcm <sup>-2</sup> )	Voc (mV)	FF (%)	$\eta$ (%)
V35	2 M NaI, 20 mM I <sub>2</sub>	2.30	500	67	0.80
	2 M KI, 20 mM I <sub>2</sub>	4.07	550	70	1.55
	2 M KI, 20 mM I <sub>2</sub> , pH 4.0	3.72	515	73	1.40
	4 M KI, 20 mM I <sub>2</sub>	4.78	570	65	1.76
D35	2 M NaI, 20 mM I <sub>2</sub>	0.115	350	55	0.02
	2 M KI, 20 mM I <sub>2</sub>	0.115	375	54	0.05
	4 M KI, 20 mM I <sub>2</sub>	0.344	440	46	0.07

Table 7. Detailed photovoltaic parameters of the J-V curves reported in Figure 7.5.

Moving from NaI to KI is possible to observe a significant improvement in the efficiency of the cells based on V35. Although no experiments were made in order

to investigate this difference, it is possible to speculate that is probably related to the ability of glycolic chains to coordinate small cations, such as  $\text{Na}^+$ . The effect is formally the same exhibited by the well-known crown ethers, and more likely results in a reduced conductivity of the electrolyte that lowers the performances. Experiments conducted employing a buffer solution at pH 4.0, reports lower values. The decrease in open-circuit voltage is due to the polarization induced on the surface by  $\text{H}^+$  ions, that shifts positively the potential of the CB of  $\text{TiO}_2$ .<sup>91,105</sup> However,  $J_{\text{sc}}$  would be expected to increase, due to the larger driving force for electron-injection. Here, it is actually observed the opposite trend, indicating that acidic pH (generally necessary to water-soluble complexes to avoid desorption) is not indicated for this system and confirming previously statements about the stability of the dye in neutral water. The additional improvement observed by using a higher concentration of KI, is probably due to the further shift in the equilibrium that suppresses free iodine concentration.<sup>97</sup> Finally, should be noticed that, in these conditions, no current was recorded in the devices fabricated employing D35.

At a later stage, the effects of guanidinium salts and chenodeoxycholic acid (structure of CDCA reported in Figure 7.6) were studied separately and together, in order to have insights on their properties. Table 8 reports the results obtained.

Dye	Electrolyte	Jsc ( $\text{mAcm}^{-2}$ )	Voc (mV)	FF (%)	$\eta$ (%)
V35	4 M KI, 20 mM $\text{I}_2$ , 0.2 GuSCN	3.83	550	68	1.42
	4 M KI, 20 mM $\text{I}_2$ , 0.5 GuSCN	3.33	555	67	1.25
D35	4 M KI, 20 mM $\text{I}_2$ , 0.5 GuSCN	1.43	532	61	0.46
V35	2 M KI, 20 mM $\text{I}_2$ , 0.2 GuSCN	3.22	545	68	1.20
	2 M KI, 20 mM $\text{I}_2$ , 0.5 GuSCN	2.32	550	69	0.89
D35	2 M KI, 20 mM $\text{I}_2$ , 0.5 GuSCN	0.104	488	46	0.23
V35	4 M KI, 20 mM $\text{I}_2$ , cheno <sup>[a]</sup>	4.86	600	76	2.20
D35	4 M KI, 20 mM $\text{I}_2$ , cheno <sup>[a]</sup>	0.627	580	77	0.28
V35	4 M KI, 20 mM $\text{I}_2$ , 0.5 GuSCN, cheno <sup>[a]</sup>	4.71	582	66	1.81
D35	4 M KI, 20 mM $\text{I}_2$ , 0.5 GuSCN, cheno <sup>[a]</sup>	2.15	581	65	0.81

*Table 8.* Photovoltaic parameters of DSSCs employing GuSCN and CDCA, with Pt counter electrodes. <sup>[a]</sup> Working electrode sensitized 1:50 = dye:CDCA, electrolyte solution in neutral water saturated with CDCA.

The available data show a different trend for V35 and D35. The addition of GuSCN in the electrolyte composition, seems to have a bad effect on the performances of the hydrophilic dye. Indeed, by making a comparison between these results and the one recorded without GuSCN, the remarkable decrease of the  $J_{\text{sc}}$  causes lower efficiency. On the other hand, the addition of CDCA results in a very positive effect. The combination of the two components does not result in a



synergistic effect, reflecting the bad effect that GuSCN has on V35. Different effects are recorded for hydrophobic D35, which exhibits a synergistic effect deriving from both GuSCN and CDCA. However, the data suggest that, employed singularly, the guanidinium salt and chenodeoxycholic acid are able to provide only slightly wetting. Furthermore, the synergistic effect is not able to exceed the results obtained with V35. Finally, Table 8 confirms the better results obtained employing 4 M KI, instead of 2 M.

Due to recent good performances reached with electropolymerized PEDOT counter electrodes (on FTO glass),<sup>104</sup> a comparison between Pt and PEDOT was made. Table 9 report these results.

Dye	Electrolyte	Jsc (mAcm <sup>-2</sup> )	Voc (mV)	FF (%)	$\eta$ (%)
<b>V35</b>	4 M KI, 20 mM I <sub>2</sub> (Pt ce)	4.78	570	65	1.76
	4 M KI, 20 mM I <sub>2</sub> , cheno <sup>[a]</sup> (Pt ce)	4.86	600	76	2.20
	2 M KI, 20 mM I <sub>2</sub> , 0.5 GuSCN (Pt ce)	2.32	550	69	0.89
	4 M KI, 20 mM I <sub>2</sub> (PEDOT ce)	5.17	590	68	2.06
	4 M KI, 20 mM I <sub>2</sub> , cheno <sup>[a]</sup> (PEDOT ce)	5.26	625	74	2.45
	2 M KI, 20 mM I <sub>2</sub> , 0.5 GuSCN (PEDOT ce)	3.35	540	71	1.29
<b>D35</b>	4 M KI, 20 mM I <sub>2</sub> , cheno <sup>[a]</sup> (Pt ce)	0.627	580	77	0.28
	4 M KI, 20 mM I <sub>2</sub> , cheno <sup>[a]</sup> (PEDOT ce)	1.18	605	61	0.44

*Table 9.* Photovoltaic parameters of DSSCs employing different counter electrodes. <sup>[a]</sup> Working electrode sensitized 1:50 = dye:CDCA, electrolyte solution of neutral water saturated with CDCA.

PEDOT counter electrodes, surprisingly, outperform the platinum ones mainly because of the increased photocurrent. In addition, PEDOT counter electrodes represent a cheaper and environmental friendly alternative to Pt, since EDOT is less expensive and the electropolymerization is carried out at room temperature, using a 0.1 M of NaDS and 0.01 M of EDOT solution, in distilled water. However, it should be pointed out that the preparation of PEDOT counter electrodes must be meticulously careful, as PEDOT may easily peel off and detach from the FTO surface, increasing resistance in the cell and leading to low performances. In addition, it was noticed that a big number of samples get very damaged after one or two weeks, as the electrolyte percolates in the PEDOT matrix, leaking out of the cell and causing surlyn detachment.

Further optimization of iodine and CDCA concentration, lead to the best performance recorded employing V35 (Figure 7.6, Table 10). It should be stressed out that the efficiency achieved, 3% under 1 sun (4% under 0.5 sun) illumination, is perfectly reflecting the state-of-the-art for D35-modified dyes in water systems.<sup>95</sup> However, in the study presented here, no additives and no ionic liquids are employed, confirming the validity of this approach.

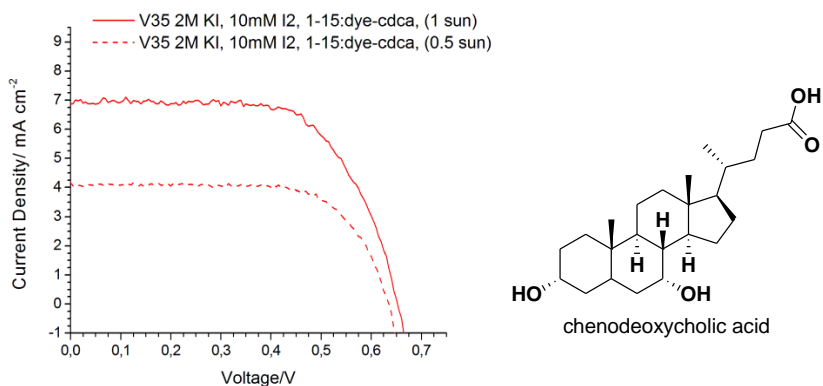


Figure 7.6 J-V curves of the most performing DSSCs based on V35 dye (left), molecular structure of CDCA (right).

Dye	$I_0/\text{Sun}$	$J_{sc}$ ( $\text{mA cm}^{-2}$ )	$V_{oc}$ (mV)	FF (%)	$\eta$ (%)
V35 <sup>[a]</sup>	1	6,85	650	67	<b>3.01</b>
	0.5	4,16	635	70	<b>4.04</b>

Table 10. Photovoltaic parameters of the J-V curves in Figure 7.6. Working electrode sensitized 1:15 = dye:CDCA, PEDOT ce, electrolyte solution: 2 M KI, 10 mM I<sub>2</sub>, sat. CDCA in distilled water.

Lower iodine concentration significantly improved the  $V_{oc}$  value, probably by reducing recombination. In addition, electrolyte realized with 10mM iodine results to be much lighter than the corresponding 20mM. Therefore, with lower amount of iodine, the dye can capture more sunlight.<sup>106</sup> In order to compare the results achieved, dyes V35 and D35 were also tested in O'Regan *et al.* best electrolyte, employing 8 M GuI and 20 mM I<sub>2</sub> in deionized water (Table 11).

Dye	Electrolyte	$J_{sc}$ ( $\text{mA cm}^{-2}$ )	$V_{oc}$ (mV)	FF (%)	$\eta$ (%)
V35	8 M GuI, 20 mM I <sub>2</sub>	3.77	500	61	1.16
	8 M GuI, 20 mM I <sub>2</sub> , cheno <sup>[a]</sup>	5.76	550	62	1.97
D35	8 M GuI, 20 mM I <sub>2</sub>	3.13	500	63	1.00
	8 M GuI, 20 mM I <sub>2</sub> , cheno <sup>[a]</sup>	5.89	520	64	1.95

Table 11. Photovoltaic parameters of DSSCs employing O'Regan's electrolyte with and without CDCA. <sup>[a]</sup>Working electrode sensitized 1:50 = dye:CDCA, electrolyte in sat. CDCA water, PEDOT ce.

Data reported in Table 11 show that by using such high concentration of guanidinium salt, wettability is so high that both hydrophilic and hydrophobic dyes perform in the same way. Measurements with and without CDCA show, once again, its remarkable impact on the performances. However, the approach based on a hydrophilic dye that does not need surfactants, as shown before, yields better efficiency.

To further investigate the hydrophilicity/hydrophobicity as a function of the amount of CDCA, and the electrolytes employed, contact angle measurements were performed (Table 12).

Dye / Dye:CDCA	Electrolyte	Contact Angle $\theta_c$ /°
V35	water <sup>[a]</sup>	41
D35	water <sup>[a]</sup>	124
V35/ 1:5	water <sup>[a]</sup>	31
D35/ 1:5	water <sup>[a]</sup>	121
V35/ 1:15	water <sup>[a]</sup>	34
D35/ 1:15	water <sup>[a]</sup>	111
V35/ 1:50	water <sup>[a]</sup>	26
D35/ 1:50	water <sup>[a]</sup>	104
V35/ 1:5	2 M KI, 10 mM I <sub>2</sub> , cheno <sup>[b]</sup>	16
D35/ 1:5	2 M KI, 10 mM I <sub>2</sub> , cheno <sup>[b]</sup>	98
V35/ 1:15	2 M KI, 10 mM I <sub>2</sub> , cheno <sup>[b]</sup>	22
D35/ 1:15	2 M KI, 10 mM I <sub>2</sub> , cheno <sup>[b]</sup>	91
V35/ 1:50	2 M KI, 10 mM I <sub>2</sub> , cheno <sup>[b]</sup>	15
D35/ 1:50	2 M KI, 10 mM I <sub>2</sub> , cheno <sup>[b]</sup>	90
V35	2 M KI, 10 mM I <sub>2</sub> <sup>[a]</sup>	41
D35	2 M KI, 10 mM I <sub>2</sub> <sup>[a]</sup>	91
V35	4 M KI, 10 mM I <sub>2</sub> <sup>[a]</sup>	43
D35	4 M KI, 10 mM I <sub>2</sub> <sup>[a]</sup>	84
D35	8 M GuI, 20 mM I <sub>2</sub> <sup>[a]</sup>	77*

\* After some time, total wetting was observed.

Table 12. Contact angle measurements. <sup>[a]</sup> Neutral water, <sup>[b]</sup> Neutral water saturated with CDCA.

The data collected in Table 12 prove that CDCA is able to provide only a negligible increase of wettability and that, as previously demonstrated by the results in Table 8, even in 1:50/D35:CDCA ratio, is not sufficient to make the current flow. Therefore, the slightly increased wettability deriving from CDCA is not sufficient to explain the remarkable enhancement in the performances and we can firmly state that the efficiency deriving from the use of CDCA in combination with V35, are not due to increased wettability. A possible explanation for the

effect of CDCA can be found in the comparison between IPCE and electron lifetime measurements performed on the most significant cell (Figure 7.7).

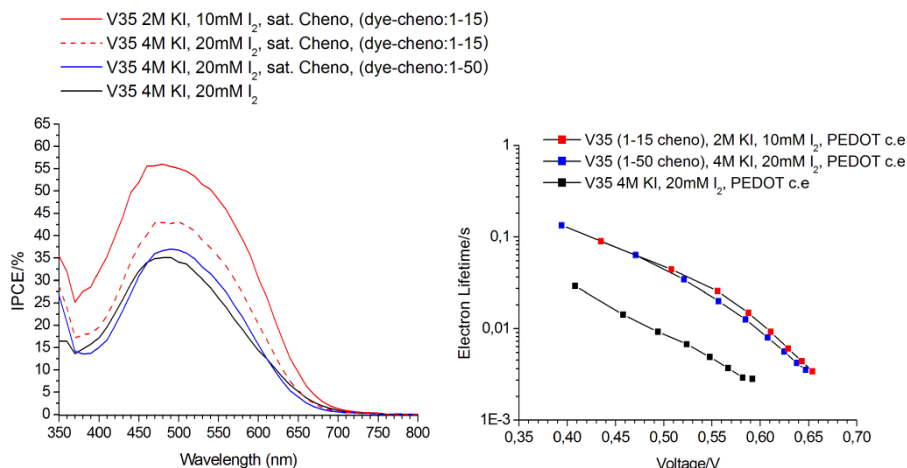


Figure 7.7 IPCE (left) and electron lifetime (right) measurements. All the cells were sealed with PEDOT ce.

These data suggest that CDCA seems to have a big influence in terms of electron lifetime. This is also supported by the significant enhancement of the  $V_{oc}$  when chenodeoxycholic acid is co-adsorbed on the surface of TiO<sub>2</sub>, indicating a reduction of the recombination processes. Infact, the main difference between the cells without CDCA and 1:50/dye:CDCA is related to the open-circuit voltage (see Table 9) that impacts on the fill factor value, enhancing the performances from 2.06% to 2.45%. Electron lifetime measurements show no significant change between the best performing cell (red), and the one employing bigger amount of CDCA and iodine (blue). On the other hand, the IPCE shows a great variance. During the optimization process, it was found that the higher the amount of CDCA is used, the higher the  $V_{oc}$  is. However, the more CDCA is employed, the less dye is absorbed on the surface, which, in turn, drops the photocurrent down. A reversed effect was observed modulating the concentration of I<sub>2</sub>. In this case, concentrations higher than 20 mM were resulting in higher current but lower  $V_{oc}$ , while concentrations lower than 10 mM yielded devices with very high open-circuit voltage, but low current. Therefore, by balancing all these effects, the optimum conditions employed are reflected by the remarkable enhancement of the IPCE spectra.

Finally, it is necessary to point out that the thickness of the scattering layer, as well as the PEDOT counter electrodes employed, played a crucial role. The initial studies, not reported here, were performed on DSSCs with one layer of active and

one layer of scattering paste (total thickness around 5.0  $\mu\text{m}$ ) and yielded approximately half of the efficiencies presented. The introduction of a second layer of scattering paste (total thickness around 7.5-8.0  $\mu\text{m}$ ) brought remarkable enhancement, probably due to a more efficient light collection.

## 7.6. Conclusion

An original approach, consisting in the development of an organic and hydrophilic, prototype dye, was employed. The critical issue of wettability has been solved and, simultaneously, desorption issues have been remarkably reduced. Significant power conversion efficiencies, of 3% and 4% under 1 sun and 0.5 sun illumination, respectively, were achieved. The efficiency, perfectly fitting in the state-of-the-art for a modified version of D35 in water, was reached employing a very simple and environmental friendly system. The roles of guanidinium salts and chenodeoxycholic acid were investigated, leading to new insights about their effects. In particular, it has been proved that CDCA, without surfactants (such as Gu-salts in big amount), only slightly improve the wettability. Therefore, its remarkable impact on the efficiency cannot be explained in terms of wettability. Finally, a comparison between the conditions developed in this study, and the ones reported by O'Regan *et al.*, confirmed the advantages introduced by the new approach.

## 8. Concluding Remarks

The research reported in this thesis has investigated new geometries of organic dyes for dye-sensitized solar cells. The new structures allow a greater variability and modulation of optical and photovoltaic properties. The prototypes presented show interesting features that should be fully explored by the realization of optimized structures, employing the most performing building blocks available. In addition, the multi-branched approach has been definitively proven to result in enhanced stability, due to a stronger interaction with TiO<sub>2</sub> semiconductor.

Asymmetric tribranched dyes can conjugate characteristics deriving from the tribranched design and the advantages of co-sensitization technique, opening many possibilities for reaching higher performances. In particular, the possibility to predict the absorption spectrum of the asymmetric tribranched from their symmetric analogous, is a powerful tool that can be used to design new structures. In this way, it would be possible to combine fragments that yield different values of photocurrent and open-circuit voltage, and maximize their effects to reach higher power conversion efficiency.

Water-based systems, combining low-cost and environmental friendly characteristics, can be the key for future commercialization. However, much fundamental research, in order to grasp and fully understand the effects deriving from water, must be done. Furthermore, new components such as dyes and, especially, redox couples, should be specifically developed for 100% water systems. Infact, iodine itself is completely insoluble in water, the binding constants of the I<sub>3</sub><sup>-</sup> specie are very different from acetonitrile, and the components used tend to sublime very easily, making critical device assembly. All these facts, made difficult the realization of devices with homogeneous electrolytes solutions and very high reproducibility. Therefore, new components are necessary in order to achieve further improvements.

# References

1. *Annual Energy Outlook*, 2013, U.S. Energy Information Administration (EIA).
2. *In Basic Research Needs for Solar Energy Utilization*, 2005, U.S. Department of Energy.
3. A. Witze, *Nature*, 2007; **445**, 14-17.
4. M. A. Green, K. Emery, Y. Hishikawa, W. Warta, E. D. Dunlop, *Prog. Photovolt: Res. Appl.*, 2013; **21**, 827–837.
5. K. Onoda, S. Ngamsinlapasathian, T. Fujieda, S. Yoshikawa, *Solar Energy Mater, Solar Cells*, 2007; **91**, 1176-1181.
6. M. Graetzel, B. O'Regan, *Nature*, 1991; **353**, 737-739.
7. S. Feldt, *Alternative Redox Couples for Dye-Sensitized Solar Cells*, Uppsala University, Ångströmlaboratoriet, 2013.
8. H. Hoppe, N. F. Sariciftci, *J. Mater. Res.* 2004; **19**, 1928-1929.
9. A. Zaban, A. Meier, B. A. Gregg, *J. Phys. Chem. B*, 1997; **101**, 7985-7990.
10. T. W. Hamann, R. A. Jensen, A. B. F. Martinson, H. Van Ryswykac, J. T. Hupp, *Energy Environ. Sci.*, 2008; **1**, 66–78.
11. E. M. Barea, J. Ortiz, F. J. Paya, F. Fernandez-Lazaro, F. Fabregat-Santiago, A. Sastre-Santos and J. Bisquert, *Energy Environ. Sci.*, 2010, **3**, 1985.
12. S. E. Koops, B. O'Regan, P. R. F. Barnes and J. R. Durrant, *J. Am. Chem. Soc.*, 2009, **131**, 4808–4818.
13. S. Meng and E. Kaxiras, *Nano Lett.*, 2010, **10**, 1238–1247.
14. T. Daeneke, A. J. Mozer, Y. Uemura, S. Makuta, M. Fekete, Y. Tachibana, N. Koumura, U. Bach and L. Spiccia, *J. Am. Chem. Soc.*, 2012, **134**, 16925–16928.
15. J. E. Kroeze, N. Hirata, S. Koops, M. K. Nazeeruddin, L. Schmidt-Mende, M. Graetzel and J. R. Durrant, *J. Am. Chem. Soc.*, 2006, **128**, 16376–16383.

16. L. Schmidt-Mende, J. E. Kroeze, J. R. Durrant, M. K. Nazeeruddin and M. Graetzel, *Nano Lett.*, 2005, **5**, 1315–1320.
17. R. Li, J. Liu, N. Cai, M. Zhang, P. Wang, *J. Phys. Chem. B*, 2010, **114**, 4461–4464.
18. B. S. Chen, D. Y. Chen, C. L. Chen, C. W. Hsu, H. C. Hsu, K. L. Wu, S. H. Liu, P. T. Chou and Y. Chi, *J. Mater. Chem.*, 2011, **21**, 1937–1945.
19. D. W. Chang, H. J. Lee, J. H. Kim, S. Y. Park, S. M. Park, L. M. Dai, J. B. Baek, *Org. Lett.*, 2011, **13**, 3880–3883.
20. M. Zhang, J. Y. Liu, Y. H. Wang, D. F. Zhou and P. Wang, *Chem. Sci.*, 2011, **2**, 1401–1406.
21. M. Xu, D. Zhou, N. Cai, J. Liu, R. Li, P. Wang, *Energy Environ. Sci.*, 2011, **4**, 4735–4742.
22. Wang, Z. S.; Li, F. Y.; Huang, C. H. *Chem. Commun.* 2000, 2063-2064.
23. Q.-H. Yao, L. Shan, F.-Y. Li, D.-D. Yin and C.-H. Huang, *New J. Chem.*, 2003, **27**, 1277–1283.
24. B. Wenger, C. Bauer, M. K. Nazeeruddin, P. Comte, S. M. Zakeeruddin, M. Grätzel, J.-E. Moser, *Proc. SPIE*, 2006, **6325**, 63250V-63250V-11.
25. R. Chen, X. Yang, H. Thian, X. Wang, A. Hagfeldt, L. Sun, *Chem Mater*, 2007, **19**, 4007.
26. Y. Ooyama, N. Yamaguchi, I. Imae, K. Komaguchi, J. Ohshita, Y. Harima, *Chem. Commun.*, 2013, **49**, 2548.
27. Y. Ooyama, S. Inoue, T. Nagano, K. Kushimoto, J. Ohshita, I. Imae, K. Komaguchi, Y. Harima, *Angew. Chem. Int. Ed.* 2011, **50**, 7429–7433.
28. S. L. Li, K. J. Jiang, K. F. Shao and L. M. Yang, *Chem. Commun.*, 2006, 2792–2794.
29. J. Cong, X. Yang, J. Liu, J. Zhao, Y. Hao, Y. Wang, L. Sun, *Chem. Commun.*, 2012, **48**, 6663–6665.
30. A. Abboto, N. Manfredi, *Dalton Trans.*, 2011, **40**, 12421.
31. Y. Hao, X. Yang, J. Cong, H. Tian, A. Hagfeldt and L. Sun, *Chem. Commun.*, 2009, 4031–4033.



32. E. Mosconi, J.-H. Yum, F. Kessler, C. J. Gomez García, C. Zuccaccia, A. Cinti, M. K. Nazeeruddin, M. Graetzel, F. De Angelis, *J. Am. Chem. Soc.* 2012, **134**, 19438–19453.
33. A. Yella, H. W. Lee, H. N. Tsao, C. Yi, A. K. Chandiran, M. K. Nazeeruddin, E. W. G. Diau, C. Y. Yeh, S. M. Zakeeruddin, M. Graetzel, *Science*, 2011, **334**, 629–634.
34. Y. Ooyama, Y. Harima, *Eur. J. Org. Chem.* 2009, 2903–2934.
35. Z. Cheng, F. Li, C. Huang, *Curr. Org. Chem.*, 2007; **11**, 1241-1258.
36. Z.-S. Wang, Y. Cui, K. Hara, Y. Dan-oh, C. Kasada, A. Shinpo, *Adv. Mater.*, 2007, **19**, 1138–1141.
37. K. Hara, T. Sato, R. Katoh, A. Furube, Y. Ohga, A. Shinpo, S. Suga, K. Sayama, H. Sugihara, H. Arakawa, *J. Phys. Chem. B*, 2003; **107**, 597.
38. S. Ito, H. Miura, S. Uchida, M. Takata, K. Sumioka, P. Liska, P. Comte, P. Pechy, M. Graetzel, *Chem. Commun.*, 2008, **41**, 5194–5196.
39. N. Koumura, Z. S. Wang, S. Mori, M. Miyashita, E. Suzuki, K. Hara, *J. Am. Chem. Soc.*, 2008; **130**, 4202.
40. D. Kim, J. K. Lee, S. O. Kang, J. Ko, *Tetrahedron*, 2007; **63**, 1913-1922.
41. C. Qin, W. Peng, K. Zhang, A. Islam and L. Han, *Org. Lett.*, 2012; **14**, 2532–2535.
42. Y. Numata, I. Ashraful, Y. Shirai and L. Han, *Chem. Commun.*, 2011; **47**, 6159–6161.
43. S. Y. Qu, C. J. Qin, A. Islam, Y. Z. Wu, W. H. Zhu, J. L. Hua, H. Tian and L. Y. Han, *Chem. Commun.*, 2012; **48**, 6972–6974.
44. S. Zhang, X. Yang, Y. Numata, L. Han, *Energy Environ. Sci.*, 2013; **6**, 1443–1464.
45. V. V. Diev, K. Hanson, J. D. Zimmerman, S. R. Forrest, M. E. Thompson, *Angew. Chem.*, 2010; **122**, 5655 –5658.
46. M. V. Martinez-Diaz, G. de la Torrea, T. Torres, *Chem. Commun.*, 2010; **46**, 7090-7108.
47. F. De Angelis, S. Fantacci, A. Selloni, M. Graetzel, M. K. Nazeeruddin, *Nano Lett.*, 2007; **7**(10), 3189-3195.

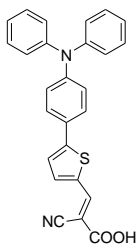
48. A. Abbotto, N. Manfredi, C. Marinzi, F. De Angelis, E. Mosconi, J. Yum, Z. Xianxi, M. K. Nazeeruddin, M. Graetzel, *Energy Environ. Sci.*, 2009; **2**, 1094-1101.
49. T. Edvinsson, C. Li, N. Pschirer, J. Schoneboom, F. Eickemeyer, R. Sens, G. Boschloo, A. Herrmann, K. Mullen and A. Hagfeldt, *J. Phys. Chem. C*, 2007, **42**, 15137-15140.
50. D. P. Hagberg, J.-H. Yum, H.-J. Lee, F. De Angelis, T. Marinado, K. M. Karlsson, R. Humphry-Baker, L. Sun, A. Hagfeldt, M. Graetzel, M. K. Nazeeruddin, *J. Am. Chem. Soc.*, 2008, **130**, 6259–6266.
51. X. Jiang, K. M. Karlsson, E. Gabrielsson, E. Johansson, M. Quintana, M. Karlsson, L. Sun, G. Boschloo, A. Hagfeldt, *Adv. Funct. Mater.* 2011, **21**, 2944–2952.
52. A. Baheti, P. Tyagi, K. R. J. Thomas, Y. C. Hsu and J. T. Lin, *J. Phys. Chem. C*, 2009, **113**, 8541–8547.
53. A. Baheti, P. Singh, C. P. Lee, K. R. J. Thomas, K. C. Ho, *J. Org. Chem.*, 2011, **76**, 4910–4920.
54. L. Cai, H. N. Tsao, W. Zhang, L. Wang, Z. Xue, M. Graetzel, B. Liu, *Adv. Energy Mater.*, 2012, **3**, 200–205.
55. I. Jung, J. K. Lee, K. H. Song, K. Song, S. O. Kang, J. Ko, *J. Org. Chem.*, 2007, **72**, 3652–3658.
56. C. Qin, W. Peng, K. Zhang, A. Islam and L. Han, *Org. Lett.*, 2012, **14**, 2532–2535.
57. D. P. Hagberg, T. Marinado, K. M. Karlsson, K. Nonomura, P. Qin, G. Boschloo, T. Brinck, A. Hagfeldt, L. Sun, *J. Org. Chem.*; 2007, **72**, 9550-9556.
58. H. Qin, S. Wenger, M. Xu, F. Gao, X. Jing, P. Wang, S. M. Zakeeruddin, M. Graetzel, *J. Am. Chem. Soc.*, 2008, **130**, 9202–9203.
59. M. K. Wang, M. F. Xu, D. Shi, R. Z. Li, F. F. Gao, G. L. Zhang, Z. H. Yi, R. Humphry-Baker, P. Wang, S. M. Zakeeruddin and M. Graetzel, *Adv. Mater.*, 2008, **20**, 4460–4463.
60. K. Hara, M. Kurashige, Y. Dan-oh, C. Kasada, A. Shinpo, S. Suga, K. Sayama, H. Arakawa, *New J. Chem.*, 2003, **27**(5), 783-785.

61. M. Lu, M. Liang, H.-Y. Han, Z. Sun, S. Xue, *J. Phys. Chem. C*, 2011, **115**, 274–281.
62. N. Zhou, L. Wang, D.W. Thompson, Y. Zhao, *Org. Lett.*, 2008, **10**, 3001.
63. T. Ishiyama, N. Miyaura, A. Suzuki, *Chem. Lett.*, 1987, 25–28.
64. R. B. Bedford, S. L. Welch, *Chem. Commun.*, 2001, 129–130.
65. N. Miyaura, A. Suzuki, *Chem. Rev.*, 1995, **95**, 2457–2483.
66. D. P. Hagberg, X. Jiang, E. Gabrielsson, M. Linder, T. Marinado, T. Brinck, A. Hagfeldt, L. Sun, *J. Mater. Chem.*, 2009, **19**, 7232–7238.
67. W.-H. Liu, I.-C. Wu, C.-H. Lai, C.-H. Lai, P.-T. Chou, Y.-T. Li, C.-L. Chen, Y.-Y. Hsu, Y. Chi, *Chem. Commun.*, 2008, **41**, 5152–5154.
68. R. Li, X. Lv, D. Shi, D. Zhou, Y. Cheng, G. Zhang, P. Wang, *J. Phys. Chem. C*, 2009, **113**, 7469.
69. D. P. Hagberg, T. Edvinsson, T. Marinado, G. Boschloo, A. Hagfeldt and L. C. Sun, *Chem. Commun.*, 2006, 2245–2247.
70. M. Akhtaruzzaman, Y. Seya, N. Asao, A. I. Islam, E. Kwon, A. E. Shafei, L. Y. Han and Y. Yamamoto, *J. Mater. Chem.*, 2012, **22**, 10771–10778.
71. T. Kitamura, M. Ikeda, K. Shigaki, T. Inoue, N. A. Anderson, X. Ai, T. Q. Lian and S. Yanagida, *Chem. Mater.*, 2004, **16**, 1806–1812.
72. C. Teng, X. Yang, C. Yang, H. Tian, S. Li, X. Wang, A. Hagfeldt, L. Sun, *J. Phys. Chem., C* 2010, **114**, 11305–11313.
73. K. M. Karlsson, X. Jiang, S. K. Eriksson, E. Gabrielsson, H. K. Rensmo, A. Hagfeldt, L. Sun, *Chem. Eur. J.*, 2011, **17**, 6415.
74. V. Leandri, R. Ruffo, V. Trifiletti, A. Abboto, *Eur. J. Org. Chem.*, 2013, **30**, 6793–6801.
75. Y. Pan, H. Lu, Y. Fang, X. Fang, L. Chen, J. Qian, J. Wang, C. Li, *Synthesis*, 2007, 1242–1246.
76. C. Wolf, S. Liu, X. Mei, A. T. August, M. D. Casimir, *J. Org. Chem.*, 2006, **71**, 3270–3273.
77. F. Y. Kwong, A. Klapars, S. L. Buchwald, *Org. Lett.*, 2002, **4**, 581–584.
78. A. Abboto, V. Leandri, N. Manfredi, F. D. Angelis, M. Pastore, J.-H. Yum, M. K. Nazeeruddin and M. Graetzel, *Eur. J. Org. Chem.*, 2011, 6195–6205.

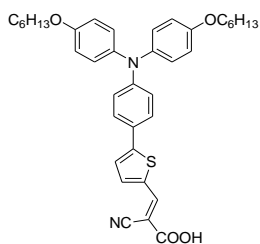
79. H.-P. Lu, C.-Y. Tsai, W.-N. Yen, C.-P. Hsieh, C.-W. Lee, C.-Y. Yeh, E. W.-G. Diau, *J. Phys. Chem. C*, 2009, **113**, 20990–20997.
80. M. Dori, K. Seintis, E. Stathatos, G. Tsigaridas, T. Y. Lin, J. T. Lin, M. Fakis, V. Giannetas and P. Persephonis, *Chem. Phys. Lett.*, 2013, **563**, 63–69.
81. J. H. Yum, S. J. Moon, R. Humphry-Baker, P. Walter, T. Geiger, F. Nuesch, M. Graetzel, M. K. Nazeeruddin, *Nanotechnology*, 2008, **19**, 424005.
82. J. Li, W. J. Wu, J. B. Yang, J. Tang, Y. T. Long, J. L. Hua, *Sci. China Chem.*, 2011, **4**, 699-706.
83. U. B. Cappel, A. L. Smeigh, S. Plogmaker, E. M. J. Johansson, Hakan Rensmo, Leif Hammarstrom, Anders Hagfeldt, Gerrit Boschloo, *J. Phys. Chem. C*, 2011, **115**, 4345–4358.
84. M. K. Nazeeruddin, F. De Angelis, S. Fantacci, A. Selloni, G. Viscardi, P. Liska, S. Ito, B. Takeru, M. Grätzel, *J. Am. Chem. Soc.*, 2005, **127**, 16835.
85. E. Borgarello, J. Kiwi, E. Pelizzetti, M. Visca, M. Grätzel, *Nature*, 1981, **289**, 158–160.
86. E. Borgarello, J. Kiwi, E. Pelizzetti, M. Visca, M. Grätzel, *J. Am. Chem. Soc.*, **103**, 6324-6329.
87. K. R. Thampi, J. Kiwi, M. Graetzel, *Nature*, 1987, **327**, 506–508.
88. M. Matsumura, S. Matsudaira, H. Tsubomura, M. Takata, and H. Yanagida, *Ind. Eng. Chem. Prod. Res. Dev.*, 1980, **19**, 415–421.
89. J. Desilvestro, M. Gratzel, L. Kavan, J. Moser, and J. Augustynski, *J. Am. Chem. Soc.*, 1985, **432**, 2988–2990.
90. N. Vlachopoulos, P. Liska, J. Augustynski, and M. Grätzel, *J. Am. Chem. Soc.*, 1988, **110**, 1216–1220.
91. Y. Liu, A. Hagfeldt, X. R. Xiao, S. E. Lindquist, *Sol. Energy Mater. Sol. Cells*, 1998, **55**, 267.
92. B. Macht, M. Turrion, A. Barkschat, P. Salvador, K. Ellmer, H. Tributsch, *Sol. Energy Mater. Sol. Cell*, 2002, **73**, 163.
93. Y. S. Jung, B. Yoo, M. K. Lim, S. Y. Lee, K. J. Kim, *Electrochim. Acta*, 2009, **54**, 6286-6291.

94. C. Law, S. C. Pathirana, X. Li, A. Y. Anderson, P. R. F. Barnes, A. Listorti, T. H. Ghaddar, B. C. O'Regan, *Adv. Mater.*, 2010, **22**, 4505–4509.
95. H. Tian, E. Gabrielsson, P. W. Lohse, N. Vlachopoulos, L. Kloo, A. Hagfeldt, L. Sun, *Energy Environ. Sci.*, 2012, **5**, 9752.
96. W. H. Lai, Y. H. Su, L. G. Teoh, M. H. Hon, *J. Photochem. Photobiol. A Chem.*, 2008, **195**, 307–313.
97. C. Law, O. Moudam, S. Villarroya-Lidon, B. O'Regan, *J. Mater. Chem.*, 2012, **22**, 23387.
98. T. Daeneke, Y. Uemura, N. W. Duffy, A. J. Mozer, N. Koumura, U. Bach, L. Spiccia, *Adv. Mater.*, 2012, **24**, 1222–5.
99. W. Xiang, F. Huang, Y.-B. Cheng, U. Bach, and L. Spiccia, *Energy Environ. Sci.*, 2013, **6**, 121.
100. Alexander B. Nepomnyashchii, A. J. Pistner, A. J. Bard, J. Rosenthal, *J. Phys. Chem. C*, 2013, **117**, 5599–5609.
101. W.-S. Han, K.-R. Wee, H.-Y. Kim, C. Pac, Y. Nabetani, D. Yamamoto, T. Shimada, H. Inoue, Heesung Choi, K. Cho, S. O. Kang, *Chem. Eur. J.*, 2012, **18**, 15368–15381.
102. R. C. White, J. E. Benedetti, A. D. Gonçalves, W. Romão, B. G. Vaz, M. N. Eberlin, C. R. D. Correia, M. a. De Paoli, and A. F. Nogueira, *J. Photochem. Photobiol. A Chem.*, 2011, **222**, 185–191.
103. S.-H. Lee, Y. Park, K.-R. Wee, H.-J. Son, D. W. Cho, C. Pac, W. Choi, S. O. Kang, *Org. Lett.*, 2010, **12**, 460–463.
104. E. Gabrielsson, H. Ellis, S. Feldt, H. Tian, G. Boschloo, A. Hagfeldt, and L. Sun, *Adv. Energy Mater.*, 2013, (Early View).
105. R. Beranek, *Adv. Phys. Chem.*, 2011, **2011**, 1–20.
106. M. Chen, X. Yang, S. Li, X. Wang, L. Sun, *Energy Environ. Sci.*, 2012, **5**, 6290–6293.

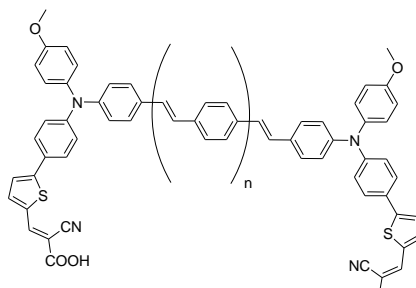
# Appendix 1



L1

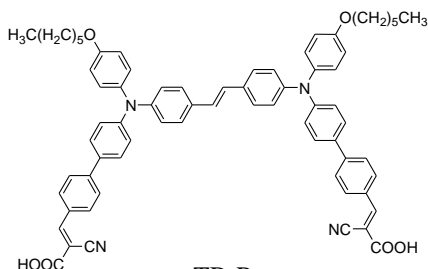


C213

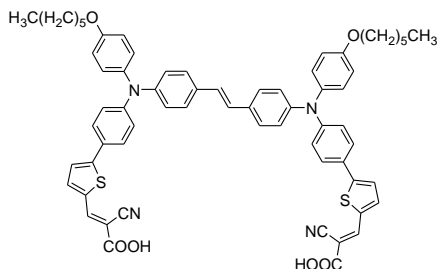


n = 0 TB-1

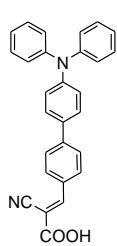
n = 1 TB-2



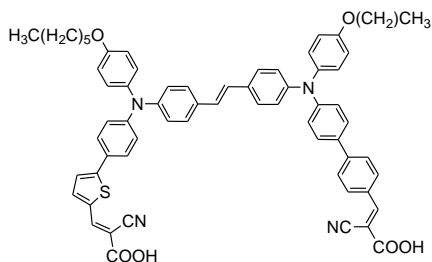
TB-P



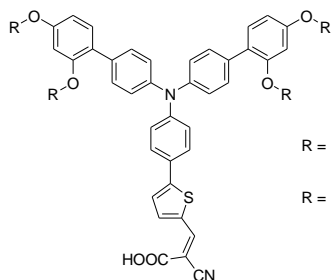
TB-T



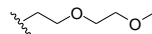
TC105



TB-PT



R =  D35

R =  V35

# Acknowledgements

I would like to express my sincere gratitude to:

Prof. Abbotto, for accepting me as a Ph.D student in his laboratory. These three years have been a fundamental step in my life, thank you for this opportunity you have given to me.

My labmates:

I will never forget the funny moments, late in the lab and during many week-ends, singing stupid cartoons openings, with Carmine Coluccini. Carmaine, I wish you the best (uhm, wait...you have something on your elbow...eheh)!

I'll never forget the nice experiences in the summer schools and, more in general, you radiant and positive character, Svitlana Karamshuk! We must keep in touch!

Luca Arosio, you are a very nice, smart and funny person. I wish you all the best, you deserve it!

Bianca Cecconi, you joined our group just before I left for the research period abroad but you immediately have revealed to be extraordinarily nice. I believe you will have a wonderful scientific future because you are very good! We did not spend much time together, but I hope we will keep in touch in the future.

Vanira Trifiletti, thanks for everything and good luck for the future!

Norberto Manfredi, and all the other funny people I forgot to report here (forgive me!). Thank you, guys!

Moving to the near labs:

Mauro Sassi, I put you in the first place because you are my favourite, you know (ok, you and Cioccio)! Ahaha! Thank you for all the funny moments, the jokes, the sweets you shared at lunch (yeah, sometimes you did it, even if I had to insist a lot...) and, most importantly, all the time you spent trying to find solutions to my scientific problems. You taught me many things and you have always been a reference point of knowledge to me! It was a pleasure to be dressed like your beloved ex-colleague, at your wedding.

Luca Beverina, I would basically say the same things I wrote for Mauro (except for the fact that I didn't have to wear a brilliant-red wig for you!). Thank you for all the time you dedicated to me and all the funny moments spent in the office!

The God of the NMR, also known as Cioccio (I cite you for third because three is the perfect number!). Thank you for all the SUPER funny moments at the NMR... It will be sooo boring to do NMRs in the future, and that makes me so sad! Thanks

for all the things you taught me. You and Elena are an amazing couple and have a wonderful family, so I really wish you all the best!

Paolo Coghi, I will not forget our lunches together and all our stupid jokes we used to do in those occasions! To eat with you have never been boring!

I would also like to thank all the people from the other lab like Nunzio, Tosi, Alessandro, Mask, Marco Vettigli, etc, that made very funny everyday in lab (sorry if i forgot anyone!).

Moving to my external internship in Sweden, I absolutely have to thank:

Prof. Anders Hagfeldt, I will never be able to thank you in an adequate way for the great opportunity you gave me. The experience in Sweden changed my life. Your research group is wonderful and I have learned an astonishing number of things during my visit. I think I can firmly say I grew up both scientifically and personally, which is the best thing one may ask for. You are an inspiration model for many people, and it is admirable the way you have remained so close to people, modest and simple, although your great scientific achievements.

Prof. Gerrit Boschloo, thank you very much for everything! I cannot wait to come back to Sweden in order to start collaborating again. Both you and Anders gave me the freedom and encouraged me to develop my own project, thank you for that. You contribute everyday to keep the group a friendly, stimulating and relaxed place where is possible to express yourself, and this is fundamental to do good research.

Marina Freitag, thank you for the time spent together and all the help and support you gave me! You and your family are wonderful and with you the group is even more close and funny. I cannot wait to spend again evenings together talking, having dinner, drinking wine, playing with Damian, etc!

Kari Sveinbjornsson and Mr. Kaito Ayatollah, oooops, I meant Kaito Aidola, no, wait...it's Kettu Aidola! Yes! No...kidding, Kerttu Aitola! Ehm...Kari...sorry for not using the proper letters to write your name, I am lazy (it was for solidarity with Kerttu's name)! You guys are amazing and I will never forget moments spent together (like when Kerttu sneaked away while we were watching "The Hobbit"! ). Kari, your speech about "being a champion" will remain in my heart forever, you can be sure. You have no idea how much it helped. I really needed it and it's something I will always try to keep in mind. Thank you.

Nick Vlachopoulos, you are wonderful! Me and Kerttu said sometimes "Nick is the soul of the group", and so it is. You are very funny, willing to help others and when you are not around we really feel the difference! I hope one day I will master electrochemistry and surprise you! Thank you for everything!

Ok, if I keep going on like this I will write a poem so, I would like to generally thank:

Hanna Ellis for having introduced me in the group immediately, making me feel like home. Yan Hao, who taught me a lot of things about solar cells and with



which I have always been able to share opinions and ideas. You are a rock, keep going on like this! Wenxing Yang and Jinbao Zhang, you two are wonderful people, funny, willing to help others, to share knowledge, hard-workers, enthusiastic....the best colleagues one may want! Meysam Pazoki, you “saved my life” a couple of times and it has always been very nice to talk with you! Pedram Narjes, Leif, Luca, Bianka, Lei, Park, Dongqin, Rayan, Justus....and all those who I am forgetting (sorry, sorry), you all have been very nice, thanks!

A special gratitude to the people from KTH:

Prof. Licheng Sun, I would like to thank you for the possibility to develop the synthetic part of my project in your group. In this occasion I learned many new things and I am very glad of this experience.

Lei Wang, Qian Gao and Haining Tian, you guys are lovely and it was a pleasure to spend some time with you in KTH! I hope to see you soon and I still would like to prepare yummy chinese dumplings with you!

Erik Gabriellsson, I would have known that offering you italian food would have made you so sweet, I would have done it before! Ahaha, kidding! You taught me new things and it was very nice to spend time in KTH with you. I know I have been very noisy, crazy, I broke stuff....well, this last part is very strange, it never happened before, I swear! Ok...it's not true, it happens regularly (I hope Sascha Ott will never read this part). Anyway...c'mon, I think you also had fun, so do not complain!

A french girly guy, also known as Quentin, whose accent made me understand nothing at the beginning! Well, now that I understand what you say (more or less) I believe it was better before! Ahaha! Kidding, kidding! Thank you for loosing my NMR tube, for remembering me that my country lost a war even against Ethiopia, for the funny moments in lab, for spotting good food with your eagle eyes...everything!

Un ringraziamento particolare ai miei genitori ed a mio nonno Gianni, che mi hanno sempre sostenuta moralmente (e finanziariamente, ahimè!) durante questi “lunghi” tre anni.

**Bis-Donor-Bis-Acceptor Tribranched Organic Sensitizers for  
Dye-Sensitized Solar Cells**

A. Abbotto, V. Leandri, N. Manfredi, F. De Angelis, M. Pastore, J.-H. Yum, M.  
K. Nazeeruddin, M. Graetzel  
*Eur. J. Org. Chem.*, **2011**, 31, 6195-6205

## Bis-Donor–Bis-Acceptor Tribranched Organic Sensitizers for Dye-Sensitized Solar Cells

Alessandro Abbotto,<sup>\*[a,b]</sup> Valentina Leandri,<sup>[a]</sup> Norberto Manfredi,<sup>[a]</sup> Filippo De Angelis,<sup>\*[b]</sup> Mariachiara Pastore,<sup>[b]</sup> Jun-Ho Yum,<sup>[c]</sup> Mohammad K. Nazeeruddin,<sup>\*[c]</sup> and Michael Grätzel<sup>[c]</sup>

**Keywords:** Conformation analysis / Dyes/pigments / Donor-acceptor systems / Energy conversion / Sensitizers

A new class of tribranched dye-sensitized solar cell (DSC) sensitizers carrying two conjugated donors and two acceptor/anchoring groups is introduced. The approach leads to significantly different optical properties and enhanced stability

with respect to related di- and monobranched dyes and yields power conversion efficiencies of up to 5.05 %, which is possibly limited by the computed nonoptimal dye packing on the semiconductor surface.

### Introduction

Solar energy has not yet found widespread use due to the high cost of crystalline silicon panels, which are not competitive with electricity generated from fossil fuels.<sup>[1]</sup> Among the new approaches to solar energy conversion, dye-sensitized solar cells (DSCs) have one of the best potential for high conversion efficiency and low-cost manufacture.<sup>[2]</sup> One strategic route to improving cell efficiencies involves the optimization of the dye-sensitizer, which captures photons to generate an electron/hole pair at the interface with the inorganic semiconductor (TiO<sub>2</sub>) and the redox electrolyte, respectively. The Ru<sup>II</sup> complex bis(2,2'-bipyridyl-4,4'-dicarboxylate)ruthenium(II) (N719)<sup>[3]</sup> is the most representative DSC sensitizer, with power conversion efficiencies exceeding 11 %.<sup>[4]</sup>

One of the main drawbacks of Ru<sup>II</sup>-bipyridyl complexes is the modest molar absorptivity of the low-energy absorption band (14200 M<sup>-1</sup>cm<sup>-1</sup> at 530 nm for N719),<sup>[3]</sup> which hinders larger photocurrent densities and thus improved efficiencies.<sup>[5]</sup> In the last years, metal-free organic dyes have been proposed as alternative sensitizers to circumvent this problem.<sup>[6]</sup> Organic dyes are readily available, easier to purify, are relatively inexpensive to manufacture, and, most of

all, are associated with an extended structural variety that can be adjusted to optimize the spectral absorption properties. Although their efficiencies are still lower than those of ruthenium sensitizers, very recently, values approaching, or even exceeding, 10% have been reported, showing the great potential of the new design.<sup>[7]</sup> The design of these efficient chromophores, in analogy with most organic sensitizers, has been based on a dipolar D- $\pi$ -A structural motif, where "D" is an electron-rich group, " $\pi$ " is a conducting bridge, and "A" an electron-poor moiety embedding the COOH anchoring functionality for grafting onto the TiO<sub>2</sub> surface. Triarylamine has been by far the most widely used D core.<sup>[8]</sup>

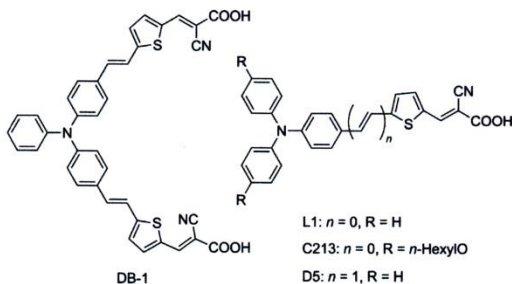
In the search for improved optical and structural properties, we,<sup>[9]</sup> and others,<sup>[10,11]</sup> have recently introduced a novel model class of dibranched dianchoring organic sensitizers composed of one donor and two anchoring groups (A- $\pi$ -D- $\pi$ -A). We have shown that the dibranched dye DB-1 (Scheme 1) offers improved optical properties (higher molar extinction coefficients and red-shifted absorption), increased photocurrent, and enhanced stability compared to its monobranched analogues.<sup>[9]</sup> Recently, a porphyrin pos-

[a] Department of Materials Science and Milano-Bicocca Solar Energy Research Center-MIB-Solar, Via Cozzi 53, 20125, Milano, Italy  
Fax: +39-02-64485400  
E-mail: alessandro.abbotto@mater.unimib.it

[b] Istituto CNR di Scienze e Tecnologie Molecolari (CNR-ISTM), Department of Chemistry, University of Perugia, Via Elce di Sotto 8, 06123, Perugia, Italy  
E-mail: filippo@thch.unipg.it

[c] Laboratory for Photonics and Interfaces, School of basic Sciences, Swiss Federal Institute of Technology, 1015 Lausanne, Switzerland  
E-mail: mdkhaja.nazeeruddin@epfl.ch

Supporting information for this article is available on the WWW under <http://dx.doi.org/10.1002/ejoc.201100821>.



Scheme 1. Reference photosensitizers.

sessing two anchoring groups has been successfully applied to DSC with a power conversion efficiency comparable to that of N719 under the same conditions.<sup>[12]</sup>

Here, we present an extension of this design, aimed at further expanding the possibility of improving the optical and energetic properties of the sensitizers. The new approach, based on a  $A-\pi-D-\pi'-D-\pi-A$  tribranched structural motif (where  $\pi'$  is other than  $\pi$ ), implies the use of two donor and two acceptor/anchoring fragments and different  $\pi$  spacers, as pictorially depicted in Figure 1. Generally speaking, the tribranched approach should allow a much larger structural variety with respect both to the  $D-\pi-A$  (Figure 1a) and  $A-\pi-D-\pi-A$  (Figure 1b) motifs due to the presence of two donor and two acceptor groups and three  $\pi$ -spacers. All of these constituent units can be fruitfully selected and combined to finely tune the donor and acceptor strength,  $\pi$ -framework extension and, ultimately, the optical, energetic, and photovoltaic response of the sensitizers.

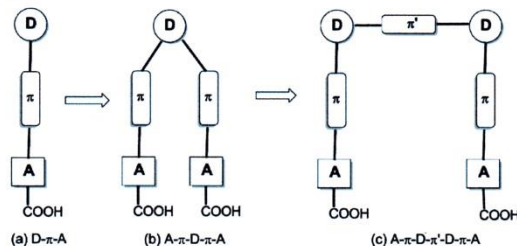
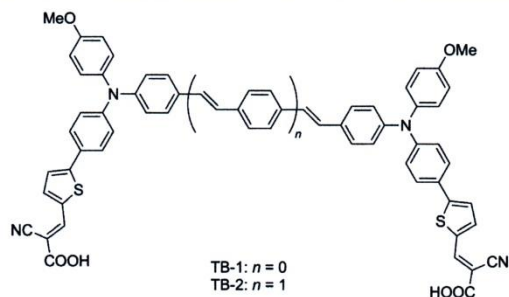


Figure 1. Schematic representation of monobranched  $D-\pi-A$ , dibranched  $A-\pi-D-\pi-A$ , and tribranched  $A-\pi-D-\pi'-D-\pi-A$  (this work) structural motifs.

To design the new tribranched prototypes, we selected some of the most common donor and  $\pi$ -spacer groups. Namely, as donor cores we have adapted the common triarylamino group<sup>[8]</sup> by using the *trans*-4,4'-bis(diarylamino)-stilbene and *trans*-4,4'-bis(diarylamino)distyrylbenzene building blocks. The simple thiophene-based  $\pi-A-COOH$  arm of L1<sup>[13]</sup> and C213<sup>[14]</sup> (Scheme 1), which we previously chose as reference monobranched dyes, and which have been used in other previously reported sensitizers,<sup>[15,16]</sup> was selected as a side-branch. Based on these premises, we designed the tribranched dyes TB-1 and TB-2 (Scheme 2).



Scheme 2. Investigated tribranched organic sensitizers.

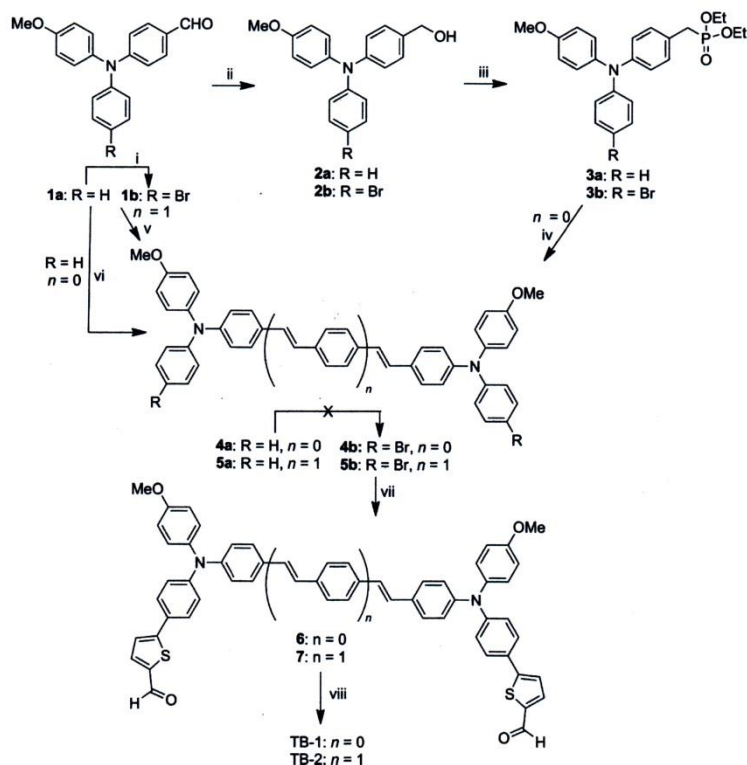
Here, we wish to report the fabrication of DSCs with the novel sensitizers, and to disclose their photoelectrochemical properties and stability data, which were measured under various conditions. DFT/TDDFT calculations have been performed in order to highlight the main properties associated with the tribranched geometry, both in solution and on  $TiO_2$  models.

## Results and Discussion

### Synthesis, Spectroscopic, and Electrochemical Characterization

TB-1 and TB-2 were synthesized according to Scheme 3. 4-[*N*-(4-Methoxyphenyl)-*N*-phenylamino]benzaldehyde (**1a**)<sup>[17]</sup> was brominated in high yields to **1b** using *N*-bromosuccinimide (NBS) in anhydrous *N,N*-dimethylformamide (DMF) while keeping the temperature between  $-5$  and  $0$  °C. At temperatures below  $-10$  °C the yields were much more modest (less than 50%) whereas at higher temperatures ( $0$  °C to r.t.) a complex mixture of brominated products was recovered. After reduction to the corresponding brominated alcohol **2b**, the phosphonate **3b** was directly prepared in one step with  $I_2$ , using  $P(OEt)_3$  as a solvent. Horner–Wittig condensation between diethyl methylphosphonate **3b** and aldehyde **1b** afforded the electron-rich brominated *trans*-4,4'-bis(diarylamino)stilbene intermediate **4b**. Similarly *p*-phenylenevinyllogue derivative **5b** was prepared using tetraethyl 1,4-phenylenebis(methylene)diphosphonate<sup>[18]</sup> and two equivalents of aldehyde **1b**. It should be noted that aromatic bromination of the corresponding precursors **4a** and **5a**, which were obtained in a similar manner to that described above from **1a** and **3a**, always lead to complex mixtures of mono- and polybrominated derivatives, regardless of reaction conditions. Unfortunately, this result prevented us from fully exploiting the high-yielding McMurry reaction of **1a**, which easily allowed the isolation of gram-quantities of **4a** in only one step. The two bromoderivatives **4b** and **5b** were then submitted to the same reaction sequence, involving the microwave-mediated Suzuki coupling reaction with 5-formyl-2-thienylboronic acid<sup>[13]</sup> to give the corresponding 2-thiophenecarbaldehydes **6** and **7**. The final Knoevenagel condensation step with cyanoacetic acid and piperidine, under microwave irradiation (which led to improved yields), afforded the corresponding piperidinium carboxylate derivatives of TB-1 and TB-2. The corresponding carboxylic acids were then isolated after treatment with saturated aqueous  $NH_4Cl$ .

The absorption and emission spectra of TB-1 and TB-2 are shown in Figure 2. The main optical parameters, together with those of reference mono- and dibranched dyes, are collected in Table 1. Both TB-1 and TB-2 present two bands in the visible region. Comparison with the absorption peak of the corresponding 4,4'-bis(diarylamino)stilbene **4a** and bis(diarylamino)distyrylbenzene **5a** building blocks (393 and 415 nm in  $CH_2Cl_2$ , respectively) shows that the higher energy visible band (393 and 421 nm in  $CH_2Cl_2$  for TB-1 and TB-2, respectively) is attributed to a local



Scheme 3. Synthesis of TB-1 and TB-2. Reagents and conditions: (i) NBS, DMF,  $-5$  to  $0$  °C, 3 h; (ii)  $\text{NaBH}_4$ , EtOH,  $0$  °C to r.t.; (iii)  $\text{I}_2$ ,  $\text{P}(\text{OEt})_3$ ,  $0$  °C to r.t.; (iv)  $n = 0$ , **1a** or **1b**,  $t\text{BuOK}$ , THF,  $0$  °C to r.t.; (v)  $n = 1$ , tetraethyl 1,4-phenylenebis(methylene)diphosphonate,  $t\text{BuOK}$ , THF,  $0$  °C to r.t.; (vi)  $\text{TiCl}_4$ , Zn, pyridine, THF; (vii) 5-formyl-2-thienylboronic acid,  $[\text{Pd}(\text{dppf})\text{Cl}_2]$ ,  $\text{K}_2\text{CO}_3$ , MeOH/toluene,  $70$  °C, 10 min, microwave irradiation; (viii) cyanoacetic acid, piperidine, EtOH or toluene,  $100$  °C, microwave irradiation followed by  $\text{NH}_4\text{Cl}$ .

transition of the donor core (see the Supporting Information, Figure S1), whereas the lower energy band is associated to the  $\pi$ - $\pi^*$  intramolecular charge transfer (CT) tran-

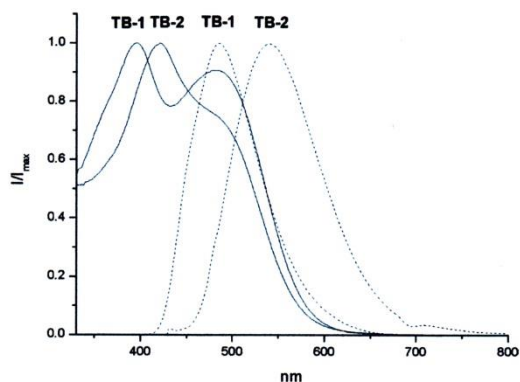


Figure 2. Normalized absorption (solid line) and emission (dashed line) spectra of TB-1 and TB-2 in DMSO.

sition from the electron-rich bis(diarylamino) moieties to the 2-cyanoacrylic acid acceptor end-groups. Indeed, the absorption peaks are almost identical in the two dyes, as a consequence of the presence of the same donor-acceptor side arm. Upon addition of a small amount of HCl, the spectrum remains unchanged, confirming that both dyes are present as carboxylic acids.<sup>[9]</sup> This picture was con-

Table 1. Absorption and emission parameters of TB-1 and TB-2 compared to reference dyes.

Compound	$\lambda_{\text{abs}} / \text{nm}$ ( $\epsilon / \text{M}^{-1} \text{cm}^{-1}$ )	$\lambda_{\text{em}} / \text{nm}$ ( $\Phi$ ) <sup>[a]</sup>
TB-1 <sup>[b]</sup>	397 (40 900)	485 (0.058) <sup>[c]</sup>
	478 (35 800)	
TB-2 <sup>[b]</sup>	421 (54 000)	540 (0.013) <sup>[d]</sup>
	480 (40 200)	
DB-1 <sup>[e]</sup>	494 (44 500)	
L1 <sup>[f]</sup>	410 (25 800)	549
C213 <sup>[g]</sup>	482 (27 500)	660

[a] Fluorescence quantum yield; Coumarin 540A was used as a standard (0.58 in EtOH). [b] This work (DMSO). [c]  $\lambda_{\text{exc}} = 397$  nm. [d]  $\lambda_{\text{exc}} = 421$  nm. [e] Ref.<sup>[9]</sup> (EtOH). [f] Ref.<sup>[13]</sup> (*tert*-butyl alcohol/acetonitrile, 1:1). [g] Ref.<sup>[14]</sup> (THF).

firmed by investigating the emission properties. Excitation at  $\lambda_{\text{max}}$  produced fluorescence spectra that were different in TB-1 and TB-2, according to their different donor cores, and resembled those of **4a** (473 nm in  $\text{CH}_2\text{Cl}_2$ ) and **5a** (504 nm in  $\text{CH}_2\text{Cl}_2$ ), respectively.

The donor–acceptor CT band of the tribranched dyes is hypsochromically shifted with respect to the monobranched dye C213, although the former chromophores have a more extended  $\pi$ -conjugated system. At the same time, TB-1 and TB-2 present a significant hyperchromic effect, likely for the same reason. Similar, albeit less pronounced, hypsochromic effects are observed when the optical properties of the tribranched dyes are compared with those of the dibranched sensitizer DB-1. In conclusion, the tribranched geometry induces a negligible blueshift but a substantial increase in absorbance with respect to mono- and dibranched dyes. In addition, a second and more intense visible band at higher energy is present due to local transitions of the donor core, thus enabling more efficient sunlight harvesting in this region.

The electrochemical properties of TB-1 and TB-2 were examined by cyclic voltammetry in dimethylformamide (DMF). Using a glassy carbon working electrode, Pt counter electrode, and 0.05 M tetrabutylammonium hexafluorophosphate [ $\text{TBA}(\text{PF}_6)$ ] as a supporting electrolyte, the potentials measured vs.  $\text{Fc}^+/\text{Fc}$  were converted into normal hydrogen electrode (NHE) potentials by addition of +0.63 V. TB-1 and TB-2 showed half-wave potentials corresponding to molecular oxidation potentials at +0.91 and +0.98 V vs. NHE, respectively. Their reduction potentials were detected at –0.87 and –0.97 V vs. NHE, respectively. By using the value of –4.5 eV vs. vacuum for NHE,<sup>[19]</sup> the HOMO/LUMO energies were calculated as –5.4/–3.6 and –5.5/–3.5 eV for TB-1 and TB-2, respectively.

### Computational Investigation

To investigate the electronic structure of the representative TB-1 standalone dye and in relation to its constituent subunits, DFT/TDDFT calculations were performed on TB-1 and on the monobranched L1 and C213 systems. As shown in Figure 3, in which the energy levels of the Molecular Orbitals (MOs) are reported, the introduction of the  $\pi$  conjugated bridge linking the two monobranched subunits, induces a significant perturbation (mixing) among the occupied MOs. The strong mixing among the highest occupied MOs of the isolated building blocks is also evident by looking at the plots of the HOMO, HOMO–1, HOMO–2, LUMO, LUMO+1, and LUMO+2 of TB-1 reported in Figure 4. Taking the C213 dye as a reference monobranched unit, it can be seen that the HOMO, which is located at –5.90 eV in C213, is split in the tribranched system into three levels: the HOMO at –5.77 eV [mainly localized on the donor *trans*-4,4'-bis(diarylamino)stilbene core], the HOMO–1 at –6.18 eV (essentially extended on the two monobranched units), and the HOMO–2 at 6.91 eV (resulting from the strong mixing of the MOs of the linker and

of the C213 blocks). As expected, the interaction between the virtual orbitals is less pronounced, with the quasi-degenerate LUMO and LUMO+1, being the combinations of the LUMOs on the two monobranched units, and the LUMO+2 localized on the linking  $\pi$  bridge. Although a comparison between experimental electrochemical potentials and calculated HOMO/LUMO energy levels is not straightforward, we notice a rather good agreement between the calculated and experimental HOMO energy, whereas the calculated LUMO is substantially less negative than the electrochemical estimate. This is due to the employed exchange–correlation functional, which contains a large percentage of Hartree–Fock exchange (ca. 42%), but which, however, allows us to nicely reproduce the optical properties of the dyes.

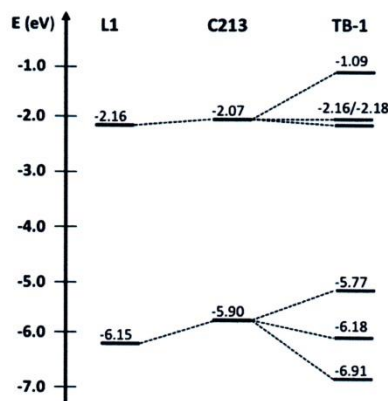


Figure 3. Molecular orbital levels of L1, C213, and TB-1. The values were computed in the gas phase at the MPWIK/6-31G\* level.

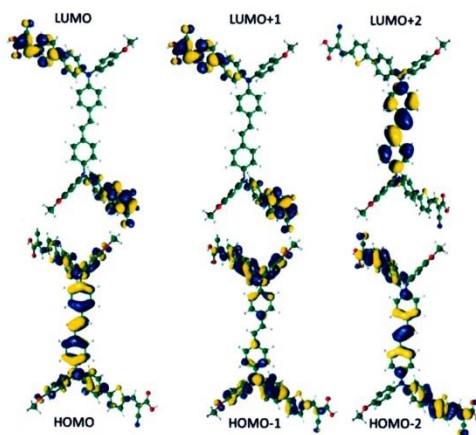


Figure 4. Isodensity surfaces of the HOMO, HOMO–1, HOMO–2, LUMO, LUMO+1, and LUMO+2 of TB-1.

The effect of the geometry of the tribranched dyes on the optical properties of the sensitizer is shown in Table 2, in which the lowest excitation energies and the corresponding oscillator strengths of the three dyes in the gas phase are compared. As could be expected on the basis of the molecular orbital energy diagram depicted in Figure 3, the lowest absorption peak moves to longer wavelengths on going from L1 to C213 as a consequence of HOMO destabilization induced by the two electron-donor hexyloxy substituents, coupled to only a slight LUMO energy upshift. Comparison of the calculated values with the experimentally determined band maxima is not straightforward because the deprotonated dye was measured for L1, whereas the protonation state of C213 is not clear. However, because protonation/deprotonation can shift the absorption maxima by up to 0.3 eV,<sup>[20]</sup> the data presented here can be considered to be in good overall agreement with the experimental values. An absorption maximum of 479 nm was calculated for C213, which can be compared with the 482 nm experimental value. For the protonated dye L1, a 461 nm absorption maximum was calculated, which can be compared to the 404 nm maximum measured for the deprotonated dye.

Table 2. Computed lowest excitation wavelengths and oscillator strengths in the gas phase and DMSO solution for TB-1, L1, and C213.

Compound	$\lambda_{\text{abs}}$ / nm vacuum/DMSO	Oscillator strength vacuum/DMSO
TB-1	457/495	1.940/1.903
L1	421/461	1.228/1.316
C213	436/479	1.222/1.316

In the tribranched structure, the computed lowest absorption band is slightly red-shifted compared with C213 both in vacuo and in solution, with an oscillator strength almost 70% larger than that of the monobranched systems. The calculated value in solution (495 nm) is in excellent agreement (within 0.1 eV) with the 478 nm experimental data. The lowest energy and most intense transition of TB-1 turns out to be a mixing of HOMO  $\rightarrow$  LUMO (65%), HOMO-1  $\rightarrow$  LUMO+1 (20%), and HOMO  $\rightarrow$  LUMO+2 (5%) orbital excitations. The mixed nature of the main TB-1 optical transition is responsible for the modest redshift computed for this system compared with C213 [495 vs. 479 nm in dimethyl sulfoxide (DMSO) solution], despite the sizeable reduction of the HOMO-LUMO gap computed for TB-1 compared with C213 (3.61 vs. 3.83 eV).

To gain insight into the possible interaction between the newly synthesized TB-1 dye and the nanostructured TiO<sub>2</sub> semiconductor, we examined the optimized geometry of TB-1 and docked the resulting structure (with no further geometry optimization) onto extended TiO<sub>2</sub> models. The optimized structure of TB-1 shows two conformers, a more stable conformer with a *transoid* arrangement of the two branches (Figure 5A) and a less stable conformer (Figure 5B) corresponding to a *cisoid* arrangement of the two branches. The A *transoid* conformer was calculated to be

5.3 kcal/mol more stable than the B *cisoid* conformer, possibly because of the preferential arrangement of the aromatic moieties around the N-terminated bridge.

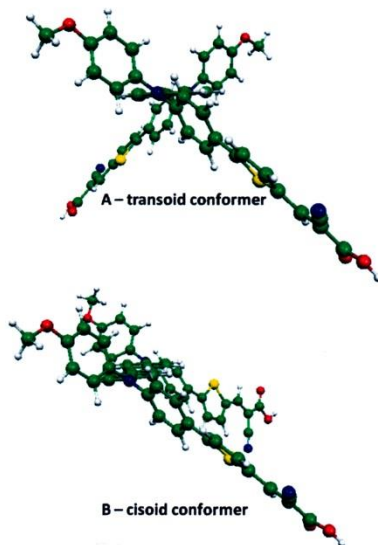


Figure 5. Optimized molecular structures of the A and B TB-1 conformers.

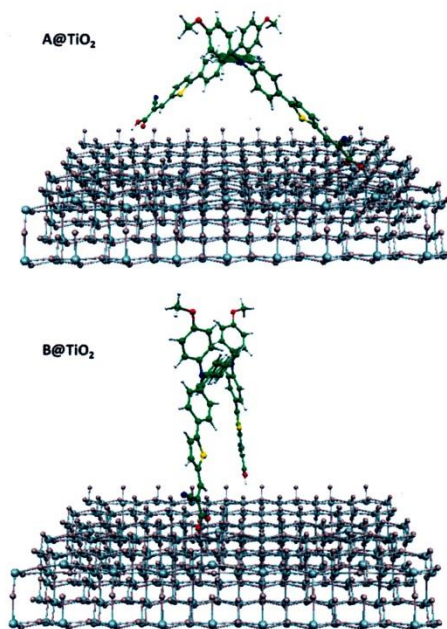


Figure 6. Possible interaction of TB-1 conformers A and B with the TiO<sub>2</sub> substrate.

As can be noticed from Figure 6, the more stable A conformer exhibits a non-optimal interaction with the  $\text{TiO}_2$  surface, which might reduce the dye molecular packing on  $\text{TiO}_2$ , which, in turn, may impact the photovoltaic performance, as discussed below. The less stable B conformer shows better dye packing on  $\text{TiO}_2$ , occupying essentially a similar space to that expected for two single branched dyes. The lower stability in solution, however, might imply that this conformer is present as a minor fraction upon adsorption onto  $\text{TiO}_2$ .

### Photovoltaic Investigation in DSCs

The new sensitizers, TB-1 and TB-2, were used to fabricate DSCs to explore the current–voltage characteristics. The incident monochromatic photon-to-current conversion efficiency (IPCE) of TB-1 plotted as a function of excitation wavelength exhibits a high value at plateau (81%) and more than 70% from 400 to 560 nm (Figure 7). In contrast, although exhibiting a photoelectrochemical response in a similar wavelength range, the IPCE of TB-2 showed a slightly lower maximum value of 75%. The integrated current under the IPCE curve is 10.8 and 9.5  $\text{mA cm}^{-2}$ , for TB-1 and TB-2, respectively, which is consistent with the photocurrent of solar cells under standard global AM 1.5 solar conditions (see below). The main photovoltaic parameters are shown in Figure 8 and Table 3. The TB-1 cell showed a 10.9  $\text{mA cm}^{-2}$  short circuit current density ( $J_{\text{sc}}$ ), 641 mV of open circuit voltage ( $V_{\text{oc}}$ ), and 72.5% fill factor ( $ff$ ) at standard global AM 1.5 solar conditions. Thus, the TB-1 power conversion efficiency  $\eta$ , derived from the equation  $\eta = J_{\text{sc}} \times V_{\text{oc}} \times ff$ , is 5.05%. Under similar conditions, the TB-2 cell performance showed a  $J_{\text{sc}}$  value of 9.65  $\text{mA cm}^{-2}$ , 662 mV  $V_{\text{oc}}$ , and a fill factor of 70.6, resulting in a power conversion efficiency ( $\eta$ ) of 4.51%. The different  $J_{\text{sc}}$  value is consistent with the estimate obtained by IPCE integration. All devices showed a very linear response of  $J_{\text{sc}}$  and a slightly higher  $ff$  under a lower light intensity (see Table 3).

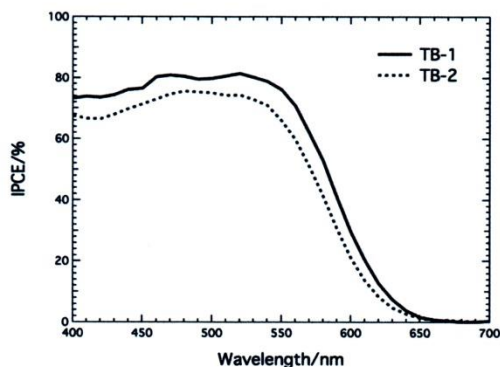


Figure 7. Photocurrent action spectra of TB-1 and TB-2 DSCs.

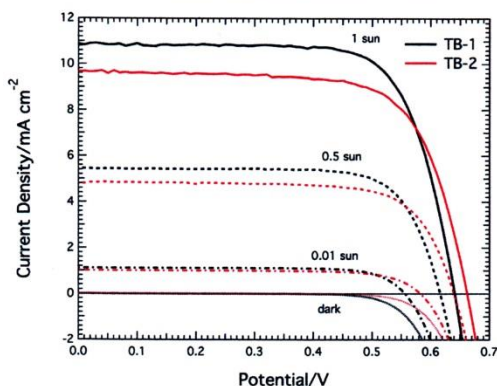


Figure 8. The  $J/V$  characteristics of DSCs based on TB-1 and TB-2 under various light intensities.

Table 3. Photovoltaic parameters of TB-1 and TB-2 compared with reference dyes.

Compound	$I_0$ / sun	$J_{\text{sc}}$ / $\text{mA cm}^{-2}$	$V_{\text{oc}}$ / V	$FF$ / %	$\eta$ / %
TB-1	1	10.9	641	72.5	5.05
	0.5	5.45	616	74.5	5.01
	0.10	1.10	558	76.6	4.75
TB-2	1	9.65	662	70.6	4.51
	0.5	4.84	640	72.6	4.50
	0.10	0.99	584	73.6	4.30
L1 <sup>[13]</sup>	1	5.42	735	69	2.75
	1	12.8	620	66	5.20
C213 <sup>[14]</sup>	1	11.9	775	74.7	6.88

It is interesting to compare the photovoltaic data obtained for TB-1 and TB-2 with the previously reported device data obtained for the related L1 and C213 dyes. A survey of such data is reported in Table 3, showing that the difference between TB-1 and the better performing C213 is mainly related to an approximate 20% increase in  $V_{\text{oc}}$  obtained for the latter, which, together with a 9% (3%) increase in  $J_{\text{sc}}$  ( $ff$ ), provides an overall 36% increase in  $\eta$ . The incorporated long alkoxy chain in C213 could also justify the higher  $V_{\text{oc}}$ . Indeed, Hagberg et al. have recently shown a correlation between  $V_{\text{oc}}$  and bulky butoxy chains.<sup>[16]</sup> A similarly higher  $V_{\text{oc}}$  is obtained for L1, despite the fact that a larger amount of LiI (0.1 and 0.05 M, respectively) was used than in the present investigation (0.05 M).<sup>[13,14]</sup> Thus, it is quite unlikely that the reduced  $V_{\text{oc}}$  value obtained with TB-1 and TB-2 is due to the composition of the electrolyte, which renders the higher  $J_{\text{sc}}$ . We could speculate that the unfavorable interaction with  $\text{TiO}_2$  discussed on the basis of the structural parameters of the dye is responsible for the lower  $V_{\text{oc}}$ , whereby the non-optimal dye packing on the semiconductor surface would allow the oxidized species in the electrolyte to approach the surface, thus increasing recombination between electrons injected into  $\text{TiO}_2$  and the electrolyte. However, we did not observe increased recombination rates in TB-1 and TB-2 when compared with mono-



branched dye D5 (see the Supporting Information, Figure S6).<sup>[21]</sup> Moreover, the measured dye loadings<sup>[22]</sup> of TB-1 ( $4.8 \times 10^{-8} \text{ mol cm}^{-2}$ ) and TB-2 ( $4.1 \times 10^{-8} \text{ mol cm}^{-2}$ ) on 3- $\mu\text{m}$   $\text{TiO}_2$  films were 96 and 82% with respect to that of monobranched dye D5 ( $4.1 \times 10^{-8} \text{ mol cm}^{-2}$ ) under same conditions. In other words, neither overloaded dyes nor fast recombination were observed in TB-1 and TB-2.

We previously reported that dibranched dyes, having two anchoring groups, showed good stability data when employed in DSCs.<sup>[9]</sup> It was thus interesting to test the temporal stability of DSCs fabricated with the new TB-1 and TB-2 dyes. Figure 9 shows the photovoltaic performance changes during a long-term accelerated ageing of TB-1 and TB-2 sensitized solar cells using an ionic liquid electrolyte (1,3-dimethylimidazoliumiodide/1-ethyl-3-methylimidazoliumiodide/1-ethyl-3-methylimidazolium tetracyanoborate/iodine/*N*-butylbenzimidazole/guanidinium thiocyanate with molar ratio 12:12:16:1.67:3.33:0.67) under light soaking at full intensity ( $100 \text{ mW cm}^{-2}$ ) at  $60^\circ\text{C}$ . Values for  $J_{\text{sc}}$ ,  $V_{\text{oc}}$ ,  $ff$ , and  $\eta$  were recorded over a period of 1000 h. The overall efficiencies of TB-1 and TB-2 remained at 88 and 74% of the initial value, respectively, after light soaking. These stabilities are an improvement over our previously reported dibranched dye DB-1, which exhibited a 67% residual value. The  $J_{\text{sc}}$  values of both TB-1 and DB-2 showed a drop at the initial ageing stage but recovered after 300 h of ageing. The reason for this drop of  $J_{\text{sc}}$  is not clear at this stage. The losses in  $\eta$  are mainly caused by the drop in  $V_{\text{oc}}$ , namely 68 and 55 mV for TB-1 and TB-2, respectively,

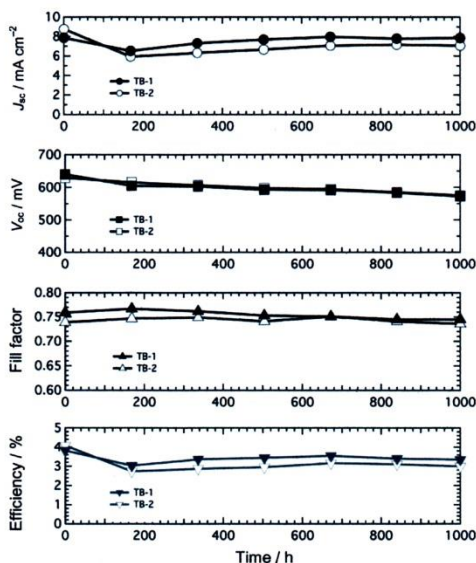


Figure 9. Photovoltaic parameter ( $J_{\text{sc}}$ ,  $V_{\text{oc}}$ ,  $ff$ , and  $\eta$ ) variations with ageing time for the devices sensitized with TB-1 (closed symbols) and TB-2 (open symbols) based on ionic liquid electrolyte during successive light soaking for 1000 h.

which is likely caused by protonation processes that take place during light soaking, leading to a positive shift of the  $\text{TiO}_2$  band edge.<sup>[23]</sup>

## Conclusions

We have introduced a novel design based on tribranched organic sensitizers, carrying two donors, two acceptors, three  $\pi$  spacers, and two anchoring points. Such molecular architecture should provide more variety in the sensitizer chemical structure, allowing further structural optimization that can be tailored to achieve the desired properties. Comparison of DSCs based on the tribranched dyes TB-1 and TB-2 with the corresponding monobranched system C213 shows a decrease in power conversion efficiency, mainly due to lower photovoltages in the former system. This was ascribed to the selected electrolyte for higher photocurrents, and to the computed non-optimal interaction with the  $\text{TiO}_2$  surface, which might reduce the molecular packing of the dye and favor detrimental recombination between the semiconductor and oxidized electrolyte. However, it should be noted that the twisted structure of the adsorbed *transoid* conformer is particularly suitable for efficient interaction with the chemisorption sites, for which a distance of 10.2 Å was measured.<sup>[24]</sup> Furthermore, such adsorption geometry inhibits aggregation as a result of steric hindrance. Indeed, the efficiency stabilities of DSCs based on TB-1 and TB-2 after light soaking are improved with respect to dibranched DB-1, which, in turn, offers increased stability with respect to the corresponding monobranched dyes.<sup>[9]</sup> Although the two first prototypes did not offer improved power conversion efficiencies with respect to the conventional uni-dimensional design, we believe that the tribranched design could trigger the development of optimized systems through the incorporation of appropriate new branches.

## Experimental Section

**General:** NMR spectra were recorded with a Bruker AMX-500 spectrometer operating at 500.13 MHz ( $^1\text{H}$ ). Coupling constants are given in Hz. High resolution mass spectra (HRMS) were recorded with a Bruker Daltonics ICR-FTMS APEX II spectrometer equipped with an electrospray ionization (ESI) source. Flash chromatography was performed with Merck grade 9385 silica gel 230–400 mesh (60 Å). Reactions were performed under nitrogen in oven-dried glassware and monitored by thin layer chromatography using UV light (254 and 365 nm) as a visualizing agent. All reagents were obtained from commercial suppliers at the highest purity grade and used without further purification. Anhydrous solvents were purchased from Sigma-Aldrich and used without further purification. Toluene and MeOH were dried with  $\text{CaCl}_2$  and  $\text{MgSO}_4$ , respectively. Extracts were dried with  $\text{Na}_2\text{SO}_4$  and filtered before removal of the solvent by evaporation. Melting points are uncorrected. Absorption spectra were recorded with a V-570 Jasco spectrophotometer. Emission spectra were recorded with a FP6200 Jasco spectrofluorometer. Fluorescence spectra were collected by exciting at the maximum of absorption. Fluorescence quantum yields  $\Phi$  were recorded by using the relative comparative method with a standard sample of known  $\Phi$  value and optically dilute solu-

tions.<sup>[25]</sup> Coumarin 540A in EtOH ( $\Phi = 0.58$ ) was used to estimate fluorescence quantum yields.<sup>[26]</sup> The absorbance at excitation wavelengths were kept below 0.1. Refractive index (DMSO 1.477, EtOH 1.359) corrections were included in order to account for the different solvents of the test and the reference solutions. Infrared spectra (IR) were recorded with an ATR-FTIR Perkin–Elmer Spectrum 100 spectrometer.

**4-[*N*-(4-Bromophenyl)-*N*-(4-methoxyphenyl)amino]benzaldehyde (1b):** A solution of NBS (0.65 g, 3.63 mmol) in anhydrous DMF (3 mL) was slowly added to a stirred solution of 4-[*N*-(4-methoxyphenyl)-*N*-phenylamino]benzaldehyde (**1a**)<sup>[17]</sup> (1.00 mg, 3.30 mmol) in the same solvent (10 mL). The solution was kept at  $-5$  to  $0$  °C for 3 h. The reaction mixture was poured into water (50 mL) and the formation of a yellow precipitate was observed. The solid was filtered under reduced pressure to yield the pure product (1.12 g, 2.93 mmol, 89%) as a green gummy solid. <sup>1</sup>H NMR ([D<sub>6</sub>]DMSO):  $\delta = 9.77$  (s, 1 H), 7.72 (d,  $J = 8.8$  Hz, 2 H), 7.56 (d,  $J = 8.8$  Hz, 2 H), 7.18 (d,  $J = 8.9$  Hz, 2 H), 7.13 (d,  $J = 8.8$  Hz, 2 H), 7.02 (d,  $J = 8.9$  Hz, 2 H), 6.87 (d,  $J = 8.7$  Hz, 2 H), 3.78 (s, 3 H) ppm.

**4-[*N*-(4-Methoxyphenyl)-*N*-phenylamino]benzyl Alcohol (2a):** A solution of NaBH<sub>4</sub> (0.22 g, 5.81 mmol) in THF (15 mL) was added to an ice-cold and stirred solution of **1a** (1.48 g, 4.88 mmol) in the same solvent (25 mL). The mixture was warmed to r.t. and stirred overnight. The solvent was partially evaporated under reduced pressure, then Et<sub>2</sub>O (15 mL) and water (30 mL) were added. After separating the organic phase, the aqueous layer was extracted with Et<sub>2</sub>O (3  $\times$  15 mL). The combined organic phases were dried and the solvent evaporated to afford the product as a yellow waxy solid (1.45 g, 4.75 mmol, 97%). <sup>1</sup>H NMR (CDCl<sub>3</sub>):  $\delta = 7.24$ – $7.19$  (m, 4 H), 7.06 (d,  $J = 8.9$  Hz, 2 H), 7.03 (d,  $J = 7.5$  Hz, 2 H), 7.02 (d,  $J = 8.4$  Hz, 2 H), 6.96 (t,  $J = 7.3$  Hz, 1 H), 6.84 (d,  $J = 8.9$  Hz, 2 H), 3.80 (s, 3 H) ppm.

**4-[*N*-(4-Bromophenyl)-*N*-(4-methoxyphenyl)amino]benzyl Alcohol (2b):** A solution of NaBH<sub>4</sub> (0.23 g, 6.15 mmol) in EtOH (15 mL) was added to an ice-cold and stirred solution of **1b** (1.96 g, 5.13 mmol) in the same solvent (50 mL). The mixture was warmed to r.t. and stirred overnight. Et<sub>2</sub>O (15 mL) and water (30 mL) were then added, the organic phase was separated, and the aqueous layer was extracted with Et<sub>2</sub>O (3  $\times$  15 mL). The combined organic phases were dried and the solvent was evaporated. The product was obtained as a yellow waxy solid (1.21 g, 3.14 mmol, 61%). <sup>1</sup>H NMR ([D<sub>6</sub>]DMSO):  $\delta = 7.36$  (d,  $J = 8.9$  Hz, 2 H), 7.24 (d,  $J = 8.3$  Hz, 2 H), 7.03 (d,  $J = 8.9$  Hz, 2 H), 6.97 (d,  $J = 8.4$  Hz, 2 H), 6.93 (d,  $J = 8.9$  Hz, 2 H), 6.78 (d,  $J = 8.9$  Hz, 2 H), 5.11 (t,  $J = 5.5$  Hz, 1 H), 4.44 (d,  $J = 5.2$  Hz, 2 H), 3.75 (s, 3 H) ppm.

**Diethyl 4-[*N*-(4-Methoxyphenyl)-*N*-phenylamino]benzylphosphonate (3a):** Alcohol **2a** (1.45 g, 4.75 mmol) was dissolved in P(OEt)<sub>3</sub> (10 mL) at  $0$  °C and I<sub>2</sub> (1.27 g, 5.00 mmol) was added in one pot. The reaction mixture was warmed to r.t. and stirred overnight. The excess of P(OEt)<sub>3</sub> was distilled off under reduced pressure and the pure product was obtained after filtration through silica gel (*n*-hexane to AcOEt/petroleum ether, 8:2) as a clear oil (1.24 g, 2.91 mmol, 62%). <sup>1</sup>H NMR (CDCl<sub>3</sub>):  $\delta = 7.19$  (t,  $J = 8.5$  Hz, 2 H), 7.13 (dd,  $J = 8.6$ , 2.5 Hz, 2 H), 7.04 (d,  $J = 8.9$  Hz, 2 H), 7.00 (d,  $J = 7.6$  Hz, 2 H), 6.97 (d,  $J = 8.0$  Hz, 2 H), 6.92 (t,  $J = 7.3$  Hz, 1 H), 6.82 (d,  $J = 8.9$  Hz, 2 H), 4.06 (quintet,  $J = 7.1$  Hz, 4 H), 3.79 (s, 3 H), 3.08 (d,  $J = 21.3$  Hz, 2 H), 1.26 (t,  $J = 7.1$  Hz, 6 H) ppm.

**Diethyl 4-[*N*-(4-Bromophenyl)-*N*-(4-methoxyphenyl)amino]benzylphosphonate (3b):** Alcohol **2b** (1.21 g, 3.14 mmol) was dissolved in P(OEt)<sub>3</sub> (10 mL) at  $0$  °C and I<sub>2</sub> (0.96 g, 3.78 mmol) was added

in one pot. The reaction mixture was warmed to r.t. and stirred overnight. The excess of P(OEt)<sub>3</sub> was distilled off under reduced pressure and the pure product was obtained after filtration through silica gel (*n*-hexane to EtOH), as a clear oil (1.50 g, 2.98 mmol, 94%). <sup>1</sup>H NMR ([D<sub>6</sub>]DMSO):  $\delta = 7.37$  (d,  $J = 8.9$  Hz, 2 H), 7.19 (dd,  $J = 8.5$ , 2.3 Hz, 2 H), 7.03 (d,  $J = 8.8$  Hz, 2 H), 6.94 (d,  $J = 8.8$  Hz, 4 H), 6.69 (d,  $J = 8.8$  Hz, 2 H), 4.01 (quintet,  $J = 8.2$  Hz, 4 H), 3.75 (s, 3 H), 3.16 (d,  $J = 21.3$  Hz, 2 H), 1.25 (t,  $J = 7.1$  Hz, 6 H) ppm.

#### *p,p'*-Bis[*N*-(4-methoxyphenyl)-*N*-phenylamino]stilbene (4a)

**Route A (Scheme 3, step iv):** *t*BuOK (0.18 g, 1.60 mmol) was added to an ice-cold and stirred solution of diethyl benzylphosphonate **3a** (0.48 g, 1.12 mmol) in THF (20 mL). After 30 min, a solution of benzaldehyde **1a** (0.34 g, 1.12 mmol) in the same solvent (10 mL) was added dropwise and the resulting mixture was stirred at r.t. for 24 h. The solvent was partially evaporated under reduced pressure, then AcOEt (20 mL) and water (50 mL) were added. After collecting the organic phase, the aqueous layer was extracted with AcOEt (3  $\times$  20 mL), and the combined organic phases were dried and the solvent was evaporated under reduced pressure to afford an orange oil, which was submitted to flash chromatography (Et<sub>2</sub>O/cyclohexane, 3:7). The pure product was obtained as a yellow-orange solid (0.14 g, 0.24 mmol, 22%), m.p. 161–162 °C. <sup>1</sup>H NMR (CDCl<sub>3</sub>):  $\delta = 7.30$  (d,  $J = 8.6$  Hz, 4 H), 7.22 (t,  $J = 7.5$  Hz, 4 H), 7.08 (d,  $J = 8.9$  Hz, 4 H), 7.06 (d,  $J = 8.6$  Hz, 4 H), 6.99 (d,  $J = 8.1$  Hz, 4 H), 6.95 (t,  $J = 7.3$  Hz, 2 H), 6.91 (s, 2 H), 6.85 (d,  $J = 8.9$  Hz, 4 H), 3.81 (s, 6 H) ppm.

**Route B (Scheme 3, step vi):** Zn (2.16 g, 32.9 mmol) was suspended in anhydrous THF (50 mL) and the suspension was cooled to  $-20$  °C. TiCl<sub>4</sub> (3.13 g, 16.5 mmol) was added dropwise (formation of a yellow precipitate was observed). The suspension was heated to reflux for 30 min (gradual darkening was observed). The mixture was cooled to  $-15$  °C and a solution of benzaldehyde **1a** (2.50 g, 8.2 mmol) and anhydrous pyridine (1.69 g, 21.4 mmol) in anhydrous THF (20 mL) was added dropwise. The resulting suspension was heated to reflux for 2 h and then poured into a 3:2 mixture of water and CH<sub>2</sub>Cl<sub>2</sub> (100 mL). The dark suspension was filtered through a pad of Celite. The organic phase was separated, extracted with water (3  $\times$  30 mL), dried, and the solvent evaporated under reduced pressure to yield the pure product as a yellow solid (2.00 g, 3.48 mmol, 84%).

***p,p'*-Bis[*N*-(bromophenyl)-*N*-(4-methoxyphenyl)amino]stilbene (4b):** *t*BuOK (0.42 g, 3.70 mmol) was added to an ice-cold and stirred solution of diethyl benzylphosphonate **3b** (1.50 g, 2.97 mmol) in anhydrous THF (20 mL). After 30 min, a solution of aldehyde **1a** (1.22 g, 3.20 mmol) in the same solvent (10 mL) was added dropwise and the resulting mixture was stirred at r.t. for 24 h. The solvent was partially evaporated under reduced pressure, then Et<sub>2</sub>O (20 mL) and water (50 mL) were added. After collecting the organic phase, the aqueous layer was extracted with Et<sub>2</sub>O (3  $\times$  20 mL). The combined organic phases were dried and the solvent evaporated to afford the pure product as a yellow-orange solid (0.99 g, 1.35 mmol, 46%). <sup>1</sup>H NMR ([D<sub>6</sub>]DMSO):  $\delta = 7.60$  (d,  $J = 8.8$  Hz, 4 H), 7.52 (d,  $J = 8.8$  Hz, 4 H), 7.16 (d,  $J = 8.9$  Hz, 4 H), 7.08 (d,  $J = 8.8$  Hz, 4 H), 7.01 (s, 2 H), 7.00 (d,  $J = 8.9$  Hz, 4 H), 6.88 (d,  $J = 8.8$  Hz, 4 H), 3.78 (s, 6 H) ppm.

***p,p'*-Bis[*N*-(4-methoxyphenyl)-*N*-phenylamino]distyrylbenzene (5a):** *t*BuOK (0.11 g, 0.99 mmol) was added to an ice-cold and stirred solution of the tetraethyl 1,4-phenylenebis(methylene)diphosphonate<sup>[18]</sup> (0.15 g, 0.41 mmol) in anhydrous THF (20 mL). After 30 min, a solution of aldehyde **1a** (0.25 g, 0.82 mmol) in the same

solvent (5 mL) was added dropwise and the resulting mixture was stirred at r.t. for 36 h. The solvent was partially evaporated under reduced pressure, then AcOEt (50 mL) and water (100 mL) were added. After collecting the organic phase, the aqueous layer was extracted with AcOEt (3 × 30 mL). The combined organic phases were dried and the solvent was evaporated to afford an orange oil. The crude product was purified by flash chromatography (Et<sub>2</sub>O/cyclohexane, 7:3) to give the product as a yellow-orange solid (0.15 g, 0.22 mmol, 54%). <sup>1</sup>H NMR ([D<sub>6</sub>]DMSO): δ = 7.55 (s, 4 H), 7.48 (d, *J* = 8.9 Hz, 4 H), 7.29 (t, *J* = 8.6 Hz, 4 H), 7.20 (d, *J* = 16.2 Hz, 2 H), 7.08 (d, *J* = 16.2 Hz, 2 H), 7.07 (d, *J* = 9.0 Hz, 4 H), 7.01 (t, *J* = 6.3 Hz, 2 H), 7.00 (d, *J* = 8.4 Hz, 4 H), 6.96 (d, *J* = 9.0 Hz, 4 H), 6.89 (d, *J* = 8.4 Hz, 4 H), 3.90 (s, 6 H) ppm.

***p,p'*-Bis[*N*-(*p*-bromophenyl)-*N*-(4-methoxyphenyl)amino]distyrylbenzene (5b):** *t*BuOK (0.49 g, 4.32 mmol) was added to an ice-cold and stirred solution of the tetraethyl 1,4-phenylenebis(methylene) diphosphonate<sup>[18]</sup> (0.68 g, 1.80 mmol) and **1b** (1.38 g, 3.61 mmol) in anhydrous THF (30 mL). The resulting mixture was stirred at r.t. for 6 h. The solvent was partially evaporated under reduced pressure, then AcOEt (30 mL) and water (50 mL) were added. The combined organic phases were dried and the solvent removed under reduced pressure to afford an orange oil, which was purified by flash chromatography (CH<sub>2</sub>Cl<sub>2</sub>/hexane, 1:1) to give the product as a yellow solid (0.97 g, 1.16 mmol, 65%). <sup>1</sup>H NMR ([D<sub>6</sub>]DMSO): δ = 7.56 (s, 4 H), 7.51 (d, *J* = 8.7 Hz, 4 H), 7.42 (d, *J* = 8.9 Hz, 4 H), 7.22 (d, *J* = 16.3 Hz, 2 H), 7.11 (d, *J* = 16.4 Hz, 2 H), 7.08 (d, *J* = 8.9 Hz, 4 H), 6.97 (d, *J* = 9.1 Hz, 4 H), 6.95 (d, *J* = 9.0 Hz, 4 H), 6.89 (d, *J* = 8.9 Hz, 4 H) 3.77 (s, 6 H) ppm.

***p,p'*-Bis[*N*-(5-formyl-thien-2-yl)phenyl]-*N*-(4-methoxyphenyl)amino]stilbene (6):** A solution of 5-formyl-2-thienylboronic acid (213 mg, 1.36 mmol) and K<sub>2</sub>CO<sub>3</sub> (481 mg, 3.75 mmol) in anhydrous MeOH (3 mL) was added to a solution of dibromo derivative **4b** (250 mg, 0.34 mmol) and [Pd(dppf)Cl<sub>2</sub>] (55.7 mg, 0.068 mmol) in anhydrous toluene (2.5 mL). The mixture was heated by microwave irradiation at 70 °C for 10 min. After adding water (30 mL), the mixture was extracted with CH<sub>2</sub>Cl<sub>2</sub> (3 × 30 mL), the combined organic extracts were dried, and the solvent was removed by rotary evaporation leaving a residue that was taken up with hot EtOH. The product was obtained as a brown solid (210 mg, 0.26 mmol, 78%). <sup>1</sup>H NMR ([D<sub>6</sub>]DMSO): δ = 9.87 (s, 2 H), 8.01 (d, *J* = 4.0 Hz, 2 H), 7.68 (d, *J* = 8.7 Hz, 4 H), 7.61 (d, *J* = 4.0 Hz, 2 H), 7.53 (d, *J* = 8.7 Hz, 4 H), 7.12 (d, *J* = 8.7 Hz, 4 H), 7.11 (s, 2 H), 7.04 (d, *J* = 8.6 Hz, 4 H), 6.99 (d, *J* = 8.9 Hz, 4 H), 6.95 (d, *J* = 8.7 Hz, 4 H) 3.78 (s, 6 H) ppm.

***p,p'*-Bis[*N*-(5-formyl-thien-2-yl)phenyl]-*N*-(4-methoxyphenyl)amino]distyrylbenzene (7):** A solution of 5-formyl-2-thienylboronic acid (220 mg, 1.44 mmol) and K<sub>2</sub>CO<sub>3</sub> (510 mg, 3.95 mmol) in anhydrous MeOH (3 mL) was added to a solution of dibromo derivative **5b** (303 mg, 0.36 mmol) and [Pd(dppf)Cl<sub>2</sub>] (59 mg, 0.072 mmol) in anhydrous toluene (2.5 mL). The mixture was heated by microwave irradiation at 70 °C for 10 min. The reaction was quenched by the addition of water (30 mL) and extracted with CH<sub>2</sub>Cl<sub>2</sub> (3 × 30 mL). The combined organic extracts were dried and the solvent removed by evaporation under reduced pressure, leaving a residue that was taken up with hot EtOH. The product was obtained as a brown solid (290 mg, 0.32 mmol, 89%). <sup>1</sup>H NMR ([D<sub>6</sub>]DMSO): δ = 9.87 (s, 2 H), 8.01 (d, *J* = 4.0 Hz, 2 H), 7.69 (d, *J* = 8.7 Hz, 4 H), 7.61 (d, *J* = 3.9 Hz, 2 H), 7.58 (s, 4 H), 7.56 (d, *J* = 8.6 Hz, 4 H), 7.25 (d, *J* = 16.4 Hz, 2 H), 7.15 (d, *J* = 16.4 Hz, 2 H), 7.13 (d, *J* = 8.8 Hz, 4 H), 7.05 (d, *J* = 8.5 Hz, 4 H), 7.00 (d, *J* = 8.9 Hz, 4 H), 6.97 (d, *J* = 8.7 Hz, 4 H), 3.78 (s, 6 H) ppm.

**TB-1:** Cyanoacetic acid (0.26 g, 3.02 mmol) and a catalytic amount of piperidine were added to a solution of bis-aldehyde **6** (80 mg, 0.10 mmol) in EtOH (5 mL). The mixture was heated by microwave irradiation at 100 °C for 1 h and then water (30 mL) was added. The formed precipitate was collected and dissolved in CH<sub>2</sub>Cl<sub>2</sub>. After extracting the solution with saturated aqueous NH<sub>4</sub>Cl, the organic phase was separated, dried, and the solvent removed by rotary evaporation to afford the crude product, which was purified as a dark-red solid by recrystallization (AcOH) (0.021 g, 0.02 mmol, 23%); m.p. > 200 °C (dec.). <sup>1</sup>H NMR ([D<sub>6</sub>]DMSO): δ = 8.09 (s, 2 H), 7.69 (d, *J* = 3.9 Hz, 2 H), 7.59 (d, *J* = 8.7 Hz, 4 H), 7.50 (d, *J* = 8.7 Hz, 4 H), 7.48 (d, *J* = 3.9 Hz, 2 H), 7.10 (d, *J* = 8.9 Hz, 4 H), 7.08 (s, 2 H), 7.01 (d, *J* = 8.6 Hz, 4 H), 6.98 (d, *J* = 8.8 Hz, 4 H), 6.97 (d, *J* = 8.5 Hz, 4 H) 3.78 (s, 6 H) ppm. IR (neat): ν̄ = 3500–2000 (s), 2217 (m), 1712 (s), 1571 (vs), 1502 (vs), 1424 (vs), 1317 (vs), 1283 (s), 1239 (vs), 1178 (vs), 1059 (s), 1027 (s), 797 (s) cm<sup>-1</sup>. HRMS-ESI: *m/z* = 463.11390 [(M – 2H)/2 requires 463.11164], 419.12302 [(M – 2COOH)/2 requires 419.12181]. C<sub>56</sub>H<sub>40</sub>N<sub>4</sub>O<sub>6</sub>S<sub>2</sub>: calcd. C 72.39, H 4.34, N 6.03; found C 72.28, H 4.76, N 6.29.

**TB-2:** Cyanoacetic acid (0.33 g, 3.89 mmol) and a catalytic amount of piperidine were added to a solution of bis-aldehyde **7** (0.174 g, 0.19 mmol) in toluene (5 mL). The mixture was heated by microwave irradiation at 100 °C for 40 min. The reaction was quenched by the addition of saturated aqueous NH<sub>4</sub>Cl (30 mL). The formed solid was collected to afford, after recrystallization (AcOH), the pure product as a dark-red solid (0.081 g, 0.08 mmol, 41%); m.p. > 200 °C (dec.). <sup>1</sup>H NMR ([D<sub>6</sub>]DMSO): δ = 8.43 (s, 2 H), 7.97 (d, *J* = 3.9 Hz, 2 H), 7.68 (d, *J* = 8.7 Hz, 4 H), 7.63 (d, *J* = 3.9 Hz, 2 H), 7.59 (s, 4 H), 7.56 (d, *J* = 8.7 Hz, 4 H), 7.25 (d, *J* = 16.3 Hz, 2 H), 7.15 (d, *J* = 16.3 Hz, 2 H), 7.14 (d, *J* = 8.7 Hz, 4 H), 7.06 (d, *J* = 8.4 Hz, 4 H), 7.00 (d, *J* = 8.8 Hz, 4 H), 6.99 (d, *J* = 8.5 Hz, 4 H), 3.78 (s, 6 H) ppm. IR (neat): ν̄ = 3260–2000 (s), 2215 (m), 1685 (s), 1565 (vs), 1506 (vs), 1408 (vs), 1318 (vs), 1287 (vs), 1243 (vs), 1220 (vs), 1193 (vs), 1181 (vs), 1063 (m), 828 (w), 801 (w) cm<sup>-1</sup>. HRMS-ESI: *m/z* = 514.13783 [(M – 2H)/2 requires 514.13512], 470.14602 [(M – 2COOH)/2 requires 470.14529]. C<sub>64</sub>H<sub>46</sub>N<sub>4</sub>O<sub>6</sub>S<sub>2</sub>·4H<sub>2</sub>O: calcd. C 69.67, H 4.93, N 5.08; found C 70.03, H 4.67, N 5.07.

**Computational Details:** DFT and TDDFT calculations were carried out using the Gaussian03 suite of programs.<sup>[27]</sup> Following the previously proposed successful strategy,<sup>[20]</sup> the ground state geometries were optimized in the gas phase using the B3LYP exchange-correlation functional<sup>[28]</sup> and a standard 6-31G\* basis set, whereas the hybrid MPW1K functional<sup>[29]</sup> was employed for the excited state calculations. Finally, the solvation effects were taken into account by applying the non-equilibrium C-PCM method<sup>[30]</sup> as implemented in Gaussian03.

**Preparation and Characterization of DSCs:** FTO glass plates (Nippon Sheet Glass, Solar 4 mm thickness) were immersed in aqueous TiCl<sub>4</sub> (40 mM) at 70 °C for 30 min and washed with water and ethanol. A paste composed of 20 nm anatase TiO<sub>2</sub> particles for the transparent nanocrystalline layer was coated on the FTO glass plates by screen printing. The coating-drying procedure was repeated to increase the thickness to that required. The TiO<sub>2</sub> electrodes were made of an approximate 6 μm transparent layer and were gradually heated under a flow of air. After a second TiCl<sub>4</sub> treatment, the TiO<sub>2</sub> electrodes were immersed in a 0.3 mM solution of TB-1 or TB-2 in tetrahydrofuran (THF) and kept at r.t. for 18 h. The liquid electrolyte consisted of 0.6 M *N*-methyl-*N*-butyl imidazolium iodide, 0.04 M iodine, 0.05 M LiI, 0.05 M guanidinium thiocyanate, and 0.28 M *tert*-butylpyridine in 15:85 (v/v) mixture of va-

leronitrile and acetonitrile. The dye-adsorbed TiO<sub>2</sub> electrode and counter electrode were assembled into a sealed sandwich-type cell with a gap of a hot-melt ionomer film, Surlyn (25 μm, Du-Pont). For stability evaluation, the TiO<sub>2</sub> electrodes were made of an approximate 7 μm transparent layer (20 nm diameter) and approximate 5 μm scattering layer (400 nm diameter, CCIC, HPW-400). The ionic liquid electrolyte consisted of 1,3-dimethylimidazolium-iodide, 1-ethyl-3-methylimidazoliumiodide, 1-ethyl-3-methylimidazolium tetracyanoborate, iodine, *N*-butylbenzimidazole, and guanidinium thiocyanate (molar ratio 12:12:16:1.67:3.33:0.67).<sup>[31]</sup> The other procedure was identical to that mentioned above. In order to reduce scattered light from the edge of the glass electrodes of the dyed TiO<sub>2</sub> layer, a light shading mask was used on the DSCs, so the active area of DSCs was fixed to 0.2 cm<sup>2</sup>. For photovoltaic measurements of the DSCs, the irradiation source was a 450 W xenon light (Osram XBO 450, Germany) fitted with a filter (Schott 113), the power of which was regulated to the AM 1.5 G solar standard by using a reference Si photodiode equipped with a color-matched filter (KG-3, Schott) in order to reduce the mismatch in the region of 350–750 nm between the simulated light and AM 1.5 G to less than 4%. The measurement of incident photon-to-current conversion efficiency (IPCE) was plotted as a function of excitation wavelength by using the incident light from a 300 W xenon lamp (ILC Technology, USA), which was focused through a Gemini-180 double monochromator (Jobin Yvon Ltd.). The measurement settling time between applying a voltage and measuring a current for the *I*-*V* characterization of DSCs was fixed to 40 and 200 ms for liquid and ionic liquid electrolytes, respectively.

**Supporting Information** (see footnote on the first page of this article): Absorption spectra of **4a** and **5a**, <sup>1</sup>H NMR and FT-IR spectra of TB-1 and TB-2, recombination rates of TB-1 and TB-2.

## Acknowledgments

A. A., F. D. A., M. P., and N. M. thank the Ministero dell'Università e della Ricerca (MIUR)-FIRB (Grant No. RBNE033KMA) and the Ministero dell'Università e della Ricerca (MIUR)-PRIN (Grant No. 2008CSNZFR). F. D. A., S. F., and M. P. thank the Fondazione Istituto Italiano di Tecnologia (IIT) Project SEED 2009 "HELYOS" for financial support. M. K. N. thanks the EU SPI-Cooperation, Collaborative Large-scale integrating project ORION FP7-NMP-LA-2009-229036 and the World Class University (WCU) program funded by the Ministry of Education, Science and Technology (Grant No. R31-2008-000-10035-0). We thank Dr. Davide Di Censo for his kind assistance.

- [1] A. J. Nozik, J. Miller, *Chem. Rev.* **2010**, *110*, 6443.
- [2] a) M. Graetzel, *Acc. Chem. Res.* **2009**, *42*, 1788; b) B. O'Regan, M. Graetzel, *Nature* **1991**, *353*, 737; M. Graetzel, *Nature* **2001**, *414*, 338.
- [3] M. K. Nazeeruddin, F. DeAngelis, S. Fantacci, A. Selloni, G. Viscardi, P. Liska, S. Ito, B. Takeru, M. Graetzel, *J. Am. Chem. Soc.* **2005**, *127*, 16835.
- [4] M. K. Nazeeruddin, C. Klein, P. Liska, M. Graetzel, *Coord. Chem. Rev.* **2005**, *249*, 1460.
- [5] H. J. Snaith, *Adv. Funct. Mater.* **2010**, *20*, 13.
- [6] a) Y. Ooyama, Y. Harima, *Eur. J. Org. Chem.* **2009**, 2903–2934; b) A. Mishra, M. Fischer, P. Bäuerle, *Angew. Chem. Int. Ed.* **2009**, *48*, 2474.
- [7] a) W. Zeng, Y. Cao, Y. Bai, Y. Wang, Y. Shi, M. Zhang, F. Wang, C. Pan, P. Wang, *Chem. Mater.* **2010**, *22*, 1915; b) H. Im, S. Kim, C. Park, S.-H. Jang, C.-J. Kim, K. Kim, N.-G.

- Park, C. Kim, *Chem. Commun.* **2010**, *46*, 1335; c) H. Choi, I. Raabe, D. Kim, F. Teocoli, C. Kim, K. Song, J.-H. Yum, J. Ko, M. K. Nazeeruddin, M. Grätzel, *Chem. Eur. J.* **2010**, *16*, 1193; d) G. Zhang, H. Bala, Y. Cheng, D. Shi, X. Lv, Q. Yu, P. Wang, *Chem. Commun.* **2009**, 2198.
- [8] Z. Ning, H. Tian, *Chem. Commun.* **2009**, 5483.
- [9] A. Abboto, N. Manfredi, C. Marinzi, F. D. Angelis, E. Mosconi, J.-H. Yum, Z. Xianxi, M. K. Nazeeruddin, M. Graetzel, *Energy Environ. Sci.* **2009**, *2*, 1094.
- [10] a) S. S. Park, Y. S. Won, Y. C. Choi, J. H. Kim, *Energy Fuels* **2009**, *23*, 3732; b) C.-H. Yang, S.-H. Liao, Y.-K. Sun, Y.-Y. Chuang, T.-L. Wang, Y.-T. Shieh, W.-C. Lin, *J. Phys. Chem. C* **2010**, *114*, 21786; c) J. A. Mikroyannidis, P. Sureshb, M. S. Royce, G. D. Sharmab, *J. Power Sources* **2010**, *195*, 3002.
- [11] D. Heredia, J. Natera, M. Gervaldol, L. Otero, F. Fungo, C.-Y. Lin, K.-T. Wong, *Org. Lett.* **2010**, *12*, 12.
- [12] C. Y. Lee, C. She, N. C. Jeong, J. T. Hupp, *Chem. Commun.* **2010**, *46*, 6090.
- [13] a) D. P. Hagberg, T. Marinado, K. M. Karlsson, K. Nonomura, P. Qin, G. Boschloo, T. Brinck, A. Hagfeldt, L. Sun, *J. Org. Chem.* **2007**, *72*, 9550; b) W.-H. Liu, I.-C. Wu, C.-H. Lai, C.-H. Lai, P.-T. Chou, Y.-T. Li, C.-L. Chen, Y.-Y. Hsu, Y. Chi, *Chem. Commun.* **2008**, 5152.
- [14] R. Li, X. Lv, D. Shi, D. Zhou, Y. Cheng, G. Zhang, P. Wang, *J. Phys. Chem. C* **2009**, *113*, 7469.
- [15] a) S. Kim, J. K. Lee, S. O. Kang, J. Ko, J.-H. Yum, S. Fantacci, F. De Angelis, D. Di Censo, M. K. Nazeeruddin, M. Graetzel, *J. Am. Chem. Soc.* **2006**, *128*, 16701; b) X. Jiang, T. Marinado, E. Gabriellson, D. P. Hagberg, L. Sun, A. Hagfeldt, *J. Phys. Chem. C* **2010**, *114*, 2799.
- [16] D. P. Hagberg, X. Jiang, E. Gabriellson, M. Linder, T. Marinado, T. Brinck, A. Hagfeldt, L. Sun, *J. Mater. Chem.* **2009**, *19*, 7232.
- [17] Y.-J. Cheng, J. Luo, S. Hau, D. H. Bale, T.-D. Kim, Z. Shi, D. B. Lao, N. M. Tucker, Y. Tian, L. R. Dalton, P. J. Reid, A. K.-Y. Jen, *Chem. Mater.* **2007**, *19*, 1154.
- [18] N. Zhou, L. Wang, D. W. Thompson, Y. Zhao, *Org. Lett.* **2008**, *10*, 3001.
- [19] A. J. Bard, L. R. Faulkner in *Electrochemical Methods, Fundamentals and Application*, Wiley-VCH, Hoboken, **2001**.
- [20] a) M. Pastore, E. Mosconi, F. De Angelis, M. Graetzel, *J. Phys. Chem. C* **2010**, *114*, 7205; b) M. Pastore, S. Fantacci, F. De Angelis, *J. Phys. Chem. C* **2010**, *114*, 22742.
- [21] D. P. Hagberg, T. Edvinsson, T. Marinado, G. Boschloo, A. Hagfeldt, L. Sun, *Chem. Commun.* **2006**, *21*, 2245.
- [22] M. Grätzel, *J. Photochem. Photobiol. A: Chem.* **2004**, *164*, 3.
- [23] J.-H. Yum, R. Humphry-Baker, S. M. Zakeeruddin, M. K. Nazeeruddin, M. Grätzel, *Nano Today* **2010**, *5*, 91.
- [24] V. Shklover, Yu. E. Ovchinnikov, L. S. Braginsky, S. M. Zakeeruddin, M. Graetzel, *Chem. Mater.* **1998**, *10*, 2533.
- [25] a) J. N. Demas, G. A. Crosby, *J. Phys. Chem.* **1971**, *75*, 991; b) A. T. R. Williams, S. A. Winfield, J. N. Miller, *Analyst* **1983**, *108*, 1067.
- [26] R. F. Kubin, A. N. Fletcher, *Chem. Phys. Lett.* **1983**, *99*, 49.
- [27] M. J. Frisch, G. W. Trucks, H. B. Schlegel, G. E. Scuseria, M. A. Robb, J. R. Cheeseman, J. A. Montgomery Jr., T. Vreven, K. N. Kudin, J. C. Burant, J. M. Millam, S. S. Iyengar, J. Tomasi, V. Barone, B. Mennucci, M. Cossi, G. Scalmani, N. Rega, G. A. Petersson, H. Nakatsuji, M. Hada, M. Ehara, K. Toyota, R. Fukuda, J. Hasegawa, M. Ishida, T. Nakajima, Y. Honda, O. Kitao, H. Nakai, M. Klene, X. Li, J. E. Knox, H. P. Hratchian, J. B. Cross, V. Bakken, C. Adamo, J. Jaramillo, R. Gomperts, R. E. Stratmann, O. Yazyev, A. J. Austin, R. Cammi, C. Pomelli, J. W. Ochterski, P. Y. Ayala, K. Morokuma, G. A. Voth, P. Salvador, J. J. Dannenberg, V. G. Zakrzewski, S. Dapprich, A. D. Daniels, M. C. Strain, O. Farkas, D. K. Malick, A. D. Rabuck, K. Raghavachari, J. B. Foresman, J. V. Ortiz, Q. Cui, A. G. Baboul, S. Clifford, J. Cioslowski, B. B. Stefanov, G. Liu, A. Liashenko, P. Piskorz, I. Komaromi, R. L. Martin, D. J. Fox, T. Keith, M. A. Al-Laham, C. Y. Peng, A.

- Nanayakkara, M. Challacombe, P. M. W. Gill, B. Johnson, W. Chen, M. W. Wong, C. Gonzalez, J. A. Pople, *Gaussian 03*, Revision C.02, Gaussian, Inc., Wallingford, CT, 2004.
- [28] A. D. Becke, *J. Chem. Phys.* **1993**, *98*, 1372.
- [29] B. J. Lynch, P. L. Fast, M. Harris, D. G. Truhlar, *J. Phys. Chem. A* **2000**, *104*, 4811.
- [30] M. Cossi, V. Barone, *J. Chem. Phys.* **2001**, *115*, 4708.
- [31] S. Wenger, P.-A. Bouit, Q. Chen, J. Teuscher, D. D. Censo, R. Humphry-Baker, J.-E. Moser, J. L. Delgado, N. Martin, S. M. Zakeeruddin, M. Graetzel, *J. Am. Chem. Soc.* **2010**, *132*, 5164.

Received: June 7, 2011

Published Online: September 5, 2011

**Asymmetric Tribranched Dyes: an Intramolecular  
Co-Sensitization Approach for Dye-Sensitized Solar Cells**

V. Leandri, V. Trifiletti, R. Ruffo, A. Abboto

*Eur. J. Org. Chem.*, **2013**, 30, 6793–6801

## Asymmetric Tribranched Dyes: An Intramolecular Cosensitization Approach for Dye-Sensitized Solar Cells

Valentina Leandri,<sup>[a]</sup> Riccardo Ruffo,<sup>[a]</sup> Vanira Trifiletti,<sup>[a]</sup> and Alessandro Abboto\*<sup>[a]</sup>

**Keywords:** Solar cells / Dyes/Pigments / Sensitizers / Conjugation / Multianchoring

A new multidonor and multianchoring asymmetric tribranched organic photosensitizer (i.e., TB-PT) for dye-sensitized solar cells containing three different (D- $\pi$ -D, D- $\pi_1$ -A, and D- $\pi_2$ -A; D = electron-rich moiety, A = electron-poor moiety,  $\pi$  = conjugated bridge) polar branches, two donor cores, and two acceptor/anchoring groups to TiO<sub>2</sub> was investigated

and compared with the corresponding symmetric dyes. TB-PT combines the advantages arising from its  $\pi$ -extended tribranched architecture and the intramolecular cosensitization approach, which results in enhanced tailored optical and energetic properties and, eventually, photovoltaic performances.

### Introduction

In the last decades, dye-sensitized solar cells (DSSCs)<sup>[1]</sup> have become very attractive because of their easy and cheap manufacturing procedures combined with over 12% record efficiencies.<sup>[2]</sup> Metal-free organic photosensitizers, providing several advantages over conventional metal complexes, typically own a linear dipolar D- $\pi$ -A structure, in which the electron-rich (D) and the electron-poor (A) moieties are connected through a conjugated ( $\pi$ ) bridge.<sup>[3]</sup> Unfortunately, these compounds present a single, often narrow, absorption band in the visible region, related to intramolecular charge transfer, which limits sunlight harvesting. Cosensitization, that is, the use of two or more dyes having complementary absorption spectra, is an attractive strategy to reach a panchromatic absorption and to enhance light harvesting,<sup>[3,4]</sup> as in the case of the recent record efficiency.<sup>[2]</sup> However, conventional intermolecular cosensitization suffers from a number of drawbacks: (1) The concentration of each cosensitizing dye on the TiO<sub>2</sub> surface is about half of that in the absence of cosensitization, which thus negates the beneficial effects of improved optical properties. (2) Well-separated complementary absorption bands of the two dyes implies the presence of a region in the cosensitized spectrum in which the absorption intensity is very low.<sup>[5]</sup> (3) Intermolecular charge- and energy-transfer processes decrease cell performances as a result of intimate mixing of the two dyes.<sup>[4]</sup>

We here propose an original approach consisting of the use of a multibranching dye in which three  $\pi$ -conjugated

branches possess complementary absorption properties (Figure 1, middle). Even if the dye is constituted by a single  $\pi$ -conjugated framework, the net result is equivalent to an intramolecular cosensitization effect. This architecture is the evolution of our previous design based on an A- $\pi_1$ -D- $\pi$ -D- $\pi_1$ -A tribranched structural motif (Figure 1, left) in which the presence of two donor and two acceptor/anchoring<sup>[6]</sup> fragments allowed enhanced optical and stability properties.<sup>[7]</sup> To further improve the optical properties through an intramolecular cosensitization approach, we have now modified the design by introducing two different D- $\pi$ -A side arms (D- $\pi_1$ -A and D- $\pi_2$ -A) with complementary absorption properties. The resulting dye can be regarded, in terms of intramolecular cosensitization, as a multichromophore structure that is derived from the combination of two linear D- $\pi$ -A dyes linked through donor end-capping moieties by a conjugated bridge. We stress that our approach differs from the other reports of intramolecular cosensitization in that the two D- $\pi$ -A arms are connected through saturated nonconjugated links, which thus limits  $\pi$ -structure extension.<sup>[8]</sup>

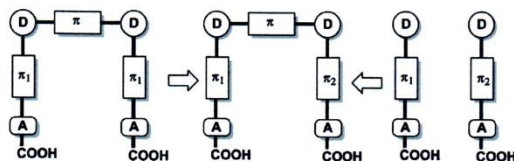


Figure 1. General design strategy for the multibranching dyes: symmetric tribranched (left), new geometry (middle), monobranching (right).

The new asymmetric dye TB-PT (see Figure 2) was designed on the basis of the most common building blocks for DSSC sensitizers, that is, D = triaryl amino, A = 2-cyanoacrylic acid, and  $\pi_1$  and  $\pi_2$  = benzene and thiophene.

[a] Department of Materials Science and Milano-Bicocca Solar Energy Research Center – MIB-Solar, University of Milano-Bicocca, INSTM Unit, Via Cozzi 53, 20125 Milano, Italy  
E-mail: alessandro.abboto@unimib.it  
Homepage: <http://www.mater.unimib.it/utenti/abboto>  
Supporting information for this article is available on the WWW under <http://dx.doi.org/10.1002/ejoc.201300962>.

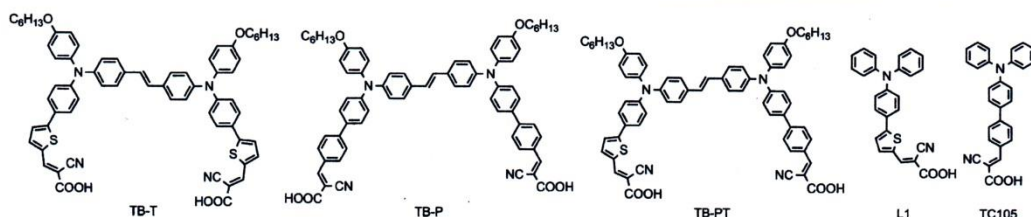


Figure 2. Symmetric (i.e., TB-T, TB-P) and asymmetric tribranched (i.e., TB-PT) dyes and monobranched reference dyes (i.e., L1 and TC105).

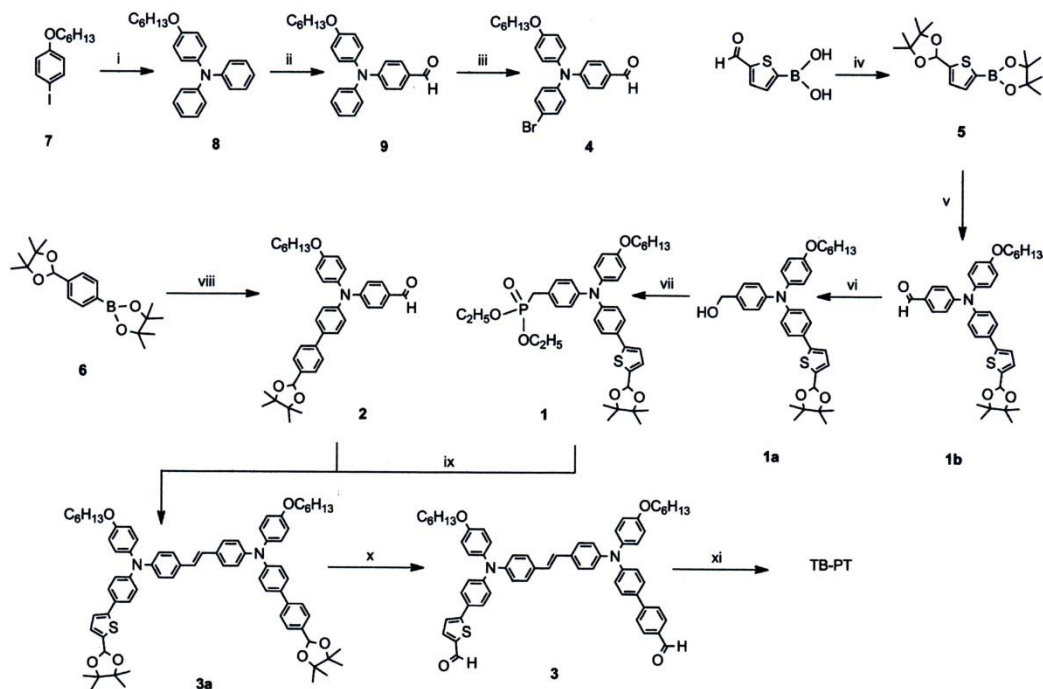
The electron-donating strength of the D moiety was increased by donor alkoxy substituents (RO-), and long linear R chains were introduced to improve the solubility and to minimize cell recombination losses.<sup>[9]</sup> TB-PT can thus be seen as the intramolecular combination of the linear dyes L1<sup>[10]</sup> and TC105<sup>[11]</sup> reported in the literature (Figure 2). The new dye was investigated in terms of its optical, electrochemical, and photovoltaic properties and compared with the corresponding symmetric tribranched dyes TB-P and TB-T (Figure 2). We will show how the optical response of the asymmetric dye TB-PT can be effectively obtained from a linear combination of the absorption bands of the sym-

metric dyes TB-P and TB-T by validating the intramolecular cosensitization model.

## Results and Discussion

### Synthesis, Spectroscopic, and Electrochemical Characterization

TB-PT was conveniently prepared, with steps that provided products in yields from 70% to quantitative, by a convergent route characterized by the Horner–Emmons condensation of branched precursors 1 and 2 (Scheme 1, see



Scheme 1. Synthesis of TB-PT. Reagents and conditions: (i) Diphenylamine, 1,10-phenanthroline, CuCl, KOH, toluene, reflux; (ii) DMF, POCl<sub>3</sub>, CH<sub>2</sub>Cl<sub>2</sub>, -5 °C to r.t.; (iii) *N*-bromosuccinimide (NBS), DMF, -18 °C; (iv) pinacol, *p*-toluenesulfonic acid (PTSA), toluene, reflux; (v) 4, Pd(dppf)Cl<sub>2</sub> [dppf = 1,1'-bis(diphenylphosphanyl)ferrocene], K<sub>2</sub>CO<sub>3</sub>, toluene/MeOH, microwave; (vi) NaBH<sub>4</sub>, THF, r.t.; (vii) P(OEt)<sub>3</sub>, I<sub>2</sub>; (viii) 4, Pd(dppf)Cl<sub>2</sub>, K<sub>2</sub>CO<sub>3</sub>, toluene/MeOH, microwave; (ix) *t*BuONa, THF, r.t.; (x) 10% HCl/THF, 50 °C; (xi) cyanoacetic acid, piperidine (cat.), CHCl<sub>3</sub>, reflux.



the Supporting Information for the synthesis of symmetric dyes TB-P and TB-T. Asymmetric bis-aldehyde **3** was submitted, in the last step, to double Knoevenagel condensation with a 25-fold excess amount of cyanoacetic acid to afford pure TB-PT as a dark solid. Both side building blocks were prepared by starting from common triarylamine block **4** through a Suzuki–Miyaura cross-coupling reaction with the *p*-formylboronic esters of thiophene and benzene, in their protected forms **5** and **6**, respectively. A divergent approach, similar to that used for the previously described tribranched dyes,<sup>[7b]</sup> was tested but discarded as a result of lower reproducibility and yields.

TB dyes exhibit two UV/Vis absorption bands (Figure 3), one more intense at lower energies (430–490 nm), which is due to intramolecular D– $\pi$ -A charge transfer of the side arms, and one at higher energies (385–395 nm), which is due to a local transition of the donor core.<sup>[6]</sup> The main quantitative optical parameters are collected in Table 1. In close agreement with the design strategy, the absorption spectrum of TB-PT nicely combines the optical features of the symmetric counterparts TB-P and TB-T. In particular, the intramolecular charge-transfer peak of the asymmetric chromophore is bathochromically and hypsochromically shifted relative to the corresponding band of TB-P and TB-T, respectively. Even more significant is the fact that the integrated intensity of the asymmetric dye absorption is higher than that of both symmetric compounds (see oscillator strengths in Table 1), and this suggests a cooperative enhancement effect of the two different side arms.

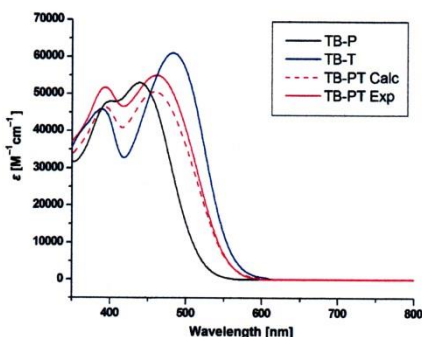


Figure 3. Absorption spectra of symmetric (i.e., TB-T, TB-P) and asymmetric (i.e., TB-PT) tribranched dyes in THF (solid line); calculated spectrum of TB-PT according to Equation (1) (dashed line).

The premise of the strategy proposed here was to demonstrate that the new molecule is actually equivalent to an intramolecular mixture of two different molecules with complementary absorption properties. Indeed, we found that both the position and intensity of the experimental spectrum of TB-PT could be nicely predicted (dashed line in Figure 3) by simply applying a 1:1 linear combination of the spectra of the symmetric dyes, as shown in Equation (1), in which  $\epsilon$  is the molar absorptivity at each wavelength. The calculated and the experimental spectra nicely match in

Table 1. Optical and electrochemical parameters of the dyes.<sup>[a]</sup>

Dye	$\lambda_{\text{abs}}$ [nm] ( $\epsilon \times 10^{-4} \text{ M}^{-1} \text{ cm}^{-1}$ )	$f^{[b]}$	HOMO <sup>[c]</sup> [eV]	LUMO <sup>[c]</sup> [eV]
TB-T	388 (4.6)	1.96	−5.7	−3.5
	482 (6.1)			
TB-P	401 (4.8)	1.58	−5.5	−3.1
	439 (5.3)			
TB-PT	394 (5.2)	1.98	−5.6	−3.4
	460 (5.5)			

[a] In THF. [b] Oscillator strength measured in the 350–800 nm range. [c] From cyclic voltammetry potential measurements vs. ferrocene/ferrocenium (Fc/Fc<sup>+</sup>); energy levels were calculated by using a value of −5.2 eV vs. vacuum for Fc/Fc<sup>+</sup> (−4.5 eV vs. vacuum for NHE).

$$\epsilon_{\text{TB-PT}} = 0.50\epsilon_{\text{TB-P}} + 0.50\epsilon_{\text{TB-T}} \quad (1)$$

shape, and the difference in intensity is within experimental error. The optical response of the target dye TB-PT can thus be effectively obtained from a linear combination of the absorption bands of the symmetric dyes, in agreement with the proposed intramolecular cosensitization model. The perfect matching between the experimental and the predicted spectrum of TB-PT is valuable in terms of the design of new panchromatic dyes with predefined optical properties once the absorption properties of the two constituting monobranched units are properly selected and investigated.

The electrochemical properties and HOMO/LUMO energies of dyes TB-P, TB-T, and TB-PT were measured by cyclic voltammetry (CV) and spectroelectrochemical measurements. The current potential profiles are shown in Figure 4 and the derived HOMO and LUMO energies are collected in Table 1 and graphically depicted in Figure S1 (Supporting Information) and compared to DSSC reference energies (conduction band of TiO<sub>2</sub> and Nerst potential of the redox pair I<sub>3</sub><sup>−</sup>/I<sup>−</sup>). All the observed oxidative waves were reversible. It is clearly seen from the electrochemical data that, similarly to the optical properties, TB-PT combines the energetic properties of TB-P and TB-T. In particular, the HOMO/LUMO energies of TB-PT lie in between those of the two symmetric dyes. Spectroelectrochemical analysis,

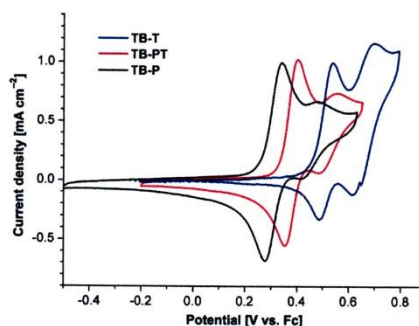


Figure 4. Cyclic voltammetry traces (vs. Fc) of dyes TB-P, TB-T, and TB-PT.

showing the change in the absorption properties of dye TB-PT upon oxidation, is described in the Supporting Information (Figure S2). The potential (0.45 V vs. Fc) was applied until no change in the optical properties was observed.

### Photovoltaic Investigation in DSSCs

The dyes were used as photosensitizers in DSSCs by using a double-layer TiO<sub>2</sub> film (20 nm particles 10 μm layer + scattering 4 μm layer) in the presence of chenodeoxycholic acid (CDCA)<sup>[12]</sup> as a deaggregating co-adsorbent agent (Table 2). Two electrolyte solutions were tested by varying the concentrations of LiI. The best average power conversion efficiencies were measured by using the electrolyte Z960 (1.0 M 1,3-dimethylimidazolium iodide, 0.03 M I<sub>2</sub>, 0.05 M LiI, 0.10 M guanidinium thiocyanate, and 0.50 M 4-*tert*-butylpyridine in acetonitrile/valeronitrile, 85:15). Table 2 summarizes the photovoltaic parameters in comparison with the DSSC benchmark dye N719 [bis(2,2'-bipyridyl-4,4'-dicarboxylate)ruthenium(II) bis(tetrabutylammonium) salt].<sup>[13]</sup> The overall conversion efficiencies PCE were derived from the equation  $PCE = J_{sc} \times V_{oc} \times FF$ , in which  $J_{sc}$  is the short circuit current density,  $V_{oc}$  is the open circuit voltage, and FF is the fill factor. Figure 5 shows the photocurrent–voltage curves of the devices.

Table 2. Photovoltaic parameters for TB-based DSSCs.

Dye	CDCA/dye	$J_{sc}$ [mA cm <sup>-2</sup> ]	$V_{oc}$ [mV]	FF	PCE [%]
TB-P	100:1	10.0	722	0.66	4.8
TB-T	100:1	10.9	687	0.65	4.9
TB-PT	100:1	11.7	708	0.66	5.4
N719	1:1	14.4	707	0.69	7.1

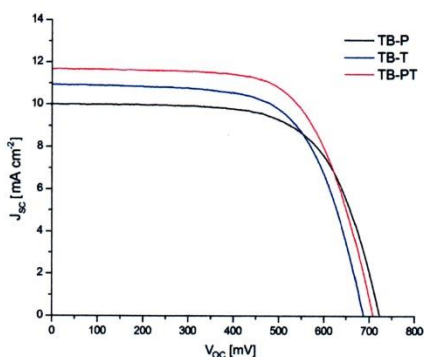


Figure 5. Current–voltage characteristics of DSSCs sensitized by TB-P, TB-T, and TB-PT.

In agreement with the superior optical properties and oscillator strength (Table 1), the asymmetric dye TB-PT exhibited the highest current and approximately 10% improved power conversion efficiency relative to the two symmetric dyes. The absolute efficiency of TB-PT is not very high if compared to recent values on organic sensitizers.<sup>[3]</sup>

However, it should be noted that our goal was to demonstrate, in addition to enhanced optical properties, improved photovoltaic efficiencies relative to the symmetric counterparts, as achieved. The very simple structure of the conventional donor, spacer, and acceptor groups and the nature of the monobranched reference dyes L1 and TC105 were not selected with the goal of reaching, at this time, higher efficiencies close to those of present record dyes.

The incident monochromatic photon-to-current conversion efficiencies (IPCE, 0–100%) of the devices based on the three dyes are shown in Figure 6. TB-PT summarizes the conversion properties of the two symmetric molecules over the whole range. To investigate this term in deeper detail, we separately examined the two constituting factors of IPCE according to the equation  $IPCE(\lambda) = LHE(\lambda) \times APCE(\lambda)$  (Figure 7) in which LHE (0–100%) is the light-harvesting efficiency associated to the ability of the cell to harvest light and APCE (0–100%) is the absorbed monochromatic photon-to-current conversion efficiency; this term gives the true quantum efficiency of the cell of generating electric current (internal quantum efficiency), and it is related to the electron injection efficiency from the dye to the semiconductor oxide, the dye regeneration efficiency, and the charge collection efficiency.<sup>[1]</sup> IPCE and LHE are experimentally determined. APCE is thus derived by dividing the IPCE number by LHE. Given that LHE can be directly measured only for transparent dye-coated films, as similarly performed for previous representative studies,<sup>[2]</sup> the whole set of comparative IPCE, LHE, and APCE spectra was recorded and derived for transparent 9 μm thick nanocrystalline TiO<sub>2</sub> monolayers. It is evident that APCE is excellent ( $\approx 100\%$ ) for almost the entire range of visible light, whereas the external quantum efficiency IPCE is much more modest, limited by the low LHE.

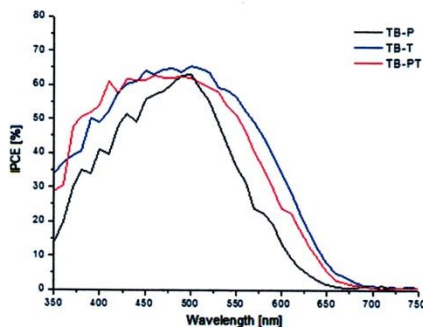


Figure 6. Incident photon-to-electric current conversion efficiencies as a function of wavelength of DSSCs sensitized by TB-P, and TB-PT.

Electrochemical impedance spectroscopy (EIS) was used to further investigate the comparative behavior of the three dyes in DSSC.<sup>[14]</sup> In this experiment, a small sinusoidal voltage stimulus of a fixed frequency was applied to an electrochemical cell and its current response was measured. The alternating current (ac) behavior of an electrochemical sys-

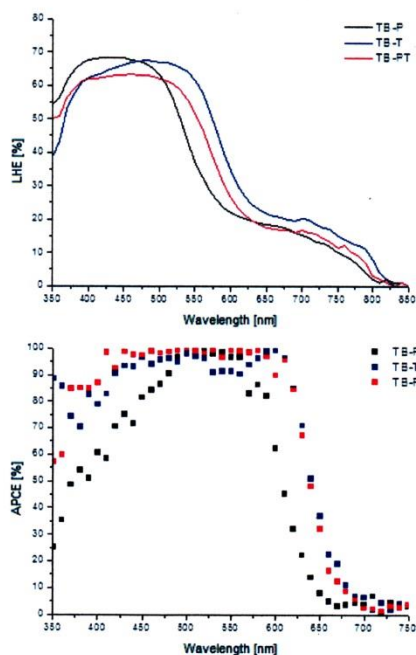


Figure 7. LHE (top) and APCE (bottom) as a function of wavelength of the DSSCs sensitized by TB-P, TB-T, and TB-PT.

tem can be investigated by sweeping the frequency over several orders of magnitude (generally from a few mHz to several MHz). The analysis of the impedance spectra is usually performed in terms of Nyquist plots in which the imaginary part of the impedance is plotted as a function of the real part over the range of frequencies. The impedance of the cell can be described by an equivalent circuit model (Figure 8, inset), in which the different cell components and their interfaces are treated as discrete electrical elements.<sup>[14]</sup> Under illumination under open-circuit voltage conditions, the DSSC Nyquist plot shows three arcs corresponding to the  $I^-/I_3^-$  redox process at the counter electrode in the high-frequency region ( $10^4 \div 10^2$  Hz), the  $TiO_2$ /dye/electrolyte interface at intermediate frequencies ( $1 \div 10$  Hz), and the Nernst diffusion within the electrolyte of the ionic species ( $I^-$ ) in the low-frequency region ( $0.01 \div 1$  Hz).<sup>[14]</sup> Under these conditions, the properties of the  $TiO_2$ /electrolyte interface can be derived from the central arc in terms of recombination resistance ( $R_{rec}$ ) and chemical capacitance for charge accumulation ( $C_\mu$ ). Both parameters are associated to charge-transfer (recombination) phenomena and represent detrimental back processes between the injected electrons in the oxide and the oxidized form of the electrolyte.<sup>[15]</sup>

Figure 8 shows the Nyquist plots for the DSSC devices obtained by EIS at the open circuit voltage under  $250 \text{ W m}^{-2}$  ( $0.25 \text{ sun}$ ) illumination. The data can be fitted by using the equivalent circuit reported in the inset of the

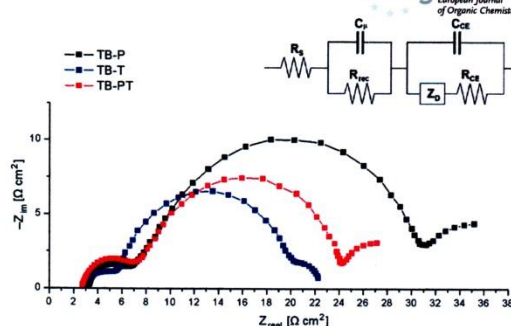


Figure 8. Nyquist plots of DSSCs sensitized by TB-P, TB-T, and TB-PT. Continuous lines represent the data fitting by using the equivalent circuit shown in the onset.

figure in which, in addition to the  $TiO_2$ /electrolyte interface parameters,  $R_s$  is the serial resistance [mainly due to the fluorine-doped tin oxide (FTO) layers],  $Z_D$  is the Warburg diffusion of the ionic species ( $I^-$ ) in the electrolyte, and  $R_{CE}$  and  $C_{CE}$  are the charge-transfer resistance and double-layer capacity at the counter electrode, respectively. The results of the EIS investigation are summarized in Table 3.  $R_{rec}$  values can be determined by the width of the central arc, whereas the capacitance  $C_\mu$  can be deduced by fitting the data with the equivalent circuit in Figure 8. The apparent electron lifetime in the oxide,  $\tau_n$ , can thus be calculated from  $\tau_n = R_{rec} C_\mu$  and corresponds to the angular frequency at the top of the middle arc.<sup>[14]</sup>

Table 3. Parameters calculated from EIS data plots of DSSCs based on TB-P, TB-T, and TB-PT sensitizers in comparison with the benchmark dye N719.

Dye	$R_{rec}$ [ $\Omega \text{ cm}^2$ ]	$C_\mu$ [ $\text{F cm}^{-2}$ ]	$\tau_n$ [ms]
TB-P	25	$5.8 \times 10^{-4}$	15
TB-T	14	$8.1 \times 10^{-4}$	11
TB-PT	17	$5.7 \times 10^{-4}$	10
N719	15	$1.1 \times 10^{-3}$	16

Yet again, asymmetric sensitizer TB-PT exhibited intermediate properties between those of symmetrical TB-P and TB-T. For the three dyes, the most relevant parameter, that is, the recombination resistance,  $R_{rec}$ , was comparable, or even slightly higher, than that of the benchmark dye N719. Therefore, detrimental charge recombination from  $TiO_2$  to the electrolyte is equally or less efficient in the DSSCs by using the three organic dyes than for the N719 sensitizer. This result is consistent with their APCE spectra. However, the corresponding capacitances, which probe the charge carrier accumulation in the oxide film and the density of states in the band gap, are lower than the reference DSSC by one order of magnitude. The net result is lower electron lifetimes, which affects cell performance.

## Conclusions

In conclusion, a new multidonor–multiacceptor/anchoring tribranched asymmetric dye, TB-PT, with two different

side dipolar branches having complementary absorption properties was designed and investigated as a DSSC sensitizer. The optical, electrochemical, and photovoltaic properties were compared with those of the corresponding symmetric counterparts, TB-P and TB-T. The results suggested a cooperative enhancement of the two different branches in terms of light-harvesting properties. Indeed, the measured current density of the DSSC based on TB-PT was higher than those of cells based on the symmetric dyes, resulting in an approximately 10% increase in the power conversion efficiency.

A novel intramolecular cosensitization strategy to enhance the optical response and, ultimately, the photovoltaic efficiency of DSSCs was demonstrated. In particular, we believe that the experimental validation of Equation (1), which shows that the panchromatic behavior of a new sensitizer can be built by appropriately selected constituting molecules with complementary optical and photovoltaic properties, will facilitate the search for new efficient sensitizers.<sup>[16]</sup>

## Experimental Section

**General:** NMR spectra were recorded with an instrument operating at 500.13 (<sup>1</sup>H) and 125.77 MHz (<sup>13</sup>C). <sup>13</sup>C signals were assigned on the basis of the results of J-MOD experiments. HRMS measurements were performed by using a ESI source and an ion trap (Fourier transform ion cyclotron resonance FT-ICR) as a mass analyzer. Flash chromatography was performed with silica gel 230–400 mesh (60 Å). Reactions performed under a nitrogen atmosphere were performed in oven-dried glassware and monitored by thin-layer chromatography by using UV light (254 and 365 nm) as a visualizing agent. All reagents were obtained from commercial suppliers at the highest purity and used without further purification. Anhydrous solvents were purchased from commercial suppliers and used as received. Extracts were dried with anhydrous Na<sub>2</sub>SO<sub>4</sub> and filtered before removal of the solvent by evaporation.

**1-(Hexyloxy)-4-iodobenzene (7):** A procedure reported in the literature was adapted with some modifications.<sup>[17]</sup> 1-Bromohexane (3.81 mL, 27.30 mmol) and K<sub>2</sub>CO<sub>3</sub> (12.56 g, 90.91 mmol) were added at room temperature to a solution of 4-iodophenol (9.99 g, 45.43 mmol) in dry acetone (50 mL). After stirring at reflux for 30 h, the mixture was filtered to remove the solid, and the solvent was evaporated under reduced pressure. The residual oil was extracted (CH<sub>2</sub>Cl<sub>2</sub>) and washed with 3 M NaOH, water, and brine. The organic phase was dried, filtered, and concentrated in vacuo to give the desired product as a colorless oil (6.64 g, 21.82 mmol, 85%).

**4-(Hexyloxy)-N,N-diphenylamine (8):** A procedure reported in the literature was adapted with some modifications.<sup>[18]</sup> A two-necked, round-bottomed flask equipped with a Dean–Stark apparatus was charged with diphenylamine (4.59 g, 27.10 mmol) and toluene (50 mL). Then, 7 (5.51 g, 18.12 mmol), 1,10-phenanthroline (652 mg, 3.61 mmol), cuprous chloride (358 mg, 3.61 mmol), and potassium hydroxide (4.06 g, 72.30 mol) were added. The reaction mixture was heated at reflux for 20 h, and then, water (150 mL) was added. The crude product was extracted with CH<sub>2</sub>Cl<sub>2</sub>, and the organic layer was washed with water, dried, and filtered. After removing the solvent under reduced pressure, the residue was purified by column chromatography (petroleum ether/CH<sub>2</sub>Cl<sub>2</sub>, 1:1) on silica gel to obtain a colorless oil (4.39 g, 12.71 mmol, 70%).

**4-[(4-(Hexyloxy)phenyl)(phenyl)amino]benzaldehyde (9):** Phosphorus oxychloride (0.752 mL, 8.21 mmol) was added dropwise to dry DMF (0.634 mL, 8.22 mmol) at –5 °C. The formation of a white solid was observed, and the reaction was kept at –5 °C for 15 min. CH<sub>2</sub>Cl<sub>2</sub> (30 mL) was added, and the solid was allowed to reach room temperature. After complete dissolution, 8 (2.04 g, 5.91 mmol) was added, and the mixture was stirred for 24 h. The reaction was quenched by the addition of water saturated with K<sub>2</sub>CO<sub>3</sub>, and the organic phase was washed with water (3 × 120 mL), dried, and filtered. Purification by column chromatography over silica gel (CH<sub>2</sub>Cl<sub>2</sub>/cyclohexane, 1:1) resulted in a yellow oil (2.10 g, 5.63 mmol, 95%). <sup>1</sup>H NMR (CDCl<sub>3</sub>): δ = 9.78 (s, 1 H), 7.64 (d, *J* = 8.8 Hz, 2 H), 7.32 (dd, *J* = 7.5, 7.4 Hz, 2 H), 7.17 (d, *J* = 7.5 Hz, 2 H), 7.14 (t, *J* = 7.4 Hz, 1 H), 7.1 (d, *J* = 8.9 Hz, 2 H), 6.94 (d, *J* = 8.8 Hz, 2 H), 6.89 (d, *J* = 8.9 Hz, 2 H), 1.46–1.44 (t, 2 H), 3.91 (t, *J* = 6.6 Hz, 2 H), 1.81–1.71 (m, 2 H), 1.52–1.42 (m, 2 H), 1.40–1.30 (m, 4 H), 0.90 (t, *J* = 7.0 Hz, 3 H) ppm. <sup>13</sup>C NMR (CDCl<sub>3</sub>): δ = 190.35 (CH), 157.08 (C), 153.66 (C), 146.11 (C), 138.52 (C), 131.33 (CH), 129.60 (CH), 128.43 (CH), 128.39 (C), 125.79 (CH), 124.77 (CH), 118.05 (CH), 115.62 (CH), 68.25 (CH<sub>2</sub>), 31.57 (CH<sub>2</sub>), 29.24 (CH<sub>2</sub>), 25.73 (CH<sub>2</sub>), 22.60 (CH<sub>2</sub>), 14.04 (CH<sub>3</sub>) ppm. HRMS (ESI): calcd. for [M + Na]<sup>+</sup> C<sub>25</sub>H<sub>27</sub>NNaO<sub>2</sub> 396.19340; found 394.19267.

**4-[(4-Bromophenyl)(4-(hexyloxy)phenyl)amino]benzaldehyde (4):** A solution of freshly recrystallized NBS (863 mg, 4.85 mmol) in DMF (10 mL) was added dropwise to a stirred solution of 9 (1.81 g, 4.85 mmol) in DMF (15 mL). The mixture was left at –18 °C for 15 h and then poured into water (50 mL). Diethyl ether was added, and the resulting organic phase was washed with water (4 × 120 mL), dried, and filtered. Removal of the solvent under reduced pressure yielded the pure product (2.06 g, 4.55 mmol, 94%) as a yellow gummy oil. <sup>1</sup>H NMR (CDCl<sub>3</sub>): δ = 9.80 (s, 1 H), 7.66 (d, *J* = 8.8 Hz, 2 H), 7.41 (d, *J* = 8.8 Hz, 2 H), 7.08 (d, *J* = 8.9 Hz, 2 H), 7.03 (d, *J* = 8.8 Hz, 2 H), 6.96 (d, *J* = 8.7 Hz, 2 H), 6.89 (d, *J* = 8.9 Hz, 2 H), 3.91 (t, *J* = 6.6 Hz, 2 H), 1.81–1.71 (m, 2 H), 1.52–1.42 (m, 2 H), 1.40–1.31 (m, 4 H), 0.90 (t, *J* = 7.1 Hz, 3 H) ppm. <sup>13</sup>C NMR (CDCl<sub>3</sub>): δ = 190.38 (CH), 157.25 (C), 153.14 (C), 145.35 (C), 138.16 (C), 132.61 (CH), 131.35 (CH), 128.95 (C), 128.36 (CH), 126.86 (CH), 118.69 (CH), 117.24 (C), 115.73 (CH), 68.28 (CH<sub>2</sub>), 31.57 (CH<sub>2</sub>), 29.22 (CH<sub>2</sub>), 25.73 (CH<sub>2</sub>), 22.61 (CH<sub>2</sub>), 14.05 (CH<sub>3</sub>) ppm. HRMS (ESI): calcd. for [M + Na]<sup>+</sup> C<sub>25</sub>H<sub>26</sub>NNaO<sub>2</sub>Br 474.10391; found 474.10369.

**4,4,5,5-Tetramethyl-2-[5-(4,4,5,5-tetramethyl-1,3-dioxolan-2-yl)thiophen-2-yl]-1,3,2-dioxaborolane (5):** A solution of 5-formyl-2-thiophenylboronic acid (802 mg, 5.14 mmol), 2,3-dimethyl-butane-2,3-diol (3.02 g, 25.70 mmol), and a catalytic amount of *p*-toluenesulfonic acid in toluene (40 mL) was heated at reflux by using a Dean–Stark receiver for 2 h. The reaction mixture was then washed with water (3 × 100 mL), dried, and filtered, and the solvent was evaporated under reduced pressure. The product was purified over silica gel (petroleum ether/ethyl acetate, 4:1) to give the desired product as light yellow needle-shaped crystals (1.22 g, 3.60 mmol, 71%); m.p. 128.5–129.5 °C. <sup>1</sup>H NMR (CDCl<sub>3</sub>): δ = 7.49 (d, *J* = 3.5 Hz, 2 H), 7.194 (d, *J* = 3.5 Hz, 2 H), 6.20 (s, 1 H), 1.32 (s, 12 H), 1.29 (s, 6 H), 1.28 (s, 6 H) ppm. <sup>13</sup>C NMR (CDCl<sub>3</sub>): δ = 151.00 (C), 136.82 (CH), 127.22 (CH), 96.48 (CH), 84.07 (C), 83.09 (C), 24.73 (CH<sub>3</sub>), 24.20 (CH<sub>3</sub>), 22.07 (CH<sub>3</sub>) ppm; the signal for the carbon atom directly attached to boron was not observed owing to quadrupolar relaxation. C<sub>17</sub>H<sub>27</sub>BO<sub>4</sub>S (338.27): calcd. C 60.36, H 8.06; found C 60.38, H 7.83.

**4-[(4-(Hexyloxy)phenyl)[4-[5-(4,4,5,5-tetramethyl-1,3-dioxolan-2-yl)thiophen-2-yl]phenyl]amino]benzaldehyde (1b):** Pd(dppf)-

Cl<sub>2</sub>:CH<sub>2</sub>Cl<sub>2</sub> (91 mg, 0.110 mmol), **5** (400 mg, 1.18 mmol), and K<sub>2</sub>CO<sub>3</sub> (628 mg, 4.55 mmol) were added to a solution of **4** (0.411 g, 0.910 mmol) in toluene/MeOH (1:1, 6 mL) in a microwave vial. The resulting mixture was heated in a microwave reactor at 75 °C for 20 min. After cooling to room temperature, the reaction mixture was poured into water and extracted with diethyl ether. The organic phase was washed with water (3 × 100 mL), dried, filtered, and concentrated under reduced pressure. Flash chromatography purification (cyclohexane/ethyl acetate, 9:1) gave the product as an orange sticky oil (414 mg, 0.710 mmol, 78%). <sup>1</sup>H NMR (CDCl<sub>3</sub>): δ = 9.78 (s, 1 H), 7.67 (d, *J* = 8.7 Hz, 2 H), 7.52 (d, *J* = 8.6 Hz, 2 H), 7.16–7.08 (m, 6 H), 7.00 (d, *J* = 8.7 Hz, 2 H), 6.90 (d, *J* = 8.9 Hz, 2 H), 6.18 (s, 1 H), 3.96 (t, *J* = 6.5 Hz, 2 H), 1.83–1.72 (m, 2 H), 1.52–1.42 (m, 2 H), 1.38–1.30 (m, 10 H), 1.29 (s, 6 H), 0.90 (t, *J* = 7.0 Hz, 3 H) ppm. <sup>13</sup>C NMR (CDCl<sub>3</sub>): δ = 190.11 (CH<sub>3</sub>), 157.22 (C), 153.24 (C), 145.55 (C), 144.32 (C), 142.91 (C), 138.34 (C), 131.28 (CH), 130.63 (C), 128.90 (C), 128.39 (CH), 127.04 (CH), 126.90 (CH), 125.46 (CH), 122.33 (CH), 118.75 (CH), 115.76 (CH), 96.72 (CH), 83.02 (C), 68.27 (CH<sub>2</sub>), 31.57 (CH<sub>2</sub>), 29.25 (CH<sub>2</sub>), 25.74 (CH<sub>2</sub>), 24.27 (CH<sub>3</sub>), 22.59 (CH<sub>2</sub>), 22.08 (CH<sub>3</sub>), 14.05 (CH<sub>3</sub>) ppm. HRMS (ESI): calcd. for [M + Na]<sup>+</sup> C<sub>36</sub>H<sub>41</sub>NNaO<sub>4</sub>S 606.26485; found 606.26500.

**4-[(4-(Hexyloxy)phenyl)]{4-[5-(4,4,5,5-tetramethyl-1,3-dioxolan-2-yl)thiophen-2-yl]phenyl}amino]phenyl-MeOH (1a)**: A solution of NaBH<sub>4</sub> (63.0 mg, 1.65 mmol) in THF (5 mL) was added dropwise to a solution of **1b** (740 mg, 1.27 mmol) at –10 °C in THF (25 mL). The mixture was stirred for 5 h at room temperature and then quenched by the addition of water. Ethyl acetate was added, and the resulting organic phase was washed with water (3 × 110 mL), dried, filtered, and concentrated under reduced pressure. The pure product was isolated as a light yellow sticky oil (709 mg, 1.21 mmol, 95.2%). <sup>1</sup>H NMR (CDCl<sub>3</sub>): δ = 7.41 (d, *J* = 8.7 Hz, 2 H), 7.23 (d, *J* = 8.5 Hz, 2 H), 7.10–7.03 (m, 6 H), 6.99 (d, *J* = 8.7 Hz, 2 H), 6.84 (d, *J* = 8.9 Hz, 2 H), 6.17 (s, 1 H), 3.95 (t, *J* = 6.5 Hz, 2 H), 1.82–1.73 (m, 2 H), 1.52–1.42 (m, 10 H), 1.40–1.33 (m, 10 H), 1.31 (s, 6 H), 0.93 (t, *J* = 7.0 Hz, 3 H) ppm. <sup>13</sup>C NMR (CDCl<sub>3</sub>): δ = 156.00 (C), 147.56 (C), 147.25 (C), 145.26 (C), 141.60 (C), 139.99 (C), 134.71 (C), 128.25 (CH), 127.72 (C), 127.43 (CH), 127.21 (CH), 126.57 (CH), 123.23 (CH), 122.32 (CH), 121.47 (CH), 115.38 (CH), 96.83 (CH), 83.04 (C), 68.23 (CH<sub>2</sub>), 64.94 (CH<sub>2</sub>), 31.63 (CH<sub>2</sub>), 29.32 (CH<sub>2</sub>), 25.79 (CH<sub>2</sub>), 24.30 (CH<sub>3</sub>), 22.65 (CH<sub>2</sub>), 22.08 (CH<sub>3</sub>), 14.12 (CH<sub>3</sub>) ppm. HRMS (ESI): calcd. for [M + Na]<sup>+</sup> C<sub>36</sub>H<sub>43</sub>NNaO<sub>4</sub>S 608.28050; found 608.28059.

**Diethyl-4-[(4-(Hexyloxy)phenyl)]{4-[5-(4,4,5,5-tetramethyl-1,3-dioxolan-2-yl)thiophen-2-yl]phenyl}amino}benzylphosphonate (1)**: Alcohol **1a** (709 mg, 1.21 mmol) was dissolved in P(OEt)<sub>3</sub> (15 mL) at –5 °C, and a solution of I<sub>2</sub> (1.27 g, 5.01 mmol) in P(OEt)<sub>3</sub> (5 mL) was added dropwise. The reaction mixture was stirred for 24 h at room temperature. The excess amount of P(OEt)<sub>3</sub> was distilled off under reduced pressure, and the pure product was obtained after flash chromatography on silica gel (CH<sub>2</sub>Cl<sub>2</sub>/ethyl acetate, 5:5) as a dark yellow oil (615 mg, 0.871 mmol, 72%). <sup>1</sup>H NMR (CDCl<sub>3</sub>): δ = 7.38 (d, *J* = 8.7 Hz, 2 H), 7.15 (d, *J* = 8.6 Hz, 2 H), 7.07–7.01 (m, 4 H), 6.99 (d, *J* = 8.3 Hz, 2 H), 6.95 (d, *J* = 8.6 Hz, 2 H), 6.82 (d, *J* = 8.9 Hz, 2 H), 6.14 (s, 1 H), 4.05 (m, 4 H), 3.92 (t, *J* = 6.5 Hz, 2 H), 3.07 (d, *J* = 21.3 Hz, 2 H), 1.82–1.73 (m, 2 H), 1.52–1.42 (m, 2 H), 1.40–1.33 (m, 10 H), 1.31 (s, 6 H), 1.26 (t, *J* = 7.1 Hz, 6 H) 0.93 (t, *J* = 7.0 Hz, 3 H) ppm. <sup>13</sup>C NMR (CDCl<sub>3</sub>): δ = 156.02 (C), 147.54 (C), 146.53 (C), 145.24 (C), 141.71 (C), 139.98 (C), 130.54/130.50 (<sup>2</sup>J<sub>C<sub>31</sub>P</sub> = 5.0 Hz, CH), 127.73 (C), 127.43 (CH), 127.08 (CH), 126.55 (CH), 125.08/125.02 (<sup>2</sup>J<sub>C<sub>31</sub>P</sub> = 6.3 Hz, C), 123.25 (CH), 122.28 (CH), 121.45 (CH), 115.37 (CH), 96.82 (CH), 82.99 (C), 68.24 (CH<sub>2</sub>), 62.11, 62.06 (<sup>2</sup>J<sub>C<sub>31</sub>P</sub> = 6.3 Hz, CH<sub>2</sub>), 33.58/

32.47 (<sup>1</sup>J<sub>C<sub>31</sub>P</sub> = 139.6 Hz, CH<sub>2</sub>), 31.59 (CH<sub>2</sub>), 29.29 (CH<sub>2</sub>), 25.74 (CH<sub>2</sub>), 24.27 (CH<sub>3</sub>), 22.60 (CH<sub>2</sub>), 22.06 (CH<sub>3</sub>), 16.42/16.37 (<sup>2</sup>J<sub>C<sub>31</sub>P</sub> = 6.3 Hz, CH<sub>3</sub>), 14.03 (CH<sub>3</sub>) ppm. HRMS (ESI): calcd. for [M + Na]<sup>+</sup> C<sub>30</sub>H<sub>42</sub>NNaO<sub>6</sub>SP 728.31452; found 728.31367.

**4,4,5,5-Tetramethyl-2-[4-(4,4,5,5-tetramethyl-1,3-dioxolan-2-yl)phenyl]-1,3,2-dioxaborolane (6)**: A solution of 4-formylphenylboronic acid (610 mg, 6.67 mmol), 2,3-dimethyl-butane-2,3-diol (3.94 g, 33.34 mmol), and a catalytic amount of *p*-toluenesulfonic acid in toluene (40 mL) was heated at reflux by using a Dean–Stark receiver for 3 h. The reaction mixture was then washed with water (3 × 100 mL), dried, and concentrated. The product was purified over silica gel (petroleum ether/ethyl acetate, 9:1) to give the desired product as colorless needle-shaped crystals (1.73 g, 5.20 mmol, 70%); m.p. 143.6–144.0 °C. <sup>1</sup>H NMR (CDCl<sub>3</sub>): δ = 7.81 (d, *J* = 8.0 Hz, 2 H), 7.49 (d, *J* = 8.0 Hz, 2 H), 6.0 (s, 1 H), 1.32 (s, 12 H), 1.29 (s, 6 H), 1.23 (s, 6 H) ppm. <sup>13</sup>C NMR (CDCl<sub>3</sub>): δ = 142.99 (C), 134.69 (CH), 125.33 (CH), 99.66 (CH), 83.71 (C), 82.62 (C), 24.87 (CH<sub>3</sub>), 24.17 (CH<sub>3</sub>), 22.17 (CH<sub>3</sub>) ppm; the signal for the carbon atom directly attached to boron was not observed owing to quadrupolar relaxation. C<sub>19</sub>H<sub>29</sub>BO<sub>4</sub> (332.25): calcd. C 68.69, H 8.80; found C 68.77, H 8.77.

**4-[[4-(Hexyloxy)phenyl]]{4'-(4,4,5,5-tetramethyl-1,3-dioxolan-2-yl)biphenyl-4-yl}amino}benzaldehyde (2)**: Pd(dppf)Cl<sub>2</sub>:CH<sub>2</sub>Cl<sub>2</sub> (111 mg, 0.137 mmol), **6** (682 mg, 2.05 mmol), and K<sub>2</sub>CO<sub>3</sub> (946 mg, 6.85 mmol) were added to a solution of **4** (620 mg, 1.37 mmol) in toluene/MeOH (1:1, 10 mL) in a microwave vial. The resulting mixture was heated in a microwave reactor at 75 °C for 20 min. After cooling to room temperature, the reaction mixture was poured into water and extracted with ethyl acetate. The organic phase was washed with water (3 × 150 mL), dried, filtered, and concentrated under reduced pressure. Flash chromatography purification (cyclohexane/ethyl acetate, 4:1) gave the product as a yellow sticky oil (633 mg, 1.10 mmol, 82%). <sup>1</sup>H NMR (CDCl<sub>3</sub>): δ = 9.80 (s, 1 H), 7.67 (d, *J* = 8.9 Hz, 2 H), 7.69–7.51 (m, 6 H), 7.21 (d, *J* = 8.6 Hz, 2 H), 7.14 (d, *J* = 8.9 Hz, 2 H), 7.01 (d, *J* = 8.2 Hz, 2 H), 6.91 (d, *J* = 8.9 Hz, 2 H), 3.96 (t, *J* = 6.5 Hz, 2 H), 1.85–1.74 (m, 2 H), 1.52–1.42 (m, 2 H), 1.39–1.32 (m, 10 H), 1.29 (s, 6 H), 0.90 (t, *J* = 7.0 Hz, 3 H) ppm. <sup>13</sup>C NMR (CDCl<sub>3</sub>): δ = 190.32 (CH), 157.18 (C), 153.49 (C), 145.46 (C), 140.57 (C), 138.70 (C), 138.47 (C), 137.05 (C), 131.32 (CH), 128.66 (C), 128.47 (CH), 128.16 (CH), 126.78 (CH), 126.70 (CH), 125.64 (CH), 118.49 (CH), 115.70 (CH), 99.72 (CH), 82.72 (C), 68.29 (CH<sub>2</sub>), 31.57 (CH<sub>2</sub>), 29.24 (CH<sub>2</sub>), 25.73 (CH<sub>2</sub>), 24.37 (CH<sub>3</sub>), 22.59 (CH<sub>2</sub>), 22.20 (CH<sub>3</sub>), 14.01 (CH<sub>3</sub>) ppm. C<sub>38</sub>H<sub>43</sub>NO<sub>4</sub> (577.76): calcd. C 79.00, H 7.50, N 2.42; found C 79.20, H 7.57, N 2.43.

**(E)-N-[4-(Hexyloxy)phenyl]-N'-4-[4-[(4-(hexyloxy)phenyl)]{4-[5-(4,4,5,5-tetramethyl-1,3-dioxolan-2-yl)thiophen-2-yl]phenyl}amino}styryl]phenyl-4'-(4,4,5,5-tetramethyl-1,3-dioxolan-2-yl)biphenyl-4-amine (3a)**: Under a nitrogen atmosphere, *t*BuOK (147 mg, 1.30 mmol) was added to a –10 °C, stirred solution of **1** (615 mg, 0.871 mmol) and **2** (503 mg, 0.871 mmol) in anhydrous THF (30 mL). The reaction immediately became red and was stirred at room temperature for 5 h. The mixture was poured into water saturated with NH<sub>4</sub>Cl, and ethyl acetate was added. The organic layer was separated, washed with water (3 × 120 mL), dried, and filtered. The solvent was removed under reduced pressure, and purification by column chromatography (petroleum ether/ethyl acetate, 4:1) gave the pure product as a yellow solid (757 mg, 0.670 mmol, 77%); m.p. 85.3–86.0 °C. <sup>1</sup>H NMR (CDCl<sub>3</sub>): δ = 7.59–7.51 (m, 4 H), 7.46 (d, *J* = 8.7 Hz, 2 H), 7.43 (d, *J* = 8.0 Hz, 2 H), 7.37 (d, *J* = 8.7 Hz, 2 H), 7.13–7.01 (m, 14 H), 6.94 (s, 2 H), 6.90–6.84 (m, 4 H), 6.18 (s, 1 H), 6.02 (s, 1 H), 3.95 (m, 4 H), 1.82–1.76 (m, 4 H), 1.51–1.42

(m, 4 H), 1.38–1.33 (m, 20 H), 1.31–1.29 (m, 12 H), 0.92 (m, 6 H) ppm.  $^{13}\text{C}$  NMR ( $\text{CDCl}_3$ ):  $\delta$  = 156.12 (C), 156.07 (C), 147.37 (C), 147.27 (C), 147.12 (C), 146.88 (C), 145.23 (C), 141.77 (C), 141.02 (C), 140.04 (C), 139.87 (C), 138.11 (C), 134.21 (C), 131.61 (C), 131.39 (C), 127.97 (C), 127.71 (CH), 127.54 (CH), 127.51 (CH), 127.16 (CH), 127.09 (CH), 126.74 (CH), 126.60 (CH), 126.51 (CH), 126.48 (CH), 126.32 (CH), 122.99 (CH), 122.91 (CH), 122.82 (CH), 122.67 (CH), 121.53 (CH), 115.40 (CH), 99.86 (CH), 96.86 (CH), 83.02 (C), 82.69 (C), 68.24 ( $\text{CH}_2$ ), 31.64 ( $\text{CH}_2$ ), 29.34 ( $\text{CH}_2$ ), 26.94 ( $\text{CH}_2$ ), 25.80 ( $\text{CH}_2$ ), 24.42 ( $\text{CH}_3$ ), 24.31 ( $\text{CH}_3$ ), 22.66 ( $\text{CH}_2$ ), 22.25 ( $\text{CH}_3$ ), 22.10 ( $\text{CH}_2$ ), 14.11 ( $\text{CH}_3$ ) ppm.  $\text{C}_{74}\text{H}_{84}\text{N}_2\text{O}_6\text{S}$  (1129.55): calcd. C 78.69, H 7.50, N 2.48; found C 78.66, H 7.62, N 2.41.

**(E)-5-(4-([4-(4-((4'-Formylbiphenyl-4-yl)[4-(hexyloxy)phenyl]amino)styryl]phenyl)[4-(hexyloxy)phenyl]amino)phenyl)thiophene-2-carbaldehyde (3):** Compound **3a** (757 mg, 0.670 mmol) was dissolved in 10% HCl/THF (1:2, 30 mL). The mixture was heated at 50 °C for 3 h and then poured into water. Ethyl acetate was added, and the organic layer was washed with water until neutral pH, dried with anhydrous  $\text{Na}_2\text{SO}_4$ , and filtered. The solvent was removed under reduced pressure, and purification by column chromatography (cyclohexane/ethyl acetate, 4:1) followed by crystallization from THF gave the pure product as an orange solid (517 mg, 0.553 mmol, 81%); m.p. 182.4–183.3 °C.  $^1\text{H}$  NMR ( $\text{CDCl}_3$ ):  $\delta$  = 10.03 (s, 1 H), 9.85 (s, 1 H), 7.92 (d,  $J$  = 8.3 Hz, 2 H), 7.72 (d,  $J$  = 8.3 Hz, 2 H), 7.71 (d,  $J$  = 4.0 Hz, 1 H), 7.51 (m, 4 H), 7.49 (m, 4 H), 7.29 (d,  $J$  = 4.0 Hz, 1 H), 7.16–7.02 (m, 12 H), 6.97 (s, 2 H), 6.88 (m, 4 H), 3.95 (m, 4 H), 1.82–1.75 (m, 4 H), 1.51–1.43 (m, 4 H), 1.39–1.33 (m, 8 H), 0.91 (m, 6 H) ppm.  $^{13}\text{C}$  NMR ( $\text{CDCl}_3$ ):  $\delta$  = 191.78 (CH), 182.52 (CH), 156.59 (C), 156.40 (C), 154.69 (C), 149.17 (C), 148.42 (C), 146.81 (C), 146.62 (C), 146.29 (C), 141.19 (C), 139.64 (C), 139.28 (C), 137.69 (CH), 134.63 (C), 132.47 (C), 132.25 (C), 131.87 (C), 130.32 (CH), 127.95 (CH), 127.85 (CH), 127.75 (CH), 127.21 (CH), 126.90 (CH), 126.79 (CH), 126.50 (CH), 125.62 (C), 123.91 (CH), 123.42 (CH), 122.68 (CH), 122.22 (CH), 121.48 (CH), 115.57 (CH), 115.52 (CH), 68.30 ( $\text{CH}_2$ ), 31.59 ( $\text{CH}_2$ ), 29.30 ( $\text{CH}_2$ ), 29.28 ( $\text{CH}_2$ ), 25.75 ( $\text{CH}_2$ ), 22.60 ( $\text{CH}_2$ ), 14.02 ( $\text{CH}_3$ ) ppm.  $\text{C}_{62}\text{H}_{60}\text{N}_2\text{O}_6\text{S}$  (929.23): calcd. C 80.14, H 6.51, N 3.01; found C 80.26, H 6.52, N 3.07.

**3-15-(4-([4-(E)-4-([4'-(2-Cyanoxy)phenyl-4-yl][4-(hexyloxy)phenyl]amino)styryl]phenyl)[4-(hexyloxy)phenyl]amino)phenyl)thiophene-2-yl]-2-cyanoacrylic acid (TB-PT):** Cyanoacetic acid (192 mg, 2.26 mmol) and a catalytic amount of piperidine were added to a solution of **3** (210 mg, 0.226 mmol) in  $\text{CHCl}_3$  (15 mL). The reaction mixture was heated at reflux for 18 h, poured into 15% HCl (100 mL), and stirred overnight at room temperature. After evaporation of the solvent, a dark precipitate was formed. Isolation of the precipitate by vacuum filtration afforded the pure product as a dark-red solid (233 mg, 0.220 mmol, 97.3%); m.p. > 200 °C (decomp.).  $^1\text{H}$  NMR ( $\text{D}_2\text{O}$ ):  $\delta$  = 8.45 (s, 1 H), 8.32 (s, 1 H), 8.10 (d,  $J$  = 8.6 Hz, 2 H), 7.92 (d,  $J$  = 4.1 Hz, 1 H), 7.88 (d,  $J$  = 8.5 Hz, 2 H), 7.72 (d,  $J$  = 8.8 Hz, 2 H), 7.67 (d,  $J$  = 8.8 Hz, 2 H), 7.63 (d,  $J$  = 4.1 Hz, 1 H), 7.54–7.50 (m, 4 H), 7.13–7.08 (m, 6 H), 7.16–6.99 (m, 6 H), 6.98–94 (m, 6 H), 3.96 (m, 4 H), 1.75–1.67 (m, 4 H), 1.47–1.38 (m, 4 H), 1.36–1.27 (m, 8 H), 0.89 (m, 6 H) ppm.  $^{13}\text{C}$  NMR ( $\text{D}_2\text{O}$ ):  $\delta$  = 164.25 (C), 163.91 (C), 156.64 (C), 156.47 (C), 154.04 (CH), 153.87 (C), 149.15 (C), 148.37 (C), 146.95 (CH), 146.57 (C), 146.04 (C), 144.36 (C), 142.11 (CH), 139.34 (C), 138.99 (C), 133.79 (C), 132.81 (C), 132.16 (C), 131.94 (CH), 131.42 (C), 130.17 (CH), 128.31 (CH), 128.29 (CH), 128.23 (CH), 127.88 (CH), 127.81 (CH), 127.15 (CH), 126.82 (CH), 126.75 (CH), 125.18 (C), 124.22 (CH), 123.58 (CH), 121.90 (CH), 121.21 (CH), 117.12 (C), 116.90 (C), 116.14 (CH), 116.12 (CH), 102.96 (C), 97.60 (C), 68.12 ( $\text{CH}_2$ ), 31.48 ( $\text{CH}_2$ ), 29.17 ( $\text{CH}_2$ ), 25.69 ( $\text{CH}_2$ ),

22.54 ( $\text{CH}_2$ ), 14.37 ( $\text{CH}_3$ ) ppm.  $\text{C}_{68}\text{H}_{62}\text{N}_2\text{O}_6\text{S}$  (1063.32): calcd. C 76.81, H 5.88, N 5.27; found C 76.51, H 6.13, N 5.29.

**Electrochemical and Spectroelectrochemical Characterization:** Dyes TB-P, TB-T, and TB-PT were submitted to electrochemical characterization. Each sample was dissolved ( $10^{-4}$  M) in a 0.1 M solution of tetrabutylammonium perchlorate (Fluka, electrochemical grade, 99.0%) in anhydrous THF (Aldrich) as the supporting electrolyte. Cyclic voltammetry (CV) was performed at a scan rate of 50 mV s $^{-1}$  by using a PARSTA273 potentiostat in a two-chamber three-electrode electrochemical cell in a glove box filled with argon ( $[\text{O}_2] < 1$  ppm). The working, counter, and pseudoreference electrodes were a glassy carbon (GC) pin, a Pt flag, and an Ag/AgCl wire, respectively. The working electrode disc was well polished with a 0.1  $\mu\text{m}$  alumina suspension, sonicated for 15 min in deionized water and washed with 2-propanol before use. The Ag/AgCl pseudoreference electrode was calibrated by adding ferrocene ( $10^{-3}$  M) to the test solution.

Spectroelectrochemical analysis of TB-PT was performed by using a three-electrode cell arranged in a thin layer quartz glass cell. The gold gauze working electrode was confined in the thin portion of the cell (wall thickness 0.5 mm) to minimize the diffusion length of the electroactive molecule. The change in the absorption properties of TB-PT upon oxidation is depicted in Figure S2 (Supporting Information). The potential (0.45 V vs. Fc) was applied until no change in the optical properties was observed.

**Fabrication of the DSSCs:** The DSSCs were prepared by adapting a procedure reported in the literature.<sup>[19]</sup> To exclude metal contamination, all of the containers were glass or Teflon and were treated with EtOH and 10% HCl prior to use. Plastic spatulas and tweezers were used throughout the procedure. FTO glass plates (Solaronix TCO 22-7, 2.2 mm thickness, 7  $\Omega\text{square}^{-1}$ ) were cleaned in a detergent solution for 15 min by using an ultrasonic bath, and then rinsed with pure water and EtOH. After treatment in a UV-O $_3$  system (Novascan PSD Pro Series – Digital UV Ozone System) for 18 min, the FTO plates were treated with a freshly prepared 40 mM aqueous solution of  $\text{TiCl}_4$  for 30 min at 70 °C and then rinsed with water and EtOH. A first transparent nanocrystalline layer (20 nm particles, Dyesol 18NR-T) was screen-printed and dried at 125 °C for 6 min. The working electrodes were screen-printed and dried again with the same procedure to obtain a 10  $\mu\text{m}$  transparent double layer. A scattering 4  $\mu\text{m}$  layer containing optically dispersing anatase particles (Dyesol WER2-O) was screen-printed on the previous electrodes. The coated films were kept in a cabinet for 5 min and then thermally treated under an air flow at 125 °C for 6 min, 325 °C for 10 min, 450 °C for 15 min, and 500 °C for 15 min. The heating ramp rate was 5–10 °C min $^{-1}$ . The thickness of the layers was measured by using a VEECO Dektak 8 Stylus Profiler. The sintered layer was treated again with 40 mM aqueous  $\text{TiCl}_4$  (70 °C for 30 min), rinsed with EtOH, and heated at 500 °C for 30 min. After cooling down to 80 °C the  $\text{TiO}_2$  coated plate was immersed into a  $2.0 \times 10^{-4}$  M solution of organic dyes in THF/EtOH (1:1) containing  $2.0 \times 10^{-2}$  M chenodeoxycholic acid (CDCA) for 20 h at room temperature in the dark. For the reference devices with N719, the plate was immersed into a  $5.0 \times 10^{-4}$  M solution of the dye in EtOH containing equimolar CDCA under the same experimental conditions. Counter electrodes were prepared according to the following procedure: A 1 mm hole was made in a FTO plate by using diamond drill bits. The electrodes were then cleaned with a detergent solution for 15 min by using an ultrasonic bath, 10% HCl, and finally acetone for 15 min by using an ultrasonic bath. After treatment in the UV-O $_3$  system for 18 min, a drop of a  $5 \times 10^{-3}$  M solution of  $\text{H}_2\text{PtCl}_6$  in EtOH was added and the thermal treatment at 400 °C for 15 min was repeated.

The dye-adsorbed TiO<sub>2</sub> electrode and Pt counter electrode were assembled into a sealed sandwich-type cell by heating with a hot-melt ionomer-class resin (Surlyn 25- $\mu$ m thickness) as a spacer between the electrodes. A drop of the electrolyte solution (Z960: 1.0 M 1,3-dimethylimidazolium iodide, 0.03 M I<sub>2</sub>, 0.05 M LiI, 0.10 M guanidinium thiocyanate, and 0.50 M 4-*tert*-butylpyridine in acetonitrile/valeronitrile, 85:15; for N719-based cells the standard electrolyte A6141 was used: 0.6 M *N*-butyl-*N*-methylimidazolium iodide, 0.03 M I<sub>2</sub>, 0.10 M guanidinium thiocyanate, and 0.5 M 4-*tert*-butylpyridine in acetonitrile/valeronitrile, 85:15) was added to the hole and introduced inside the cell by vacuum backfilling. Finally, the hole was sealed with a sheet of Bynel and a cover glass. A reflective foil at the back side of the counter electrode was taped to reflect unabsorbed light back to the photoanode.

**Photovoltaic and Photoelectrical Characterization of DSSCs:** Photovoltaic measurements of the DSSCs were performed with an antireflective layer on top of the cells under a 500 W xenon light source (ABET Technologies Sun 2000 class ABA Solar Simulator). The power of the simulated light was calibrated to AM 1.5 (100 mW cm<sup>-2</sup>) by using a reference Si cell photodiode equipped with an IR cutoff filter (KG-5, Schott) to reduce the mismatch in the region of 350–750 nm between the simulated light and the AM 1.5 spectrum. Values were recorded after 3 and 24 h and 3 and 7 d of ageing in the dark. Curves I–V were obtained by applying an external bias to the cell and measuring the generated photocurrent with a Keithley model 2400 digital source meter. Incident photon-to-current conversion efficiencies (IPCE) was recorded as a function of excitation wavelength by using a monochromator (Omni 300 LOT ORIEL) with single grating in Czerny–Turner optical design, in AC mode by using a chopping frequency of 1 Hz and a bias of white light (0.3 sun). EIS spectra were obtained by using an Eg&G PARSTAT 2263 galvanostat potentiostat. The measurements were performed in the frequency range from 100 kHz to 100 mHz under ac stimulus with an amplitude of 10 mV and no applied voltage bias. The obtained Nyquist plots were fitted by a nonlinear least-square procedure by using the equivalent circuit model in Figure 8.

**Supporting Information** (see footnote on the first page of this article): Synthesis of TB-P and TB-T, <sup>1</sup>H NMR and <sup>13</sup>C NMR spectra for all new compounds, HOMO and LUMO energy levels of the dyes (pictorial view), and spectroelectrochemical curves.

## Acknowledgments

The authors thank Consorzio per le Ricerche sui Materiali Avanzi (CORIMAV) (Pirelli S.p.A. - University of Milano-Bicocca) and the Ministero dell'Università e della Ricerca (MIUR-PRIN) (grant number 2008CSNZFR) for financial support.

- [1] a) S. F. Zhang, X. D. Yang, Y. H. Numata, L. Y. Han, *Energy Environ. Sci.* **2013**, *6*, 1443; b) B. E. Hardin, H. J. Snaith, M. D. McGehee, *Nat. Photonics* **2012**, *6*, 162; c) X. B. Chen, C. Li, M. Grätzel, R. Kostecki, S. S. Mao, *Chem. Soc. Rev.* **2012**, *41*, 7909; d) M. Grätzel, *Nature* **2001**, *414*, 338; e) A. Hagfeldt, G. Boschloo, L. Sun, L. Kloo, H. Pettersson, *Chem. Rev.* **2010**, *110*, 6595; f) M. Grätzel, *Acc. Chem. Res.* **2009**, *42*, 1788.
- [2] A. Yella, H.-W. Lee, H. N. Tsao, C. Yi, A. K. Chandiran, M. K. Nazeeruddin, E. W.-G. Diau, C.-Y. Yeh, S. M. Zakeeruddin, M. Grätzel, *Science* **2011**, *334*, 629.
- [3] For recent reviews, see: a) B. G. Kim, K. Chung, J. Kim, *Chem. Eur. J.* **2013**, *19*, 5220; b) Y. S. Yen, H. H. Chou, Y. C. Chen, C. Y. Hsu, J. T. Lin, *J. Mater. Chem.* **2012**, *22*, 8734; c) J. N. Clifford, M. Planells, E. Palomares, *J. Mater. Chem.* **2012**, *22*, 24195; d) A. Mishra, M. Fischer, P. Bäuerle, *Angew. Chem.* **2009**, *121*, 2510; *Angew. Chem. Int. Ed.* **2009**, *48*, 2474.
- [4] a) S. F. Zhang, A. Islam, X. D. Yang, C. J. Qin, K. Zhang, Y. Numata, H. Chen, L. Y. Han, *J. Mater. Chem.* **2013**, *1*, 4812; b) G. D. Sharma, S. P. Singh, R. Kurchania, R. J. Ball, *RSC Adv.* **2013**, *3*, 6036; c) C. Magne, M. Urien, T. Pauporte, *RSC Adv.* **2013**, *3*, 6315; d) C. L. Lee, W. H. Lee, C. H. Yang, *J. Mater. Sci.* **2013**, *48*, 3448; e) M. Cheng, X. C. Yang, J. J. Li, F. G. Zhang, L. C. Sun, *ChemSusChem* **2013**, *6*, 70; f) M. J. Griffith, K. Sunahara, P. Wagner, K. Wagner, G. G. Wallace, D. L. Officer, A. Furube, R. Katoh, S. Mori, A. Mozer, *Chem. Commun.* **2012**, *48*, 4145; g) N. C. Jeong, H.-J. Son, C. Prasitichai, C. Y. Lee, R. A. Jensen, O. K. Farha, J. T. Hupp, *J. Am. Chem. Soc.* **2012**, *134*, 19820; h) B. E. Hardin, A. Sellinger, T. Moehl, R. Humphry-Baker, J.-E. Moser, P. Wang, S. M. Zakeeruddin, M. Grätzel, M. D. McGehee, *J. Am. Chem. Soc.* **2011**, *133*, 10662.
- [5] J. N. Clifford, A. Forneli, H. Chen, T. Torres, S. Tan, E. Palomares, *J. Mater. Chem.* **2011**, *21*, 1693.
- [6] Y. Wu, M. Marszalek, S. M. Zakeeruddin, Q. Zhang, H. Tian, M. Grätzel, W. Zhu, *Energy Environ. Sci.* **2012**, *5*, 8261.
- [7] a) A. Abbotto, N. Manfredi, C. Marinzi, F. D. Angelis, E. Mosconi, J.-H. Yum, Z. Xianxi, M. K. Nazeeruddin, M. Grätzel, *Energy Environ. Sci.* **2009**, *2*, 1094; b) A. Abbotto, V. Leandri, N. Manfredi, F. D. Angelis, M. Pastore, J.-H. Yum, M. K. Nazeeruddin, M. Grätzel, *Eur. J. Org. Chem.* **2011**, 6195.
- [8] a) Y. P. Hong, J. Y. Liao, J. L. Fu, D. B. Kuang, H. Meier, C. Y. Su, D. R. Cao, *Dyes Pigment.* **2012**, *94*, 481; b) X. M. Ren, S. H. Jiang, M. Y. Cha, G. Zhou, Z. S. Wang, *Chem. Mater.* **2012**, *24*, 3493; c) D. Cao, J. Peng, Y. Hong, X. Fang, L. Wang, H. Meier, *Org. Lett.* **2011**, *13*, 1610; d) Y. Hong, J.-Y. Liao, D. Cao, X. Zang, D.-B. Kuang, L. Wang, H. Meier, C.-Y. Su, *J. Org. Chem.* **2011**, *76*, 8015.
- [9] Z. Ning, Y. Fu, H. Tian, *Energy Environ. Sci.* **2010**, *3*, 1170.
- [10] M. Lu, M. Liang, H.-Y. Han, Z. Sun, S. Xue, *J. Phys. Chem. C* **2011**, *115*, 274.
- [11] C. Teng, X. Yang, C. Yang, H. Tian, S. Li, X. Wang, A. Hagfeldt, L. Sun, *J. Phys. Chem. C* **2010**, *114*, 11305.
- [12] X. Jiang, T. Marinado, E. Gabrielsson, D. P. Hagberg, L. Sun, A. Hagfeldt, *J. Phys. Chem. C* **2010**, *114*, 2799.
- [13] M. K. Nazeeruddin, F. De Angelis, S. Fantacci, A. Selloni, G. Viscardi, P. Liska, S. Ito, B. Takeru, M. Grätzel, *J. Am. Chem. Soc.* **2005**, *127*, 16835.
- [14] a) F. Fabregat-Santiago, G. Garcia-Belmonte, I. Mora-Seró, J. Bisquert, *Phys. Chem. Chem. Phys.* **2011**, *13*, 9083; b) J. Halme, P. Vahermaa, K. Miettunen, P. Lund, *Adv. Mater.* **2010**, *22*, E210.
- [15] J. Bisquert, F. Fabregat-Santiago, I. Mora-Seró, G. Garcia-Belmonte, S. Giménez, *J. Phys. Chem. C* **2009**, *113*, 17278.
- [16] This work is under investigation and will be presented in due course.
- [17] K. M. Karlsson, X. Jiang, S. K. Eriksson, E. Gabrielsson, H. K. Rensmo, A. Hagfeldt, L. Sun, *Chem. Eur. J.* **2011**, *17*, 6415.
- [18] Z. Li, W. Wu, G. Qiu, G. Yu, Y. Liu, C. Ye, J. Qin, Z. Li, *J. Polym. Sci., Part A J. Polym. Sci., Part A: Polym. Chem.* **2011**, *49*, 1977.
- [19] S. Ito, T. N. Murakami, P. Comte, C. Liska, M. Grätzel, M. K. Nazeeruddin, M. Grätzel, *Thin Solid Films* **2008**, *516*, 4613.

Received: June 29, 2013

Published Online: August 20, 2013

**Organic Hydrophilic Dye for Water-Based Electrolyte  
Dye-Sensitized Solar Cells**

V. Leandri, H. Ellis, E. Gabrielsson, G. Boschloo, L. Sun, A. Hagfeldt

*(in preparation)*